Western&Graduate&PostdoctoralStudies

Electronic Thesis and Dissertation Repository

4-18-2017 12:00 AM

Photoactive Properties of Nanostructured Titania Modified Polyurethanes

Chao Chen, *The University of Western Ontario*

Supervisor: Paul A. Charpentier, *The University of Western Ontario*
A thesis submitted in partial fulfillment of the requirements for the Doctor of Philosophy degree
in Chemical and Biochemical Engineering
© Chao Chen 2017

Abstract

In order to enhance both the photoactivity and physical/mechanical properties of titania/polyurethane (PU) nanocomposites, *in-situ* polymerization and film casting were investigated. Both self-degrading PU foams and self-cleaning PU coatings were prepared. Functional monomers were prepared using DMPA (2,2-dimethylolpropionic acid) functionalized anatse TiO_2 and P25 for integration into polyurethane foam with a "grafting-from" synthetic method. This technique was found to successfully reduce the agglomeration effect of titania nanoparticles inside the foams. In addition, the photodegradation rate was enhanced by $> 120\%$ over unmodified foam at an optimized loading of 3wt% DMPA functionalized anatase TiO_2. The presence of DMPA functionalized P25 nanoparticles produced an increase in the degradation rate of 66% over the unmodified foam at an optimized 1wt% loading.

SiO_2 encapsulated anatase and rutile TiO_2 nanoparticles were successfully synthesized via a modified Stöber process, and integrated into polyurethane coatings. The SiO_2 encapsulation enhanced the anatase TiO_2 nanoparticle distribution as well as the photocatalytic activity of the polyurethane nanocomposites when the loading weight of SiO_2 was lower than 3.25wt%. By increasing the SiO_2 amount on the titania surface, the contact angle of the coatings increased from 75° to 87° for anatase phase and 70° to 78° for rutile phase. The Young's Modulus was also increased from 1.06GPa to 2.77GMPa for anatase phase and 1.06GPa to 2.17GPa for rutile phase, attributed to the silica layer giving better integration. The thermal conductivity of the polyurethane coatings was also

successfully decreased by encapsulating SiO_2 on the titania surface, which has applications for next generation high performance coatings.

In addition to nanospheres, TiO_2 nanofibers were synthesized via an environmental friendly supercritical CO_2 method and nanotubes were prepared via a hydrothermal reaction. They were encapsulated with silica via the modified Stöber process, then integrated into polyurethane coatings. With more of SiO_2 coated on the nanofibers' surface, the photocatalytic activity, UV absorbance, and hydroxyl radical formation decreased due to the shielding effect of the SiO_2 layers. These effects in part are attributed to the surface area changes. With these modified nanofibers and nanotubes, the polyurethane coatings were found to exhibit similar photoactivity trend. The mechanical strength was enhanced and the hydrophobicity of coatings was maintained upon exposure to UV irradiation.

Nanofiber shaped TiO_2 xerogel was synthesized via environmental friendly approach with supercritical CO_2 ($ScCO_2$), which when mixed within polyurethane coatings through film casting method and the coatings remain transparent. The coordination between Ti and the carboxylic acid group was investigated showing a bidentate coordination. The TiO_2 xerogel nanofibers were found to possess high UV absorbance with high UV shielding properties when integrated into polyurethane coatings. They also were found to influence the thermicity while increasing the reflective index, hence allowing more IR transfer through the coatings faster.

Key words: Anatase, Rutile, TiO_2, P25, SiO_2, DMPA, functionalize, encapsulation, polyurethane, foam, coating, supercritical CO_2, Stöber process, photoactivity, nanofiber, nanotube, xerogel, transparent, spin coating, UV-shielding.

Dedication

To the people in my life who have always believed in me, seen me at my best and worst,

and always stood by me.

Acknowledgement

Table of Contents

VII

List of figures

List of tables

List of schemes

Abbreviations

BET	Brunauer–Emmett–Teller
C16TAC	Alkyltrimethylammonium bromide
DLS	Dynamic light scattering
DMPA	2,2-dimethylolpropionic acid
DMPA-TiO$_2$	DMPA functionalized titanium dioxide nanoparticles
DMPA-TiO$_2$(A)	DMPA functionalized anatase titanium dioxide
DMPA-P25	DMPA functionalized P25
EDX	Energy-dispersive x-ray spectroscopy
FTIR	Fourier Transform Infrared
IPDI	Isophorone diisocyanate
NF	Nanofiber
NPs	Nanoparticles
NT	Nanotube
nTiO$_2$	Titanium dioxide nanoparticles
PMDI	polymeric diphenylmethane diisocyanate
PU	polyurethane
scCO$_2$	Supercritical carbon dioxide
SEM	Scanning electron microscopy
SiO$_2$	Silica Dioxide
SiO$_2$-TiO$_2$	Silica dioxide encapsulated titanium dioxide

SiO_2-TiO_2(A)	Silica dioxide encapsulated anatase titanium dioxide
SiO_2-TiO_2(R)	Silica dioxide encapsulated rutile titanium dioxide
TEM	Transmission electron microscopy
TEOS	Tetraethoxysilane
TiO_2	Titanium Dioxide
TiO_2(A)	Anatse titanium dioxide
TiO_2(R)	Rutile titanium dioxide
TIP	Titanium isopropoxide
TGA	Thermo-Gravimetric Analysis
UV-Vis	Ultraviolet-visible
XRD	X-ray diffraction

Nomenclature

A_{100}	Area in this region of 100% transmittance
A_T	Area under the transmittance curve between 700 to 1400 cm^{-1}
k_W	Reaction rate constant (%/d)
K_s	Adsorption rate constant
r_W	Photodegradation reaction rate (%/d)
t	Reaction time (h)
W	Weight loss of polymer (%)
T	thermicity of coatings

Chapter 1. Introduction

1. Overview

Since the invention of polyurethanes in 1937, they have become one of the most versatile types of polymers in existence today. Polyurethanes have been increasingly used for a wide variety of applications due to their low cost, unique physical and mechanical properties, and long usage life [1-6]. In 2010, the global market for polyurethanes was estimated at 13.7 million tons, which was expected to reach 17.9 million tons by 2016. In terms of value, polyurethanes were estimated to be worth US$33 billion in 2010 and are expected to reach US$55 billion by 2016[7, 8].

As emerging applications for polyurethane's become more complex with longer lifetimes required, conventional products are limited by having only a polymeric component. However, nanotechnology provides a new approach for introducing metal oxide nanoparticles into a polymer matrix to create higher performance products, termed polymer nanocomposites. Compare to traditional fillers, polymer nanocomposites achieve similar property enhancements with 1-5% volume addition compared to conventional loadings of fillers requiring 15-40%[9]. More importantly, some unique properties are introduced to the nanocomposite such as increased resistance to oxidation and ablation. Some of these characteristics have been transformed into commercial success including automotive parts. Although the field of adding metal oxide nanoparticles especially TiO_2 into polyurethanes is with tremendous opportunity [10-13], it is relatively unexplored how to reduce the agglomeration of nano-TiO_2 in polyurethane while examining applications in photoactive properties. Several applications to be explored in this

thesis include photo-degrading foams incorporating DMPA-TiO_2 nanoparticles, high performance coatings with TiO_2-SiO_2 core-shell structure nanoparticles, nanotubes, and nanofibers, and UV shielding transparent coatings with nanofiber-shaped TiO_2 xerogel.

2. Objectives

Polymer nanocomposites generally suffer from a serious problem which is the agglomeration effect of the nanofillers, especially TiO_2 inside the polymer, which will have a negative impact on the photocatalytic activity [14-18]. Generally speaking, there are four methods for reducing the agglomeration effect of polymer nanocomposites, melt compounding such as extrusion [19, 20], film casting [21, 22], in situ polymerization [23, 24], and in situ particle generation [25, 26]. In this thesis, two methods, in situ polymerization and film casting, are mainly applied in order to reduce the agglomeration effect. DMPA functionalized TiO_2 nanoparticles are integrated in polyurethane foams via in situ polymerization to enhance the photodegradation of polyurethane foam. SiO_2 encapsulated TiO_2 nanoparticles, nanofibers, and naotubes are integrated in polyurethane coatings via in situ polymerization to enhance the photocatalytic activity and physical chemical properties as well. Nanofiber-shaped TiO_2 xerogel mixed with polyurethane coatings were prepared via film casting and in-situ polymerization to enhance the UV shielding property while remaining transparent.

3. Literature review

Metal oxides/polymer nanocomposites are attracting tremendous interest from scientists and engineers due to their unique and widespread applications in areas such as catalysts[27], antibacteria surfaces[28], to window coatings[29]. Here we are going to investigate two types of

nanoscale metal oxides in this dissertation: TiO_2, and SiO_2, and their performance when integrated within the versatile polymer, polyurethane.

3.1. Polyurethane

Polyurethane is a polymer in which organic units are conjugated with urethane linkages (– NH – C (= O) – O –) [30, 31]. They are traditionally formed by the reaction of polyisocyanate which provides isocyanate groups and polyol which provides hydroxyl groups.   Scheme 1.1 shows the generalized urethane reaction.

$$R^1\!-\!N\!=\!C\!=\!O \ + \ R^2\!-\!O\!-\!H \longrightarrow \underset{\displaystyle R^1\!-\!N\!-\!C\!-\!O\!-\!R^2}{\overset{\displaystyle H \quad\ O}{}}$$
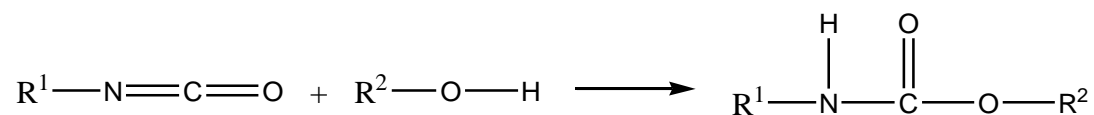
Scheme 1.1 The generalized urethane reaction.

There are generally two forms of polyurethane polymers, elastomers[32] and foams[33]. Polyurethane elastomers are synthesized following the general urethane reaction which takes place between two main raw materials, polyisocyanate and polyols. Polyisocyanates can be divided into two categories, aromatics such as polymeric diphenylmethane diisocyanate (MDI) and aliphatic such as polymeric hexane diisocyanate (HDI). Polyols generally include polyether polyols and polyester polyols. Recently, there are new environmentally friendly polyols developed which are vegetable oil contains hydroxyl group [34-36]. The urethane reaction usually requires extra conditions such as heat or UV irradiation[37, 38]. However, with the addition of certain catalysts such as tertiary amines, the reaction can proceed under ambient condition as Scheme 1.2 shows[39, 40].
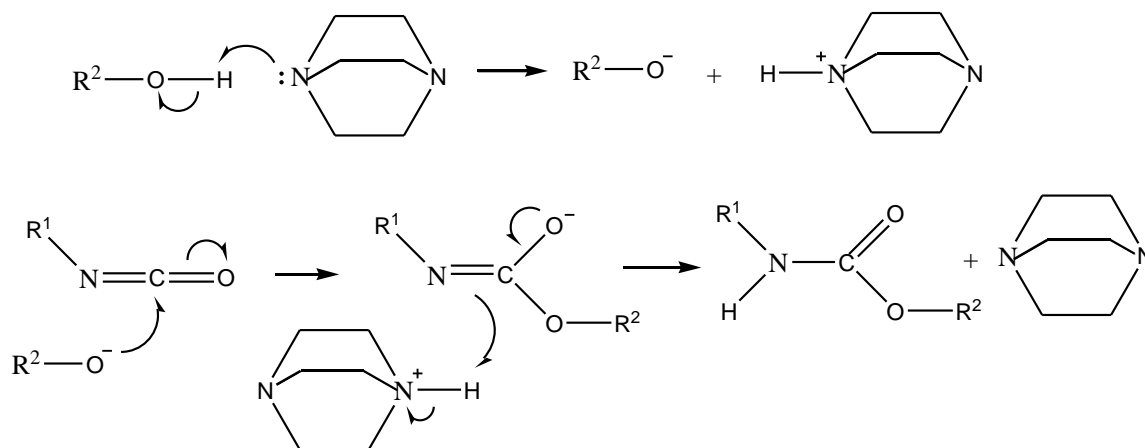
Scheme 1.2. Polyurethane reaction mechanism catalyzed by tertiary amine.

In order to synthesize polyurethane foams, additional reactive agents are required since a foaming process is involved in the reaction. Therefore, other than polyisocyanates, polyols, and catalyst, blowing agents and surfactants are also necessary [41]. During the foaming process, a blowing agent is essential because gas generation which causes bubbles depends on it. The most common blowing agent is water, which will react with isocyanate groups, producing carbon dioxide (Scheme 1.3). Surfactants which are formed by polydimethylsiloxane (PDMS) backbone and polyethylene oxide-co-propylene oxide (PEO-PPO) random copolymer grafts are necessary in the foaming process as well. They will have a significant effect on the bubble size and cell windows. Without these agents, the foaming system will experience catastrophic coalescence and eventually cause foam collapse [42-44].

n HO—R^1—OH + (n+1) OCN—R^2—NCO

$\longrightarrow$ OCN—$\big[$polyuretahne prepolymer$\big]_n$— NCO

nH$_2$O + n OCN—$\big[$polyuretahne prepolymer$\big]_n$— NCO

$\longrightarrow$ $\Big(\!-\big[$polyuretahne prepolymer$\big]_n$— NHCONH —$\Big)_n$ + CO$_2\uparrow$
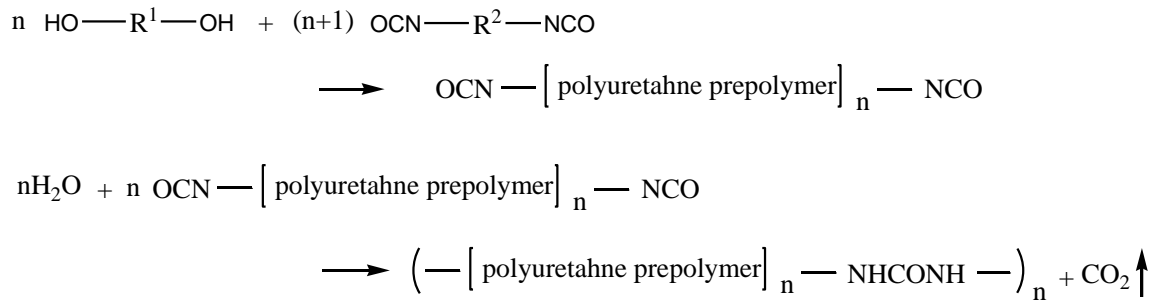
Scheme 1.3. Polyurethane foam reaction model.

In order to improve the physical and chemical properties of polyurethanes for various applications, polyurethane nanocomposites have been investigated. Kim, Hyunwoo, et al. produced the graphene/polyurethane nanocomposites successfully, improving their electrical conductivity [45]. Jain, Prashant, et al. formed a polyurethane nanocomposite with silver nanoparticles to make an antibacterial water filter[46]. Guo, Zhanhu, et al. introduced silicon carbide nanoparticles into polyurethane and enhanced the thermal stability and mechanical strength of the material[47].

Another important factor regarding polyurethane is their degradation due to their long usage life and long decomposition time after disposal. There are two main decomposition methods for polyurethane, thermal decomposition [48-50] and chemical decomposition [51-53]. However, they are both not environmental friendly due to the release of toxic agents [54, 55]. Some studies have indicated that under UV irradiation, polyurethanes are prone to photodegradation [56, 57]. Therefore, photocatalysts such as TiO$_2$ can be introduced into the polyurethane structure in order to improve its photodegradation ability. In this thesis, we are going to investigate the effect of several nanostructures on polyurethane foams and coatings.

3.2. Metal Oxides

Metal oxides nanosturctures are attracting tremendous interest from scientists and engineers due to their unique chemical and physical properties such as optical conductivity [58-60], ionic or mixed ionic/electronic conductivity [61, 62], yield strength and hardness [63, 64], and catalytic activity [65-67], which make them suitable for the applications in various fields like solar cells [68, 69], biosensors [70, 71], bone cements [72, 73], and catalysts [74-76]. Generally, metal oxides nanostructures includes aluminum oxides [77, 78], zirconium oxides [79], titanium oxides [80, 81], and other oxides such as zinc oxides [82, 83] and silica oxides [84, 85]. In this thesis, TiO_2 and SiO_2 will be investigated.

3.2.1   Titanium Dioxide

Titanium dioxide (TiO_2) is the naturally occurring oxide of titanium, which has a wide range of applications from paints to sunscreens [86-88]. Generally it consists of two different crystal structures, anatase and rutile (Figure 1.1). While rutile exhibits a band gap which is about 3.0 eV, anatase has a higher band gap which is about 3.2 eV (Figure 1.1). This difference in band gap would imply that rutile can be excited by irradiation at longer wavelengths at 413 nm compared to anatase which is 388 nm. However, anatase generally exhibits superior photocatalytic activity to rutile as a result of a significantly higher surface area which leads to higher levels of adsorbed radicals[89].
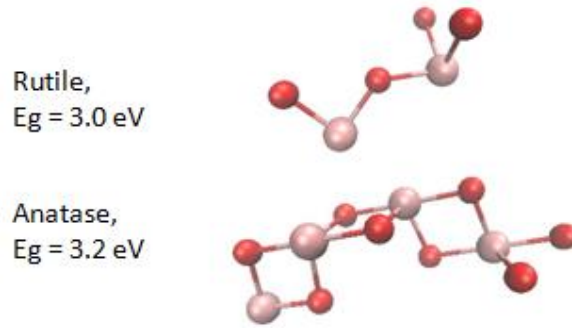
Figure 1.1. Structure and band gap energy of Rutile and Anatase TiO_2.

As shown by Xu Dong Chen et al[90], anatase TiO_2 nanoparticles will increase the photodegradation ability of polymers like polyurethane, while rutile TiO_2 nanoparticles will stabilize the polymer performance under sunlight. They investigated the photooxidation mechanism of PU which was found to proceed via oxidation on carbon atoms in the α position of urethane N–H groups. TiO_2 molecules generate various active oxygen species such as $O_2^{\bullet-}$, $HOO^{\bullet}$ and $HO^{\bullet}$ under UV irradiation. These species will attack neighboring polymer chains to absorb a hydrogen atom to form carbon-centered radicals. Finally, hydroxyl derivatives and carbonyl intermediates will be produced, leading to chain cleavage. However, how the nanoparticle size and morphology will affect the photodegradation ability of nanoTiO$_2$ is still not clear, requiring further investigation. Nano TiO_2 has a high light absorption which is mainly attributed to direct interband electronic transitions[27]. After TiO_2 nanoparticles absorb light and photons with energies equal to or higher than its band gap energy, electrons are excited from the valence band into the unoccupied conduction band. This leads to excited electrons in the conduction band and positive holes in the valence band. These charge carriers can recombine, or become trapped and react with electron donors or acceptors adsorbed on the surface of the

photocatalyst. The competition between these processes determines the overall efficiency for various applications of TiO_2 nanoparticles[27].

When nanoTiO$_2$ is irradiated by a light source which exceeds the band gap, electron-hole pairs are generated so that electrons enter the conduction band, while holes remain in the valence band. These electron-hole pairs facilitate redox reactions through the formation of adsorbed radicals on the nanoTiO$_2$ surface. The photocatalytic activity of nanoTiO$_2$ depends on the relative rates of generation and recombination of electron-hole pairs as well as the levels of adsorbed radical-forming species on the nanoTiO$_2$ surface. The research on photodecomposition of water and photooxidation of organics has provided some evidence into the mechanism. From Kesselman's study, when the photooxidation of $CHCl_3$ by oxygen is conducted in aqueous solution using 30 nm TiO_2 particles, the interfacial charge transfer rather than electron-hole generation is the rate-limiting step for the overall photodegradation process[91]. Another study also investigated the photodegradation of organic pollutants on rutile TiO_2 surface[92], which clearly demonstrated that substrate-mediated photoactivation of adsorbed oxygen is the key step in the photocatalytic oxidation of methyl chloride on TiO_2.

TiO_2 nanoparticles have a strong tendency to agglomerate [93-95] which will affect their specific surface area and therefore their photocatalytic activity. Many studies have been performed to avoid or minimize the agglomeration effect including transforming titania's shape into nanotubes or nanofibers [96, 97], shaped-controlled method [98], or modify their surface with various ligands[99, 100]. In this study, SiO_2 is encapsulated onto the surface of TiO_2 nanoparticles in order to reduce the agglomeration effect, which will form a structure of silica

aerogel whose pores will be filled by nanoparticles. It is expected that these structures will possess properties of silica aerogel without losing photoactivity.

TiO$_2$ nanotubes and nanofibers are one-dimensional (1D) nanostructure which provide higher specific surface areas and high mechanical strength[96, 101]. They have attracted much attention due to their photocatalytic property in specific crystal structure, anatase and rutile[102-104]. These so-called 1D materials have been used in many fields such as photocatalysis[105-107], solar cells[108, 109], electrochromic devices[110], biomedical coatings[111-113], drug delivery[114-116] and so on. Many methods have been developed to synthesize TiO$_2$ nanotubes and nanofibers.

Generally, there are three common methods to synthesize TiO$_2$ nanotubes; these include template preparation[117, 118], anodic oxidation[119], and chemical processing[120]. In the template preparation method, the size and morphology of the nanotubes mainly depend on the template, and nanotubes are hard to maintain their shape when separated from the template. Anodic oxidation is able to synthesize even-sized nanotubes but with relatively larger diameters. Chemical processing is the first and classic method of preparing nanotubes with the smallest size. However, different hydrothermal conditions are known to affect the mesoporous structure of the nanotubes[121].

In the chemical processing method, a single layer of TiO$_2$ nanosheets is removed by the effect of strong base solution, helping to form unsaturated bonds on both sides of the nanosheet. During the reaction, more unsaturated bonds are formed and the surface becomes more active. At a certain point, the nanosheet begins to curve in order to reduce the system energy, and forms a

tube at the end [121]. During the processing, the nanotubes tend to conjugated into a cluster, which can be reduced by increasing the ratio of TiO_2 nanocrystal and the volume of NaOH solution[121].

TiO_2 nanofibers are commonly prepared via hydrothermal methods[122], electrospinning [123, 124], and the sol-gel method[97, 125]. Recently, an environment friendly method, supercritical CO_2 has been used to synthesize TiO_2 nanofibers[97]. This is a sol-gel method which replaces the solvent with CO_2 in critical conditions. Supercritical CO_2 is a fluid state of carbon dioxide where it is held above its critical temperature and critical pressure. This methodology has attracted considerable attention in recent years due to its lack of solvent residue, inexpensive, nontoxic, and negligible surface tension, which make it an ideal approach not only for chemical extraction but also for nanomaterial synthesis [97, 126, 127].

During the supercritical CO_2 synthesis of TiO_2 nanofibers, different amounts of titanium isopropoxide (TIP) and acetic acid are added into the autoclave reactor. The reaction takes place in an experimental system, such as that shown in Figure 1.2. For example, it was previously shown at 60℃ and 6000 psi, with 6.1 mol/L acetic acid, 1.5 mol/L results in 10nm diameter nanofiber and 1.1 mol/L results in 40 nm diameter nanofiber[97].
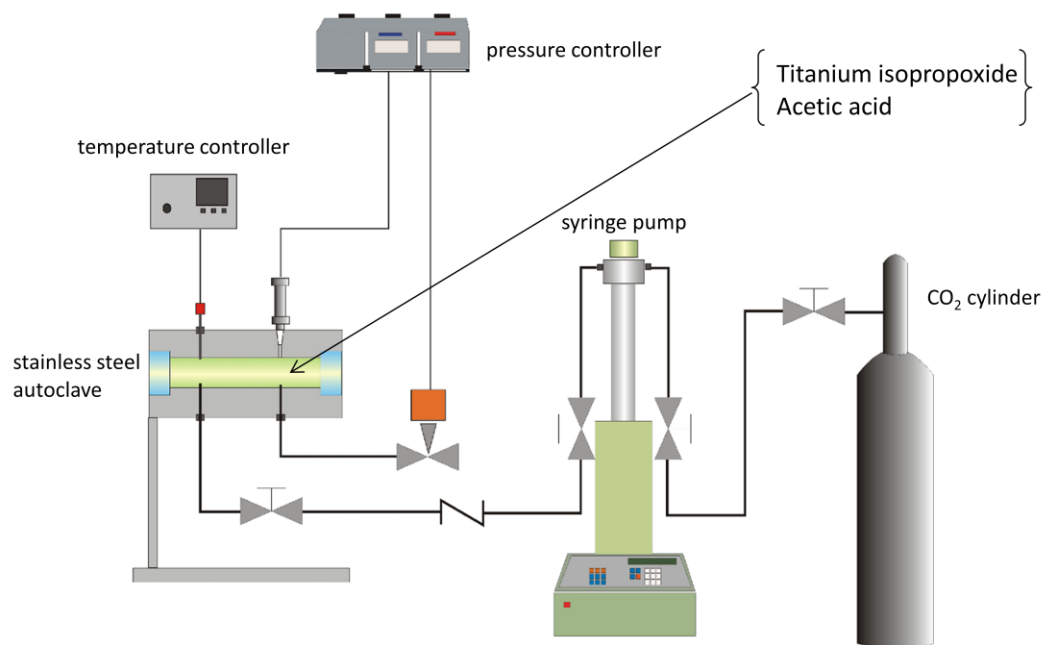
Figure 1.2. The demonstration of synthesis of TiO_2 nanofiber via supercritical CO_2.

Some studies regarding the modification of TiO_2 nanotubes and nanofibers are performed in order to improve the physical chemical property and expand the application field. The modification methods include doping with other elements such as N, C, Fe [128-130], and depositing with other metal oxides [131-133]. However, there is lack of the study of SiO_2 effect on nanotubes and nanofibers, which will be investigated in this study.

TiO_2 xerogels are of considerable interest in the metal oxide xerogel field. Due to the unique photoactivity from two different phases: anatase and rutile, high photocatalytic activity is provided [134] while other applications such as dye sensitized solar cells[135] and biosensor[136] have been reported. Other metal oxides such as SiO_2[137, 138] and V_2O_5[139, 140] are also involved in the sol-gel process and can form combined metal oxides xerogels. The conventional method to synthesize TiO_2 xerogels or modified TiO_2 xerogels is the sol-gel proces, with a typical procedure reacting titanium isopropoxide and acetic acid in methanol [141]. According to

many studies, the titanium isopropoxide and acetic acid will form a bidentate coordination [142, 143].

In this study, an environmental friendly approach using Supercritical CO_2 has been applied for the synthesis of TiO_2 xerogel. Using this technique, titanium isopropoxide and acetic acid are dissolved in supercritical CO_2 solution, then reacted in an autoclave to form TiO_2 xerogel. The as -prepared xerogel will be able to dissolve in solvent with a similar polarity of acetic acid, such as methanol or ethanol. In this case, due to the UV absorbance property of TiO_2 nanostructure[144], transparent window coatings with high UV absorbance can potentially be prepared.

A similar study has been carried out to prepare transparent polyurethane/titanium hybrid films [145]. The process includes preparing titanium sol-gel with titanium n-butoxide and water, mixing polyester and titanium sol-gel to get resin, then synthesizing a film with polymer/titanium hybrid resin and isophorone diisocyanate. The formed film presents high UV shielding properties while maintaining transparency in the visible region. However, this process involves several defects which in this study will be overcome such as synthesis complexity, and environment unfriendly solvents.

3.2.2   Silica Dioxide

Silica dioxide (SiO_2) nanoparticels are generally synthesized through the Stöber process[146, 147], which is a classic physical chemistry process for the generation of monodispersed silica particles[148]. This process involves excess of water, low molar-mass alcohol, and ammonia. The classic Stöber process is able to encapsulate silica onto the surface of other metal oxides as shown in Scheme 1.4 [146].   As the mechanism shows, hydroxyl groupd appear on the sphere

surface [149], which makes *in situ* polymerization possible since the hydroxyl groups react with

isocyanate groups during the polyurethane synthesis.

$$Si(OC_2H_5)_4 + 4H_2O \underset{\text{Esterification}}{\overset{\text{Hydrolysis}}{\rightleftharpoons}} Si(OH)_4 + 4C_2H_5OH$$

$$Si(OH)_4 + (OH)Si\!\!\equiv \overset{\text{Condensation}}{\longrightarrow} \equiv\!\!Si-O-Si\!\!\equiv$$

$$Si(OH)_4 + (OH)Me\!\!\equiv \overset{\text{Condensation}}{\longrightarrow} \equiv\!\!Si-O-Me\!\!\equiv$$
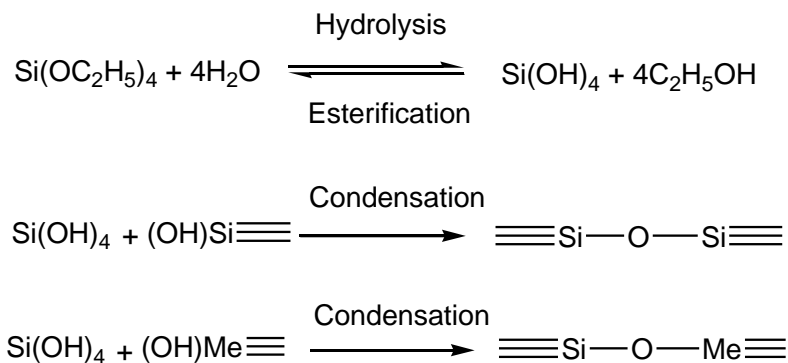
Scheme 1.4. The mechanism of modified Stöber process for silica encapsulation on metal oxide.

As a previous study has shown, the silica encapsulated metal oxide possesses a similar

structure as silica aerogel, in which the void space is replaced with metal oxide crystals [150].

Therefore, it might possess properties of silica aerogel such as thermal conductivity [151, 152]

which would lower the thermal conductivity of polymer nanocomposites, and high optical

transparency [152, 153] which would help preserve the photoavtivity of both nanoparticles and

nanocomposites.

Thermal conductivity of silica aerogels is lower than air due to its high porosity and

nanometer pore size. Silica aerogels have a very small fraction of solid silica, so it has lower

solid conductivity and transmits lower thermal energy[154]. However, since the pores of silica

aerogel are open, allowing gas to diffuse through, gases are able to transfer thermal energy to the

solid matrix. Moreover, infrared radiation is able to transfer thermal energy as well, but this is

lower when the temperature is low, and it would dominant the thermal conduction when the temperature is high.

Optical transparency is another important property of silica aerogels. This property is quite unusual for a porous material. The reason is that the aerogel microstructure is small enough compared to the wavelength of light. Transparency happens because there is a small amount of scattering in the visible region, and the scattered light has a relatively isotropic angular distribution and exhibits little multiple scattering[155].

The Stöber process has been modified in many studies to coat SiO_2 onto the surface of P25 [156, 157]. In these studies, different molar ratios of TEOS to TiO_2 from 0:1 to 6:4 or different amounts of surfactant were studied. Observable SiO_2 layers are on the surface of P25 through HR-TEM images and they were analyzed to be amorphous SiO_2. It was also found that the photocatalytic activity of the hybrid nanoparticles is driven by the adsorption rate. The main problem here is that the silica layers on the surface is not thin enough to allow free radicals generated by electron-hole pairs to reach the surface and contact with pollutants, which is why the photocatalytic activity is adsorption-driven.

A separate study applied the Stöber process to coat TiO_2 onto the surface of SiO_2 in order to obtain high-efficiency solar cells, due to the optical transparency of the SiO_2 core and the light scattering inside the TiO_2 shell [158]. In this process, TIP was used in the solution to carry out the hydrolysis and condensation reactions on the surface of SiO_2 nanoparticles. As a result, the prepared SiO_2-TiO_2 core-shell nanostructures successfully improved the solar cell energy conversion efficiency due to the introduced light scattering function. It helps to consider that

with SiO_2 layers coated, light scattering could happen as well.

Instead of the Stöber process, the sol-gel method has been used for preparation of SiO_2-TiO_2 nanostrcutures as well [159-161]. In this method, TiO_2 and SiO_2 are synthesized from precursors during one step together or two steps to form a mixture of TiO_2 and SiO_2, where there might not be a chemical linkage between these two oxides. Some results have shown that SiO_2 inside the mixture would help increase the thermal stability and allow a higher calcination temperature leading to a higher rate of anatase phase. This will suppress the TiO_2 crystal growth leading to higher surface area material, which will enhance the photocatalytic activity [160]. Another interesting study prepared a rattle-type SiO_2-TiO_2 nanoparticles via the sol-gel process [159]. This technique created a void space by applying polymer inside the process. The polymer was adsorbed onto the surface of TiO_2 nanoparticels followed by the SiO_2 coatings through precursor TEOS. The polymer layers in-between were then degraded through UV irradiation and therefore created a void space between TiO_2 core and the SiO_2 shell. As a result, these rattle-type nanoparticles show a higher photocatalytic activity; meanwhile they possess high UV-shielding performance without decomposition of the supporting organic materials. However, a disadvantage of sol-gel method could not be neglected is the environmental unfriendly and the chemical residuals.

3.3 Polyurethane nanocomposites

Polyurethane nanocomposites are nanofiller modified polyurethane in order to introduce new properties or enhance the existing properties for various applications. One of the most interesting applications developed in recent years is the shape-memory effect of polyurethane

nanocomposites [162-164]. There are two types of shape-memory polyurethane nanocomposites, thermal trigger and electric trigger. The thermal trigger nanocomposites are usually formed with silica related nanostructure [165, 166], while the electric trigger ones usually contains carbon nanotubes or graphene [167, 168]. With carbon nanotubes or graphene as the nanofiller, the electrical conductivity would be enhanced in polyurethane nanocomposites [169, 170], which is due to the electrical conductivity of these nanofillers when added above the percolation threshold.

With metal oxides used as the nanofiller in polyurethanes, the nanocomposites would exhibit enhanced optical and thermal properties for UV absorbance [171], photocatalytic activity [172], thermal stability as a flame retardant [173, 174], and thermal insulation from heat transfer or IR irradiation [175, 176]. SiO_2 related nanostructures generally introduce enhanced thermal behavior into the polyurethane nanocomposites [177], while the photoactivity and UV related property of nanocomposites are from the photocatalyst metal oxides such as TiO_2 [178]. The photocatalytic activity of polyurethane nanocomposites has been applied in the medical field for enhanced antibacterial activities [179, 180]. Polyurethane nanocomposites have been used in other medical applications such as bone cements with hydroxyapatite [181], and biocompatibility enhancement with carbon nanotubes [182].

Generally, there are three methods for preparing polyurethane nanocomposites, i.e. blending [183], the sol-gel method [184, 185], and *in-situ* polymerization [186, 187]. Blending is a method that mixes the prepared nanofillers inside the uncured polyurethane mixture or melted thermoplastic polyurethane to form nanocomposites. However, since the polyurethane usually is

cured quite fast and most of them are thermosetting, it is not widely used. The sol-gel method method dissolves the nanofiller precursor in organic solvent and mixes with polyurethane precursors. Then the mixture goes through the sol-gel process and forms the polyurethane nanocomposites. During this process, the nanofiller precursors would produce hydroxyl groups which can react with isocyanate groups, thus creating chemical linkages between the nanofiller and the polyurethane structure. In *in-situ* polymerization, nanofillers are mixed with polyurethane precursor part A which usually be polyol or polyester, and then the precursor part B usually be polyisocyanate is added to the solution, foring the polyurethane nanocomposite.

In order to have chemical connection and better distribution within the polyurethane structure, nanofillers would generally be modified with functionalized groups [188, 189]. One previous study used DMPA to functionalize the TiO_2 nanoparticles and synthesize the nano-TiO_2/polyurethane composites for antibacterial and self-cleaning coatings [190]. With bidentate coordination, one DMPA molecule would provide two hydroxyl groups which could have reaction with isocyanate groups and create chemical linkage between nano-TiO_2 and the polyurethane structure. As a result, nano-TiO_2 was well distributed in the polyurethane nanocomposites and no significant agglomeration was observed.

Nano-TiO_2/polyurethane nanocomposites commonly possess antibacterial and self-cleaning properties, which provide many new potential applications in the medical and coating fields. However, its property is limited by the agglomeration effect of TiO_2 nanostructures. Surface fictionalization with organic groups like DMPA as described above to form functional monomers would be a potential solution to reduce agglomeration. The direct sol-gel method could also

solve the agglomeration problem according to a previous study [145]. In this study, titania sol

was mixed with monomers to form a polyester/titania resin, and then reacted with IPDI to

produce polyurethane/titania nanocomposites, which appears to be transparent films with

enhanced UV shielding.

In this thesis, in order to study the reducing agglomeration of TiO_2 nanostructures in

polyurethane nanocomposites, *in-situ* polymerization was used as the primary method with

DMPA functionalized and SiO_2 encapsulated TiO_2. Another method called film casting is applied

for the TiO_2 xerogel since it would dissolve in methanol solution which gives a better

distribution and provide transparency to the polyurethane nanocomposites.

Chapter 2. "Grafting From" Approach to the Synthesis of Photo-degrading Polyurethane Foams utilizing 2,2-Dimethylolpropionic Acid Functionalized Nano-TiO$_2$

Abstract: Waste polyurethane foams are becoming a serious environmental issue due to their low degradation rates upon environmental exposure. In order to accelerate foam degradation, this work examined a "grafting-from" method in which polyurethane (PU) chains were grown directly from functionalized TiO$_2$ nanoparticle surfaces. Both anatase and P25 TiO$_2$ nanoparticles were reached with 2,2-dimethylolpropionic acid (DMPA) to produce functionalized monomers, which were subsequently used for PU foaming in a "grafting-from" polymerization approach. The photodegradation rate and degradation mechanism of synthesized PU foams was examined by exposure of foams to a UV weathering chamber from 0-250 hrs with timed water spraying. The results show that anatase TiO$_2$ nanoparticles promote an increase in the degradation rate of polyurethane foams 120% over unmodified foam at an optimized loading of 3wt% DMPA-TiO$_2$(A). The presence of DMPA functionalized P25 nanoparticles produced an increase in the degradation rate of 66% over the unmodified foam at an optimized 1wt% loading. The results of this study suggest the potential for enhancing the degradation of polyurethane foams using a nano-TiO$_2$ functional monomer approach.

Keywords: Polyurethane, DMPA, Titanium Dioxide, Photodegradation

1. Introduction

Polyurethane (PU) foams are frequently used to produce durable goods for many everyday applications and industrial uses.[41] As such they enter the municipal solid waste stream by way of discarded consumer and industrial products. One major problem is that due to the irreversible cross-linking that occurs during the thermosetting process, commercial PU foams are not susceptible to facile degradation. On the other hand, PU recycling programs are currently limited to recycling clean scrap material from specific manufacturing processes, which are shredded and processed for use in various applications such as carpet underlay[191]. While a small number of chemical recycling processes do exist, they are extremely limited by high cost, the quality of material required for recycle, and the current lack of infrastructure. Hence, the possibility for enhanced degradation of PU's is of tremendous current interest.[192-194]

Previous studies have examined the impact of UV irradiation on aromatic PU foams during UV exposure which have described the degradation process and yellowing of the foam. [56, 195, 196] Nano titanium dioxide (nTiO$_2$) has been shown to enhance the photodegradation of PU [90]. However, simple mixing approaches for integrating TiO$_2$ nanoparticles into polymers suffer from particle agglomeration, providing a limited enhancement in the degradation rate. One possible solution is "grafting-from" polymerization in which polymer chains are grown from a nanoparticle surface, providing steric stabilization and better access to the TiO$_2$ photocatalytic active sites. For instance, TiO$_2$ nanoparticles can be attached to a polyurethane matrix through NH$_2$ or OH functional groups.[197, 198] However, it remains unexplored how this "grafting-from" approach will affect the photocatalytic activity of TiO$_2$ and the mode of

photodegradation behavior.

In this study, 2,2-dimethylolpropionic acid (DMPA)-functionalized nano-TiO$_2$ molecules containing two hydroxyl groups were used to react with poly hexane diisocyanate (PMDI), providing a direct connection during nanocomposite formation (see scheme 1). It was anticipated that the agglomeration using this approach would be decreased and that the TiO$_2$ nanoparticles chemically linked to the polyurethane structure would provide superior photocatalytic sites. By utilizing the photocatalytic properties of nano-TiO$_2$ (anatase or P25),[199-201] the decomposition rate of the polyurethane foam can be potentially enhanced when exposed to sunlight.

2. Materials and Experiments

2.1 Materials. Polyols (Insulthane 200 part A) and PMDI (Insulthane 200 part B) were obtained from Line-X Coatings (Brantford, ON). 2,2-Dimethylolpropionic acid (DMPA) and anatase Titanium (IV) oxide nanopowder (TiO$_2$) with an average particle size less than 25 nm and P25 with an average particle size of 21 nm were purchased from Sigma-Aldrich (Mississauga, ON). All chemicals were used as received except DMPA which was heated under vacuum at 100ºC to remove any absorbed moisture.

2.2 Synthesis Procedure. The synthesis of DMPA-TiO$_2$ and P25 follows a procedure previously described[198]. The coordination reaction occurs between the surface of DMPA and TiO$_2$ (Scheme 1). The polyurethane foam was prepared by direct mixing of commercial product PMDI and polyols with six samples of each type of nanoparticle prepared.   Each sample was generated

using 10g of polyol (Insulthane 200 part A) and 10g of PMDI (Insulthane 200 part B), and different amounts of DMPA-TiO$_2$ (anatase, P25), i.e.: 0.0g, 0.2g, 0.4g, 0.6g, 0.8g, and 1.0g (0%, 1%, 2%, 3%, 4%, 5% by weight). The procedure is as follows: 10 g of PMDI was placed into a 150 ml polyethylene beaker, then mixed with DMPA-TiO$_2$ of different weights: 0.0g, 0.2g, 0.4g, 0.6g, 0.8g, and 1.0g, under constant magnetic stirring at 600 rpm for 3 min at room temperature in order to reach a homogeneous solution. Then, 10 g of polyol was added with constant magnetic stirring at 600 rpm for 1 min to perform the foaming process. After that, the prepared PU/nTiO$_2$ foams were cured at room temperature for 24 hours.

2.3 Characterization. The photoactivity of the as-prepared DMPA-TiO$_2$ was tested in 1ppm methylene blue solution under UV irradiation in a light simulator (Luzchen ICH1) with a light intensity of 0.635 W/m^2. The methylene blue concentration was measured after 5, 10, 15, 20, 30, 40, and 60 minutes. Brunauer–Emmett–Teller (BET) surface area data was obtained using a Micromeritics Tri Star II 3020 instrument at 77 K. Prior to the N$_2$ physisorption, the samples were degassed at 100℃ at reduced air pressure for 5 hours. Fourier Transform Infrared (FTIR) spectroscopy was used to identify the functional groups of the prepared nanoparticles and polyurethane foams. FTIR analysis was performed using a NICOLET 6700 spectrometer which provided spectra in the range of 400-4000cm^{-1} and was operated using 32 scans at 4cm^{-1} resolution for each sample. Thermo-Gravimetric Analysis (TGA) analysis was performed to characterize the prepared nanoparticles and polyurethane foams using a TA Instruments® Q-series SDT Q600 analyzer. Data were analyzed using TA Instruments® Universal Analysis 2000 software. The aforementioned analyzer provided mass loss data over the temperature range

of 25-800℃ at a constant heating rate of 20℃/min in air. The photodegradation weight loss of

PU/nTiO$_2$ foams were tested in a weathering chamber (Q-Sun Xenon Test Chamber) for 250

hours. The test specimens had dimensions of 20 mm×10 mm×0.5 mm. The irradiation utilized

was 0.55 w/m^2 which is equivalent to four noon summer sunlight. The temperature in the

chamber was 65°C with each cycle consisting of: 18 minutes irradiation plus water spray

followed by 1 hour 42 minutes irradiation. Scanning electron microscopy (SEM) was performed

for the experimental nanocomposite thin foam slices before and after weathering using a

LEO(Zeiss) 1540XB scanning electron microscope after each sample was osmium sputtered

using an Edwards Auto500 unit. Osmium was deposited at 15 mA/min for 90 seconds to achieve

a 5-7 nm osmium layer. All observations were made at 3 kV and varying magnifications.

3. Results and Discussion

3.1 Polyurethane Foam Synthesis With DMPA-TiO$_2$(A) and DMPA-P25.

As shown in Scheme 1, the nanoTiO$_2$ (anatase or P25) was treated with DMPA in

isopropanol to make a functional monomer-i.e. nTIO$_2$-DMPA (see Scheme 2.1).
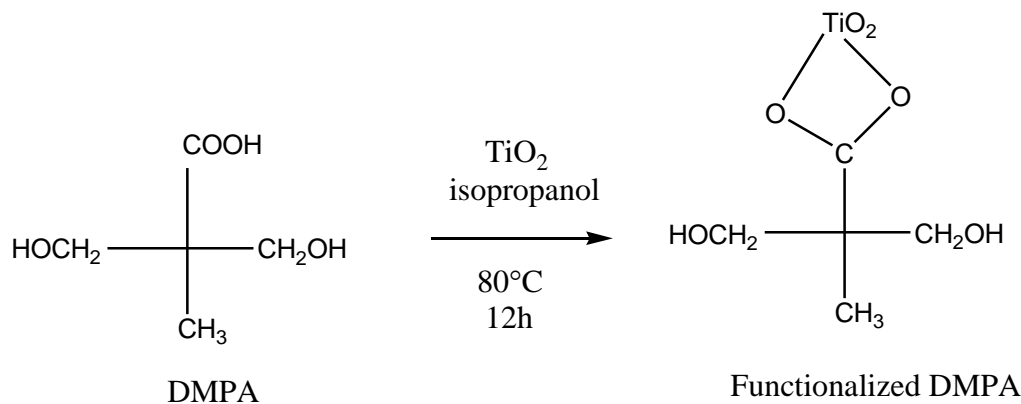
Scheme 2.1. Coordination of DMPA to the surface of nTiO$_2$.

Functional group changes accompanying the coordination of DMPA with anatase TiO_2 can be observed using FTIR spectroscopy (Figure 2.1). The hydroxyl group absorption at 3352 cm^{-1} from DMPA was broadened during nanocomposite formation. The absorption for a carboxylic acid group at 1683 cm^{-1} disappeared from the DMPA spectrum after functionalization, indicating no unreacted DMPA remained. There are no significant absorptions in the spectrum for anatase TiO_2 between 1400-1600 cm^{-1}. However, in the spectrum of functionalized TiO_2, there are three absorptions at 1558, 1471, and 1417 cm^{-1} which correspond to the presence of bidentate coordination interactions between titanium atoms and the carboxylic groups of DMPA (see inset). The identity of these absoptions has been confirmed by other studies.[202, 203]
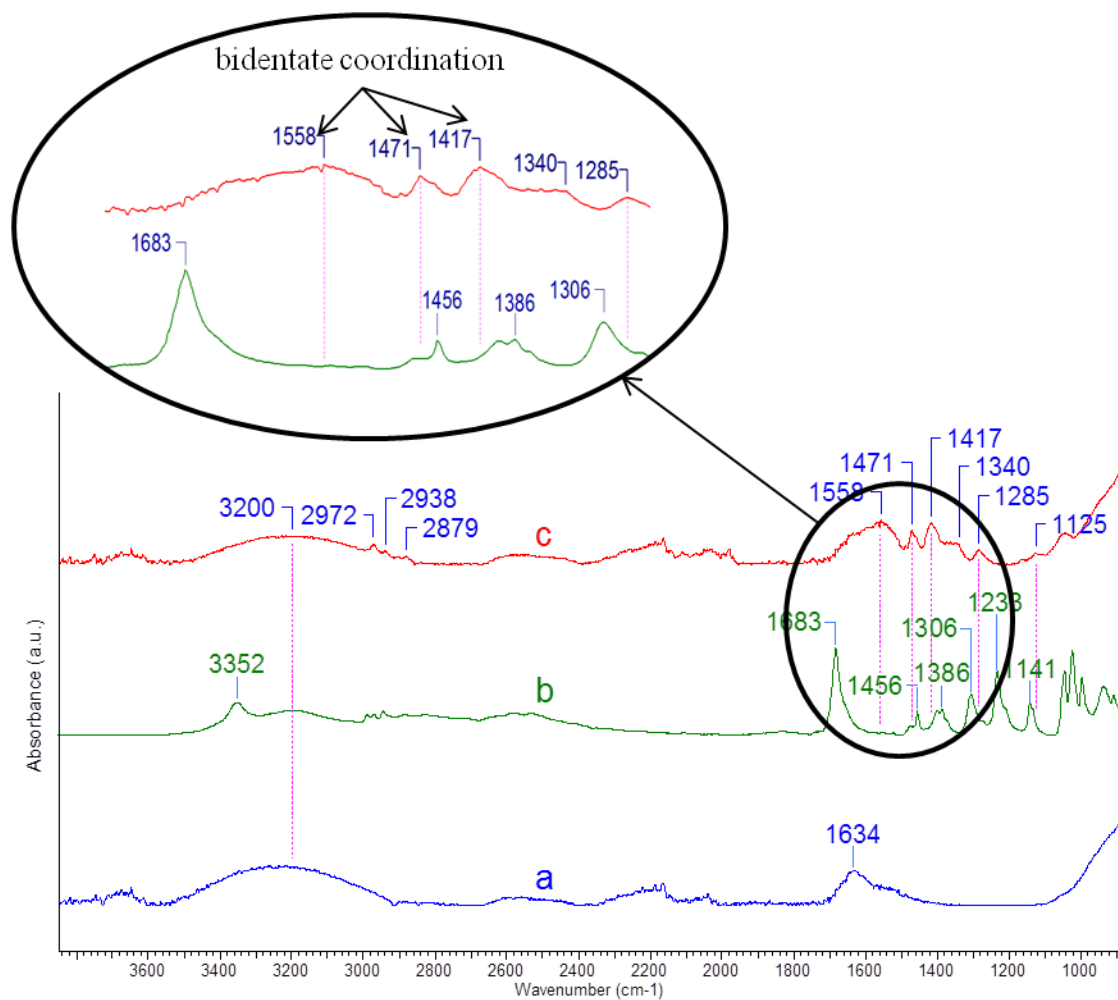
Figure 2.1. A comparison of FTIR spectra of (a) Anatase TiO$_2$, (b) DMPA, and (c) DMPA functionalized TiO$_2$(A).

From this functionalized DMPA monomer, polyurethane foams were synthesized through a "grafting-from" polymerization approach as shown in Scheme 2.2. In this methodology, the polyurethane chains were grown from the surface of the TiO$_2$ nanoparticles, which become embedded within the foam structure during the foaming process. Polyurethane foams containing both TiO$_2$ and DMPA-TiO$_2$ were prepared with the level of TiO$_2$ the same for both samples.
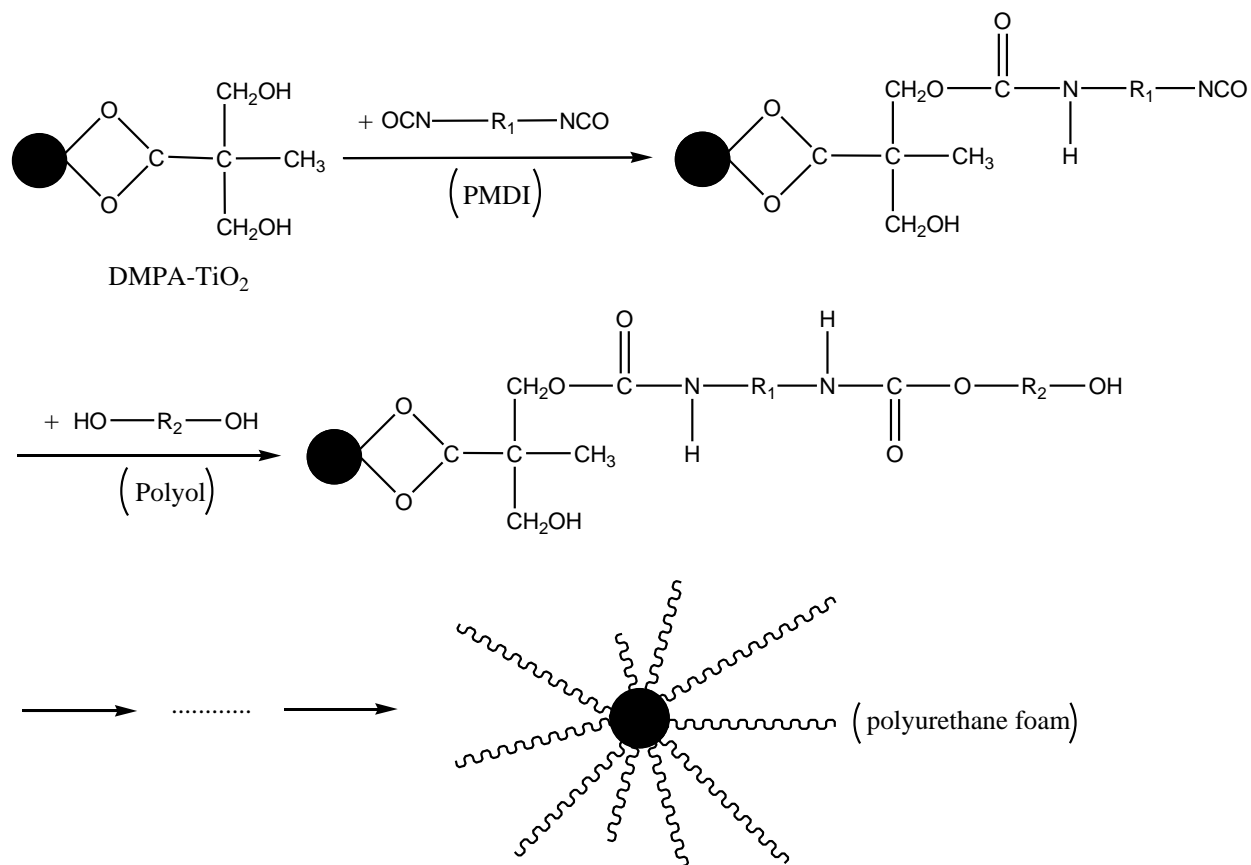
Scheme 2.2. "Grafting-from" approach for the preparation of functionalized polyurethane foam.

The SEM micrographs of polyurethane foams made by simple blending of nTiO$_2$ with those made using the "grafting-from" approach are compared in Figure 2.2. It is clear that the "grafting from" approach using DMPA-TiO$_2$ provides a better dispersion of nanoparticles than those made by simple blending of nTiO$_2$ into the foam.
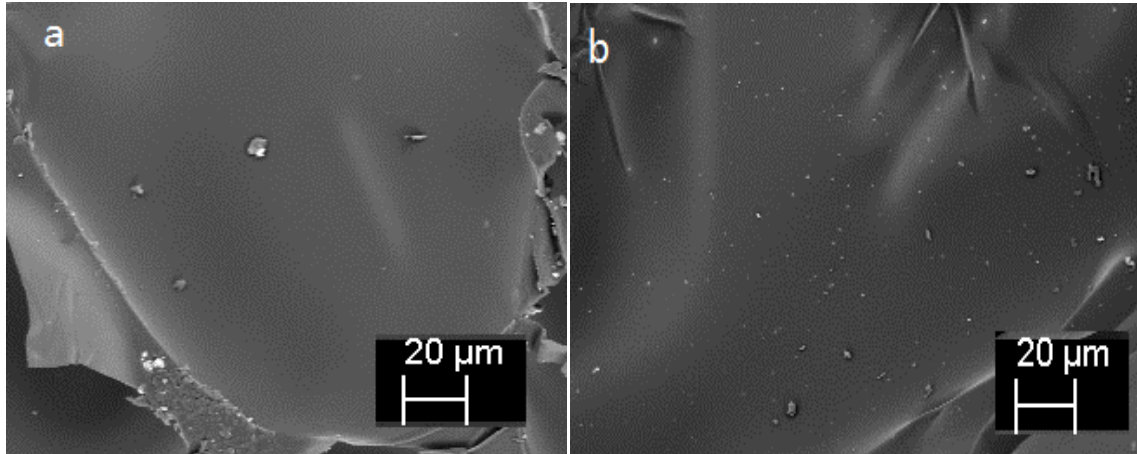
Figure 2.2. SEM images of TiO_2(A) and DMPA-TiO_2(A) in PU foams. (a): TiO_2(A)/PU composites.(b): DMPA-TiO_2(A)/PU composites.

3.2 Polyurethane Foam Degradation Kinetics.

Langmuir-Hinshelwood kinetics is a widely used approach for modeling heterogeneous photocatalytic reaction processes[204]. In order to apply the Langmuir-Hinshelwood kinetics, some assumptions need to be made.

(1) Hydroxyl radicals are formed uniformly and immediately upon irradiation.

(2) Photodegradation happens uniformly on the catalyst surface.

(3) The concentration of reactants C will be replaced by weight loss percent W due to the solid form of reactants.

(4) As catalyst is integrated within reactant, the adsorption rate constant K_s will be considered as infinite.

(5) The surface decomposition step is the rate controlling step.

Based on these assumptions, the Langmuir-Hinshelwood kinetics applied in this study is written

as:

$$r_W = \frac{dW}{dt} = \frac{k_W K_s W}{1 + K_s W} \qquad (9)$$

where r_W is the photodegradation reaction rate, W is the weight loss of polymer in terms of %,

t is the reaction time in terms of hour, k_W is the reaction rate constant and K_s is the adsorption

rate constant. Equation (9) can be rewritten as:

$$r_w = \frac{k_W}{1 + \frac{1}{K_s W}} \qquad (10)$$

As K_s is assumed equal to infinity, the final photodegradation rate equation is expressed as

follows:

$$r_w = k_w \qquad (11)$$

This equation suggests that the photodegradation of foam specimen is a zero order reaction. To

examine this relation experimentally, the weight loss results upon irradiation in the weathering

chamber were plotted according to Eqn. 11 (Figure 2.3).   The results show that nanosized

DMPA-TiO$_2$ (A) significantly affects the photodegradation ability of the polyurethane foams.

With an increase of the weight percent of DMPA-TiO$_2$, the degradation increases until a loading

of 3% weight of nanoparticles. Then, the degradation ability decreased although it was still

higher than that of unmodified PU foam. The weight loss data plot clearly indicates that when the

loading of DMPA-TiO$_2$ is 3wt%, the PU composite possesses the highest degradation rate. After

this, the degradation ability decrease is attributed to the agglomeration[94, 205] of TiO$_2$

nanoparticles, as confirmed by electron microscopy results described further below.
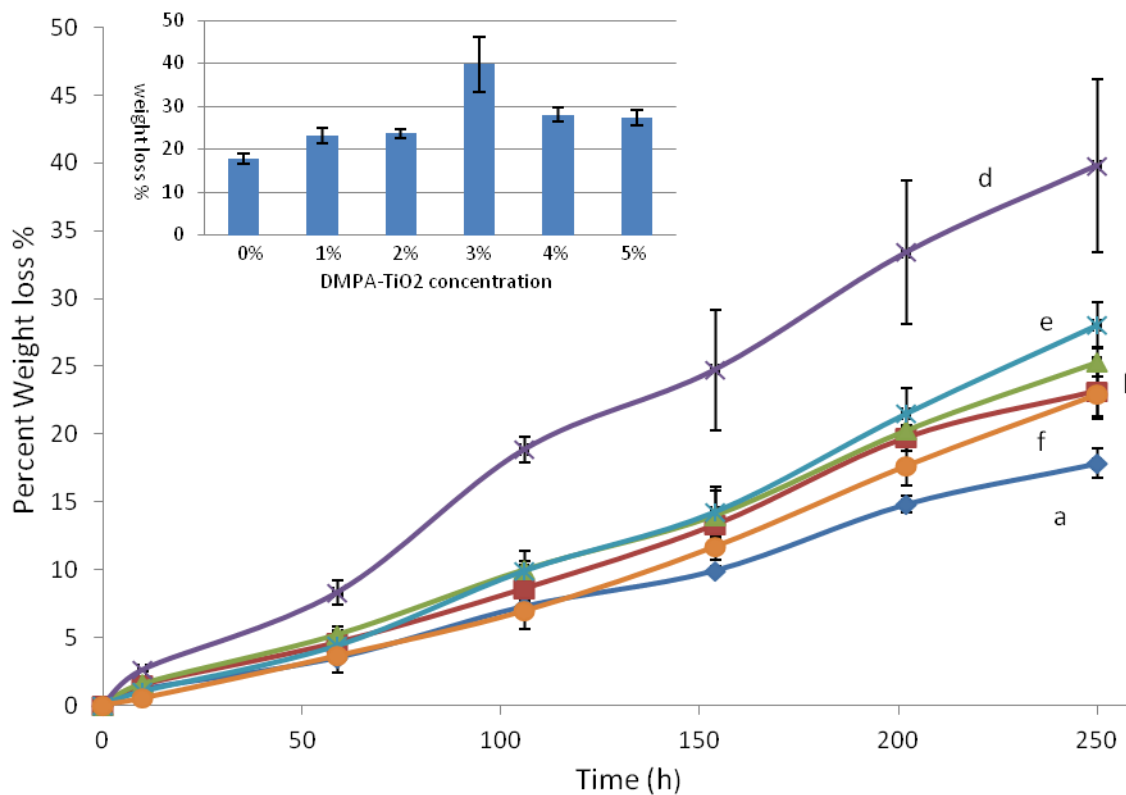
Figure 2.3. Percent weight loss of PU/DMPA-TiO$_2$(A) foams. (weathering chamber, Temperature 65°C, irradiation 0.55w/m^2). a:0wt% DMPA-TiO$_2$(A); b: 1wt% DMPA-TiO$_2$(A); c: 2wt% DMPA-TiO$_2$(A); d: 3wt% DMPA-TiO$_2$(A); e: 4wt% DMPA-TiO$_2$(A); f: 5wt% DMPA-TiO$_2$(A).

Comparing with the control experiments of PU foam modified with unfunctionalized anatase TiO$_2$ (Figure 2.4), the PU modified with DMPA-TiO$_2$ exhibits a higher photodegradation rate. Differently from DMPA-TiO$_2$, the highest photoactivity of anatase TiO$_2$ appears when the loading weight is 4%, which indicates about 58% more degradation rate than from the unmodified PU foam.
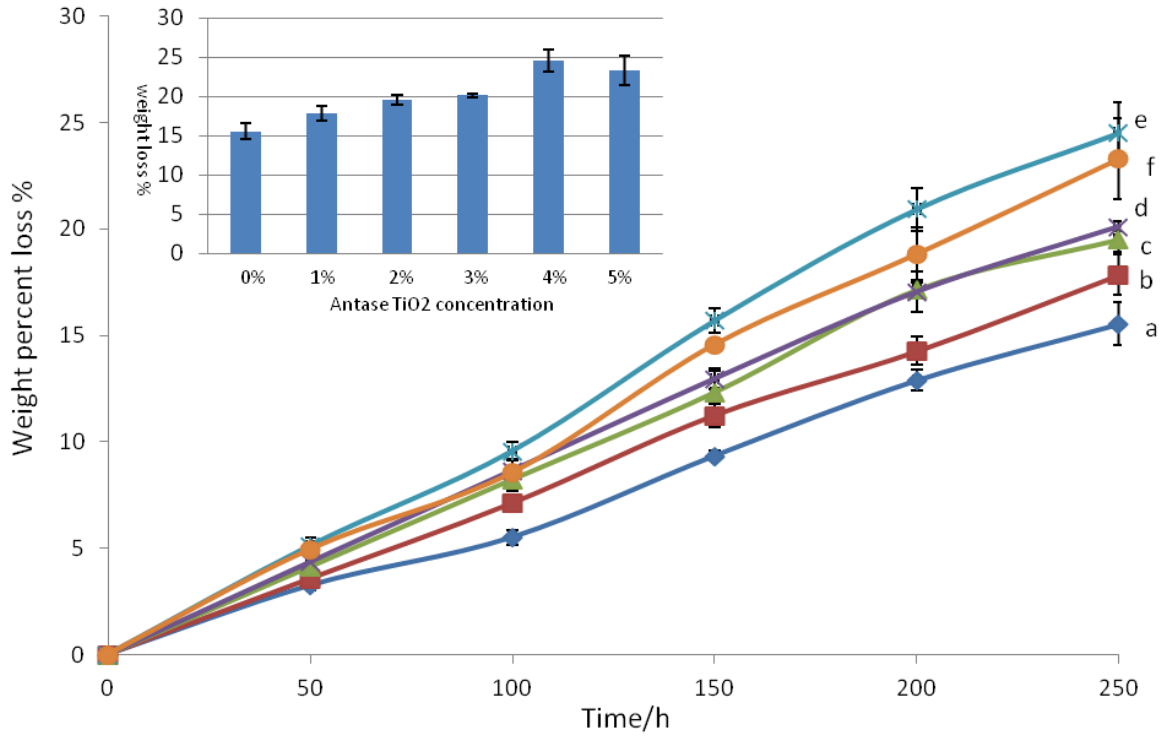
Figure 2.4. Percent weight loss of PU/ TiO$_2$(A) foams. (weathering chamber, Temperature 65°C, irradiation 0.55w/m^2). a:0wt% TiO$_2$(A); b: 1wt% TiO$_2$(A); c: 2wt% TiO$_2$(A); d: 3wt% TiO$_2$(A); e: 4wt% TiO$_2$(A); f: 5wt% TiO$_2$(A).

The weight loss results of DMPA-P25/PU composites are provided in Figure 2.5. Comparing with the unmodified PU foam, different loadings of DMPA-P25 have different effects. When the loading weight of DMPA-P25 is 1wt%, the PU foam has the highest degradation rate. With increased loading of nanoparticles, the degradation rate becomes relatively constant as shown in the inset plot.
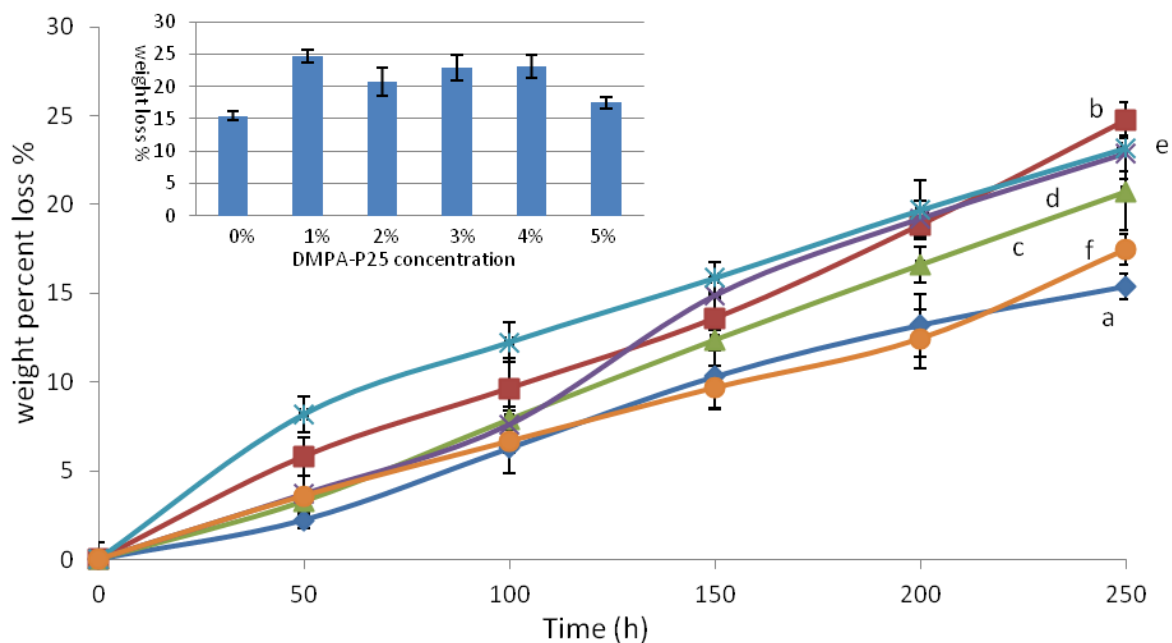
Figure 2.5. Percent weight loss of PU/DMPA-P25 foams. (weathering chamber, Temperature 65°C, irradiation 0.55w/m^2). a:0wt% DMPA-P25; b: 1wt% DMPA- P25; c: 2wt% DMPA- P25; d: 3wt% DMPA- P25; e: 4wt% DMPA- P25; f: 5wt% DMPA- P25.

Compared with the experimental data plotted results (Figures 2.3, 2.4, and 2.5), the developed kinetic model described the photocatalytic degradation reaction in a reasonable manner, with the reaction rate constants $k_w's$ provided in Table 2.1. The polyurethane foams with 0wt% loading have a similar trend and degradation rate as previously found with an oxidation reaction in PBS solution with sodium azide[206].

Table 2.1. Photodegradation rate of polyurethane foams as a function of TiO_2 nanoparticle loading (Temperature 65°C, irradiation 0.55w/m^2).

	Loading wt%	0	1	2	3	4	5
DMPA-TiO$_2$(A)	k_W %/d	1.7	2.1	2.2	3.8	2.7	2.6
TiO$_2$(A)	k_W %/d	1.5	1.7	1.9	1.9	2.4	2.2
DMPA-P25	k_W %/d	1.5	2.4	2.0	2.2	2.2	1.7

3.3 Elucidation of Polyurethane Foam Photocatalytic Mechanism

A comparison of SEM images of 3% and 5% weight loading of DMPA-TiO$_2$(A)/PU composites is provided in Figure 2.6. The TiO$_2$ nanoparticles in (b) clearly possess a larger size than in (a), showing high agglomeration occurring at this higher loading, which helps explain the weight loss results.
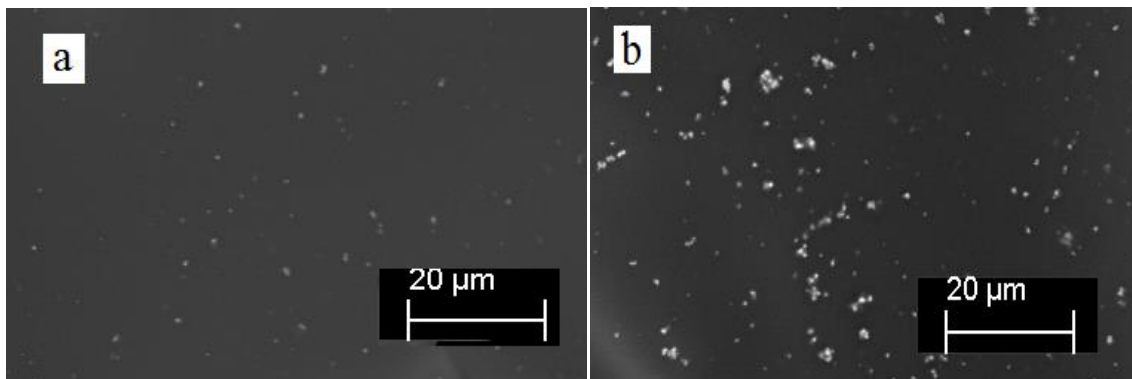
Figure 2.6. SEM images of DMPA-TiO$_2$ (A) in PU foams: (a) 3% weight DMPA-TiO$_2$(A)/PU composites, (b) 5% weight DMPA-TiO$_2$(A)/PU composites.

The photoactivity of P25 is well known to be higher than that of anatase TiO_2[207] due to the rutile TiO_2 component contained in P25 which enhances electron transfer [208]. For this enhancement of P25 in photoactivity, the rutile phase should to be in direct contact with the anatase phase. When DMPA is chemically co-ordinated to the surface of P25, it is possible that some separation of rutile and anatase phases occurs during the separation/purification process, which leads to a reduction in electron transfer. To explore this possibility, the photoactivity of these materials in methylene blue solution in water was examined (Figure 2.7). After the DMPA functionalization, although the activity of P25 and TiO_2(A) both decreased, the photoactivity of DMPA-TiO_2(A) is clearly higher than that of DMPA-P25, which helps corroborate the results found in the foam degradation experiments.
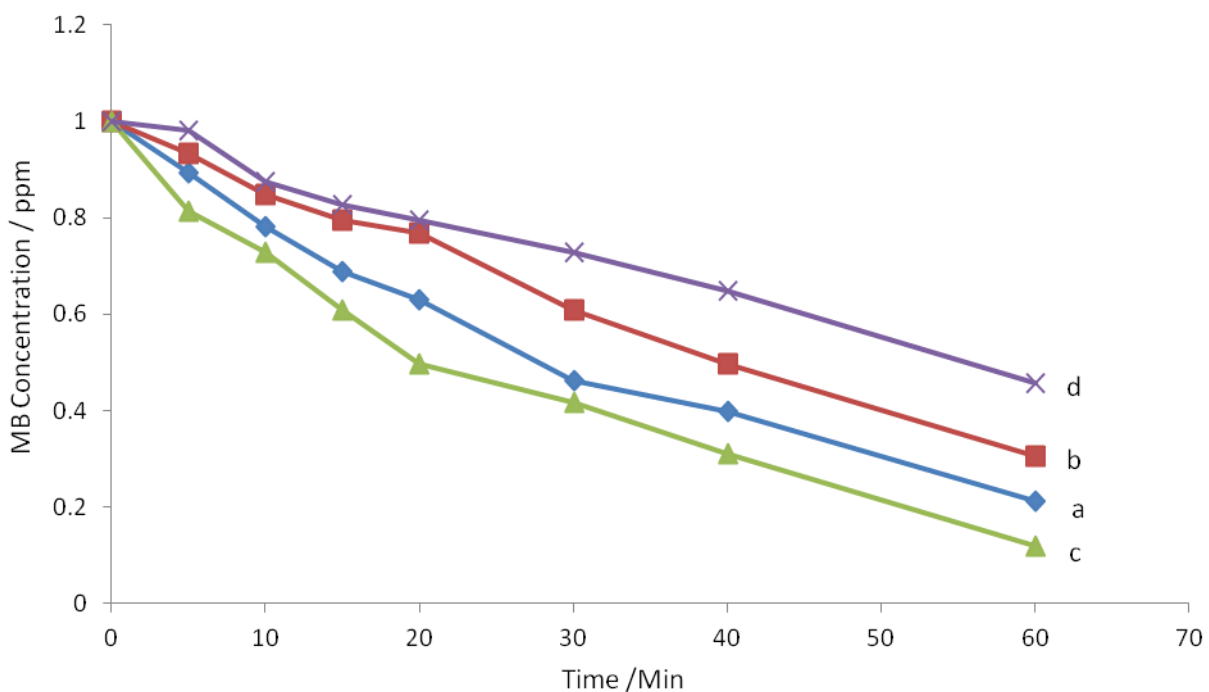
Figure 2.7. The photoactivity of different TiO_2 nanoparticles in 1ppm methylene blue solution with light intensity of 0.635 W/m^2. (a):Anatase TiO_2; (b):DMPA-TiO_2(A); (c):P25;

(d):DMPA-P25.

From the BET surface area results after DMPA functionalization (Table 2.2), both surface areas of TiO_2 (A) and P25 decreased, which in part leads to the observed decrease in photoactivity during the methylene blue testing (Figure 2.7). Moreover, the surface area of DMPA- TiO_2(A) is higher than that of DMPA-P25, which we attribute to the rutile phase of TiO_2 tending to agglomerate more than that of the anatase phase of TiO_2[209].

Table 2.2. Surface area of different types of TiO_2.

Types of TiO_2	BET Surface Area (m^2/g)
Anatase TiO_2	50.8 ± 0.17
DMPA-TiO_2(A)	10.7 ± 0.03
P25	50.6 ± 0.14
DMPA-P25	6.7 ± 0.01

The surface morphology of the polyurethane foams both modified and unmodified with DMPA-TiO_2(A) nanoparticles, before and after photodegradation are compared in Figure 2.8. Although both polyurethane foams have obvious cracks occurring after photodegradation, the specimen without TiO_2 has fewer cracks than the one containing TiO_2 which is attributed to the degradation process. TiO_2 nanoparticles are clearly observed in the specimen containing TiO_2 in the crack cross section.
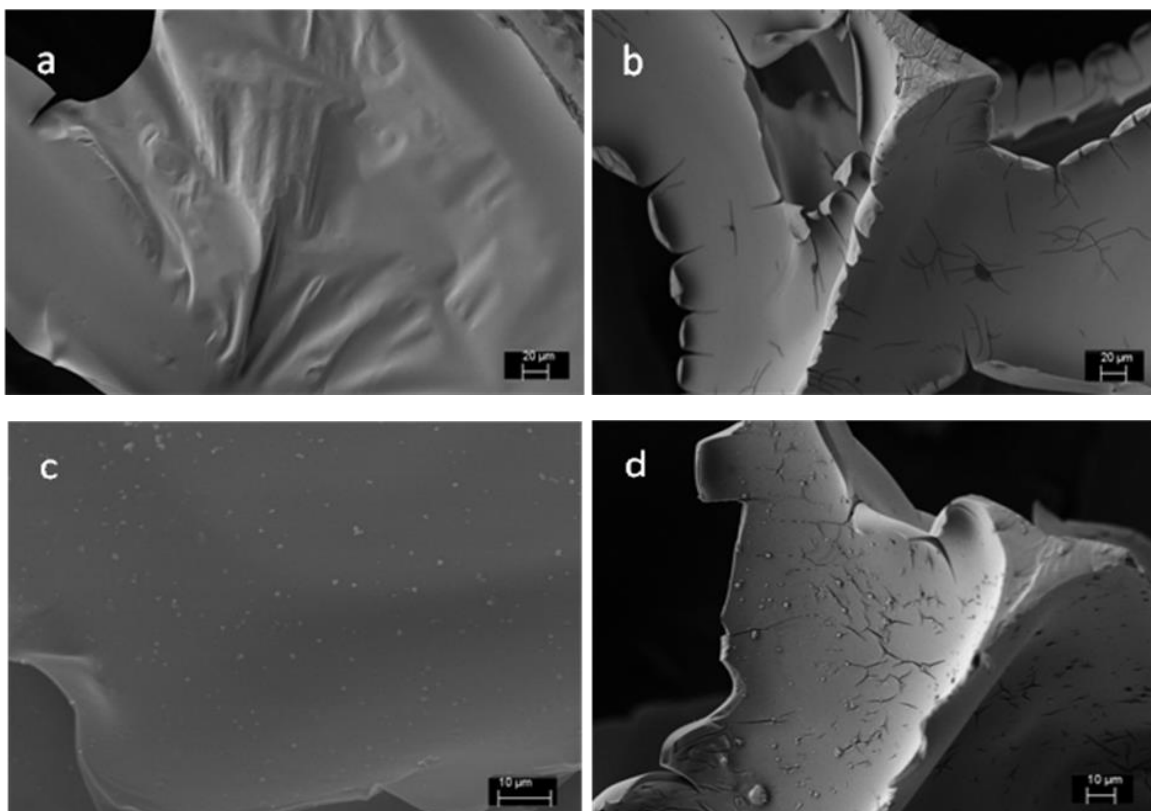
Figure 2.8. SEM images of surface morphology of polyurethane foams. (a) unmodified polyurethane foam before photo degradation; (b)unmodified polyurethane foam after photo degradation; (c)polyurethane foam modified with 3wt%DMPA-TiO2(A) before photo degradation; (d) polyurethane foam modified with 3wt%DMPA-TiO$_2$(A) after photo degradation.

According to previous works[56, 90, 195], the photodegradation of polyurethane starts from linkage loss of the urethane functional group (-NH-CO-) forming oxidant radicals. In the FTIR spectrum of unmodified polyurethane foam (Figure 2.9 curve (a) and (b)), the N-C=O group absorption at 1214 cm^{-1} has a reduction after degradation indicating the loss of the urethane bond. At 1175 cm^{-1}, a small absorption appears comparing to the spectrum before degradation, indicating the formation of branched ether which is the degradation product. There is also an

35

absorption reduction observed at 1515cm^{-1}(C-N-H) and 1705cm^{-1}(C=O) which confirms the loss

of the urethane sequence. Other functional groups have noticeable deductions at: C-H at 2948

and 2874 cm^{-1}, aromatic ring at 1410 cm^{-1}, and C-O-C at 1061 cm^{-1}. However, the only

absorption which remains is the C-C at 1594 cm^{-1}. The FTIR spectrum of polyurethane modified

with 3wt% DMPA-TiO$_2$(A) (Figure 9 curve (c) and (d)) are similar. Their mechanism in group

loss by UV radiation is similar, although the degradation rate is higher due to the TiO$_2$

photocatalytic activity. The C=O absorption at 1701cm^{-1} is lower and the formation of branched

ether at 1173cm^{-1} is higher, indicating a higher degradation rate.
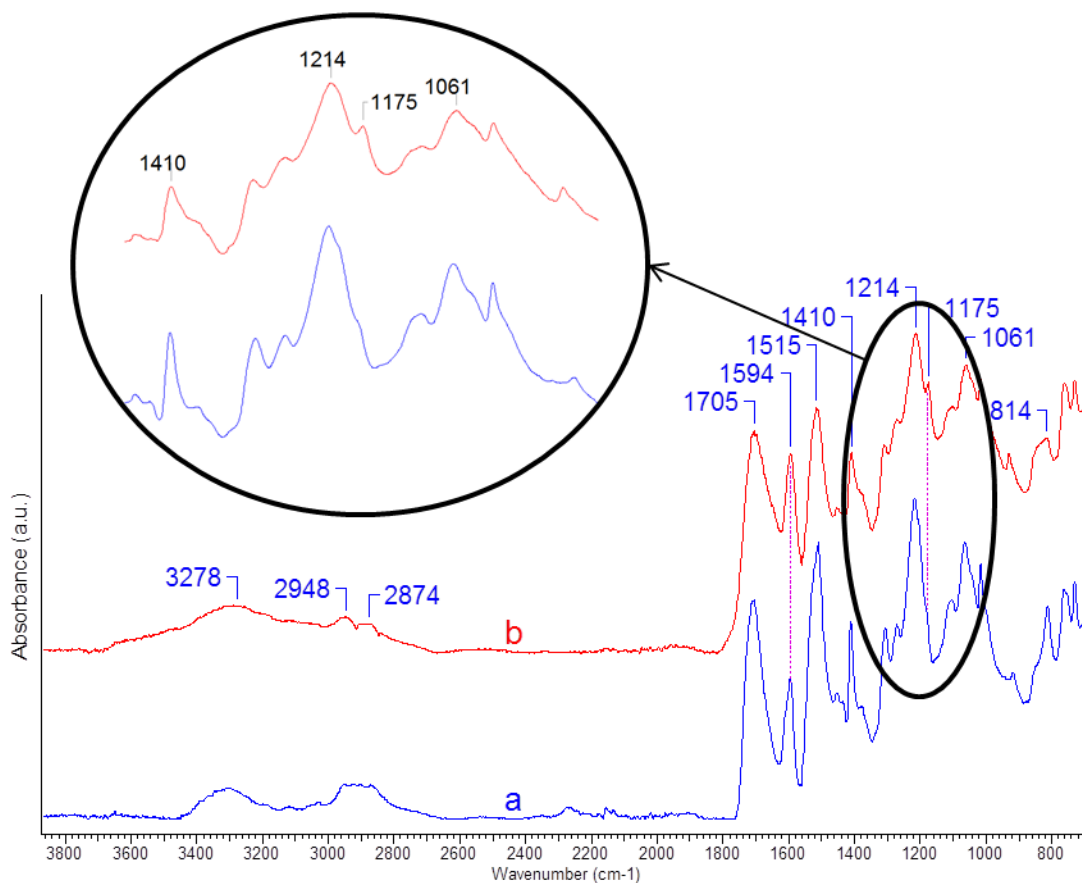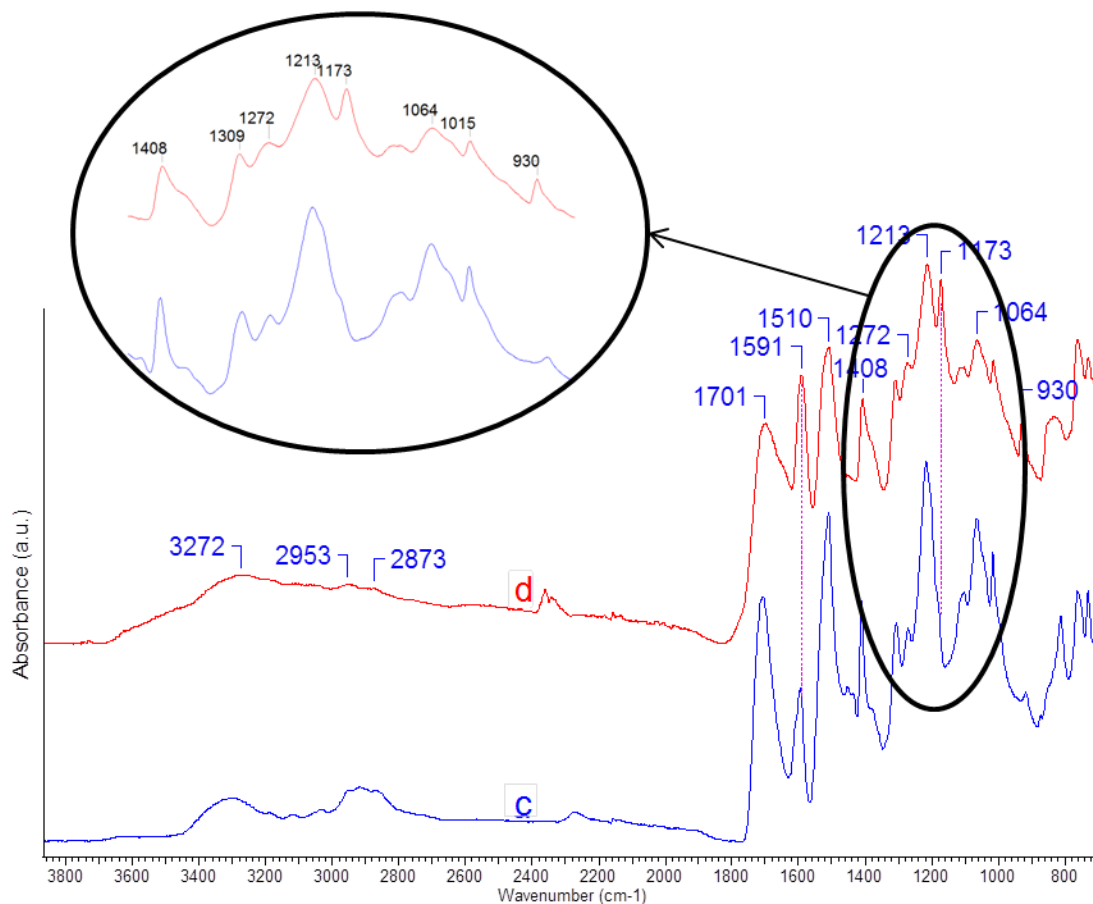
Figure 2.9. FTIR spectroscopy of polyurethane foams. (a): unmodified foams before photodegradation; (b): unmodified foams after photodegradation; (c): foams modified with 3wt% DMPA-TiO$_2$(A) before photodegradation; (d): foams modified with 3wt% DMPA-TiO$_2$(A) after photodegradation.

In addition to FTIR, TGA was utilized to investigate the decomposition process. The TGA spectroscopy results demonstrate weight differences of each component of PU before and after photodegradation (Figure 2.10 A/B). There are commonly two steps in the thermal decomposition of PU, i.e. 1) the decomposition of hard segment (isocyanate and urethane group), and 2) decomposition of the soft segment (polyol component)[210]. In the spectrum of unmodified PU (Figure 2.10 A curve (a) and (b)), three steps are observed which become more

37

evident after photodegradation. Unreacted polyol in the PU matrix may lead to the third

degradation step increase from 590℃ to 700℃. Due to the photodegradation process leading to

the loss of urethane groups, more polyol segments are separated from the foam matrix which

leads to a more obvious third step. From the FTIR results (Figure 2.9), the photodegradation

mainly happens in the hard segment, which is evident from the first step in the TGA spectrum

decreasing. When the DMPA-TiO_2(A) is chemically attached to the PU matrix after

polymerization, the unreacted polyols are connected to the matrix through the chain extender

DMPA. Therefore, only two steps were observed on Figure 2.10 B curve (a) and (b). The first

step is lower which is attributed to the photodegradation of the hard segment component while

the second step is lower but wider due to the cleavage of polyol segments.
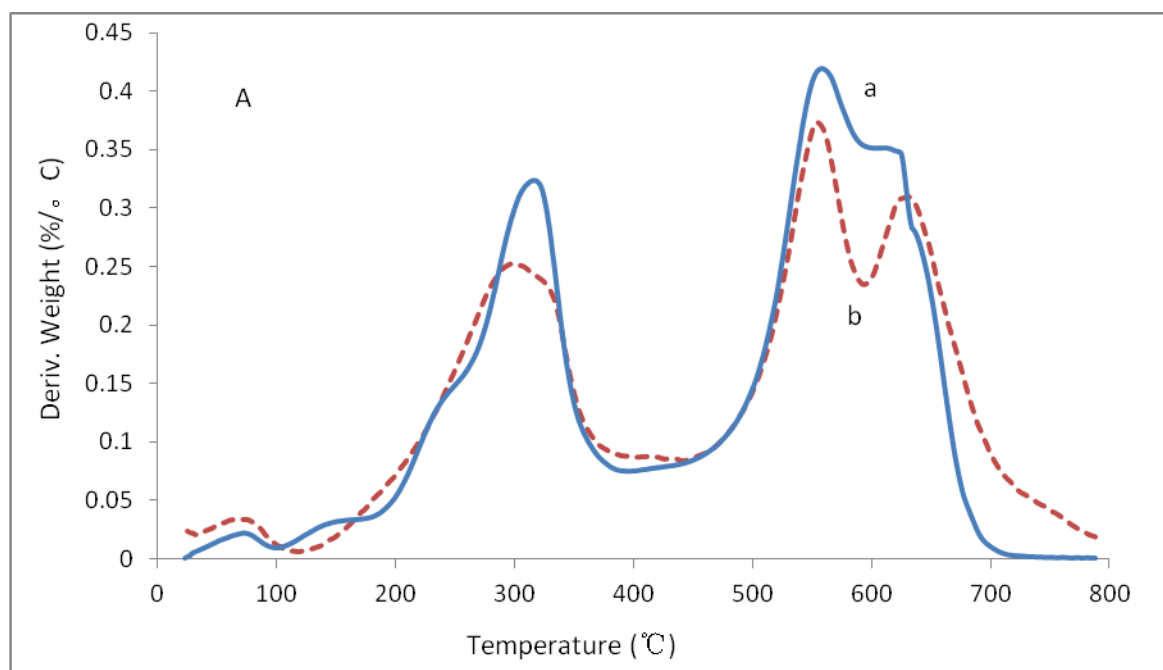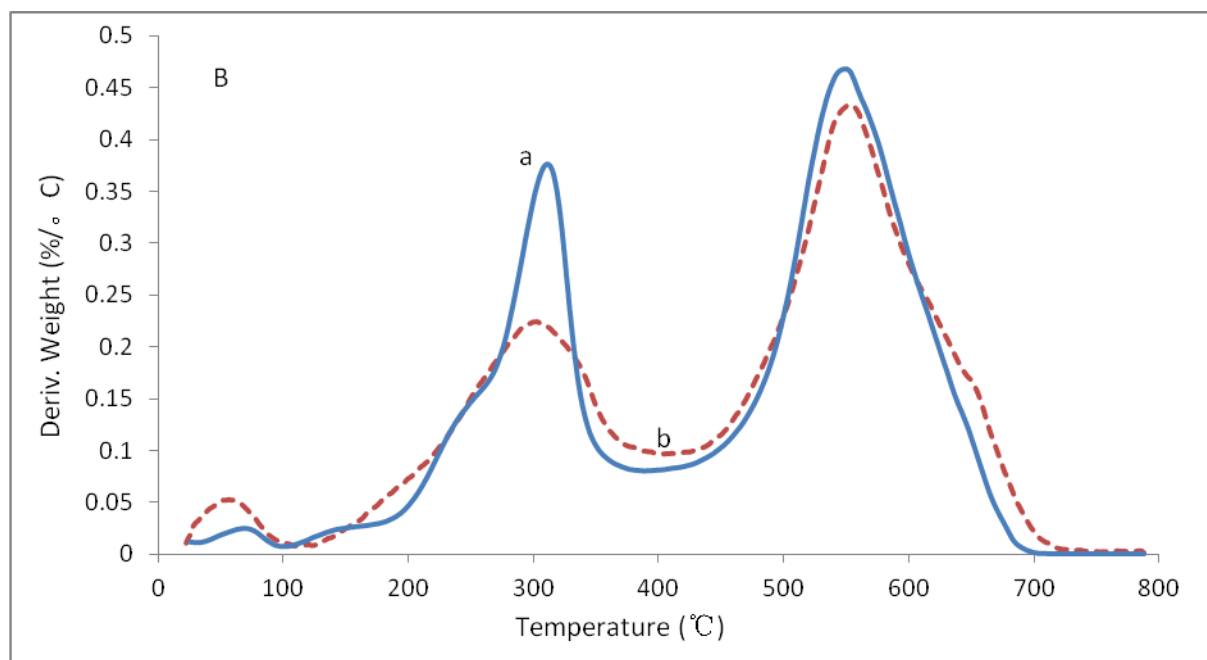
Figure 2.10. A) TGA of unmodified polyurethane foams. (a): foams before photodegradation; (b): foams after photodegradation. B) TGA of polyurethane foams modified with 3wt% DMPA-TiO$_2$(A). (a): foams before photodegradation; (b): foams after photodegradation.

4. Conclusions

A "grafting-from" approach was successfully utilized to integrate DMPA-TiO$_2$ nanoparticles into polyurethane foam structure with good dispersion. The loading of DMPA-TiO$_2$ nanoparticles was shown to have little effect on the degradation mechanism, indicating that TiO$_2$ nanoparticles function primarily as a photocatalyst. By applying Langmuir-Hinshelwood kinetics, the photodegradation of polyurethane foam appears to be a zero order reaction. Coordination of DMPA to TiO$_2$ gave DMPA-TiO$_2$(A) nanoparticles that at 3wt%, were able to increase the degradation rate of polyurethane foam by 120%. DMPA-P25 nanoparticles increased the degradation rate about 66% over unmodified polyurethane foam at a loading of 1wt%. After

functionalized with DMPA, anatase TiO_2 becomes a better photocatalyst than P25 which is

attributed from a reduction of electron transfer due to anatase/rutile surface interaction

separation.

Chapter 3. The Effect of Silica Thickness on Nano TiO$_2$ Particles for Functional Polyurethane Nanocomposites

Abstract: In order to help reduce the agglomeration of TiO$_2$ nanoparticles in polyurethane coatings while enhancing their photoactivity and mechanical/physical properties, this work examined encapsulating TiO$_2$ nanoparticles in a thin layer of SiO$_2$, prior to their nanocomposite polymerization. By applying a Stöber process, varying thicknesses of SiO$_2$ were successfully coated onto the surface of anatase and rutile TiO$_2$ nanoparticles. The methylene blue results showed that different loadings of SiO$_2$ onto the TiO$_2$ surface significantly influenced their photocatalytic activity. When the loading weight of SiO$_2$ was lower than 3.25wt%, the photocatalytic activity was enhanced, while with higher loadings, it gave lower photocatalytic activity. When the rutile phase TiO$_2$ surface was fully covered with SiO$_2$, an enhanced photocatalytic activity was observed. When these silica coated nanoparticles were applied in polyurethane coatings, increasing the amount of SiO$_2$ on the titania surface increased the coatings contact angle from 75° to 87° for anatase phase and 70° to 78° for rutile phase. The Young's Modulus was also increased from 1.06GPa to 2.77GMPa for anatase phase and 1.06GPa to 2.17GPa for rutile phase, attributed to the silica layer giving better integration. The thermal conductivity of the polyurethane coatings was also successfully decreased by encapsulating SiO$_2$ on the titania surface for next generation high performance coatings.

Keywords: SiO$_2$, TiO$_2$, Nanoparticles, Polyurethane, Mechanical Properties

1. Introduction

TiO$_2$ nanoparticles are well-known photocatalysts whose activity depends primarily on their crystal structure and specific surface area [27, 89, 211]. Anatase and rutile TiO$_2$ are two different forms of titanium dioxide[90], which have different roles when integrated into coatings. Anatase TiO$_2$ works as a photocatalyst and can be integrated into self-cleaning or antibacterial polymer coatings[190, 212], while rutile TiO$_2$ works as photosensitizer and is usually applied for UV protection[213, 214]. However, TiO$_2$ nanoparticles tend to agglomerate during their photocatalytic process, reducing their activity [93-95]. Also, agglomeration will reduce the specific surface area of TiO$_2$ nanostructures, also affecting their photocatalytic efficiency[94]. This is particularly a challenge when integrating such nanoparticles into polymer coatings [215-217]. Previously our group showed that using a functional monomer approach by directly grafting functional groups such as DMPA onto the surface of nanoparticles, both an improved photocatalytic effect and enhanced dispersion in monomer and solventwas provided, [198, 218] enabling an improved photocatalytic behavior when integrated into polyurethane.

Previously, SiO$_2$/TiO$_2$-core/shell structures showed that SiO$_2$ limited the agglomeration of TiO$_2$ particles, therefore optimizing their light scattering properties to produce highly efficient dye-sensitized solar cells[158]. Moreover, a sol-gel process including the synthesis of TiO$_2$ was conducted in other studies showing that SiO$_2$ could control the photocatalytic activity [160, 219, 220]. The aforementioned synthesized mixture of SiO$_2$-TiO$_2$ nanoparticles and SiO$_2$-TiO$_2$ core-shell nanostructures exhibited enhanced photoactivity whereas SiO$_2$ showed none. Moreover, using inorganic materials such as SiO$_2$ coated TiO$_2$ for reducing the decomposition

effect of polymer substrates but still maintaining or even enhancing the catalytic property was studied by Ren, Yuan, et al[159]. However, the agglomeration and photoactivity of TiO_2 particles coated with different thickness of SiO_2 layers is unexplored when embedded into polyurethane coatings, and it is unknown how this will affect the coatings physical and chemical properties.

In this study, we examine how SiO_2 will affect both the rutile ($TiO_2(R)$) and anatase ($TiO_2(A)$) forms of titanium dioxide when different thicknesses of SiO_2 are coated onto the surface of TiO_2 nanoparticles and their subsequent effect when integrated into polyurethane coatings. In addition, the thermal conductivity and surface hydrophobicity of the polyurethane coatings embedded with these nanoparticles was studied in order to examine the effect of silica on the coating properties.

2. Materials and Experiments

2.1 Materials. Alkyltrimethylammonium bromide (C16TAC) (Sigma Aldrich, >95%), tetraethoxysilane (TEOS, 99.0%) (Sigma Aldrich), methanol (Caledon Laboratories, Ontario, Canada), aqueous ammonia solution (28%)(Caledon Laboratories, Ontario, Canada), anatase TiO2 (Sigma Aldrich, <25nm, 99.7%), rutile TiO2 (Sigma Aldrich, <100nm, 99.5%), poly aspartic ester (Bayer MaterialScience), poly hexamethylene diisocyanate (Bayer MaterialScience), isophorondiamine-isobutyraldimine (Bayer MaterialScience), methylene blue (Caledon Laboratories, Ontario, Canada) were purchased and used as is.

2.2 Synthesis Procedure. Silica encapsulated TiO_2 nanoparticles were prepared by using a modified Stöber process [146, 148]. During this experiment, 1g of anatase or rutile TiO_2 was

dispersed in 50ml of methanol and was sonicated for 30 minutes (solution A). About 0.2g of

C16TAC, 17.7g of deionizer water and 7.2g of 28% aqueous ammonia solution were added in

100mL of methanol (solution B). The desired amount of TEOS (0.12ml, 0.24ml, 0.36ml, 0.48ml)

was added into solution B, the weight ratio of SiO_2 to TiO_2 were calculated to be 3.25:100,

6.50:100, 9.75:100, 13.0:100, respectively. Solution A was mixed with solution B with the

mixture stirred for 24 hours at room temperature. Then the mixture was centrifuged and washed

with methanol, and the final product was dried in a vacuum oven at 50°C for 48 hours.

The polyurethane coatings were prepared by mixing SiO_2-TiO_2, polyaspartic ester mixture and

poly hexamethylene diisocyanate at a ratio of 5:425:250 by weight. The polyaspartic ester

mixture was prepared by mixing poly aspartic ester and catalyst (isophorondiamine-

isobutyraldimine) at a ratio of 4:1 by weight. The SiO_2-TiO_2 nanoparticles were first physically

mixed with polyol and then dispersed in acetone, with the polyisocyanate mixed with polyol

solution. The resulting mixture was then cast onto Teflon petri dishes and cured in air at room

temperature. After the complete evaporation of acetone, a thin lay of coating was formed.

Step 1. Synthesis of SiO₂-TiO₂ nanoparticles

Step 2. Synthesis of PU/SiO₂-TiO₂ nanocomposites
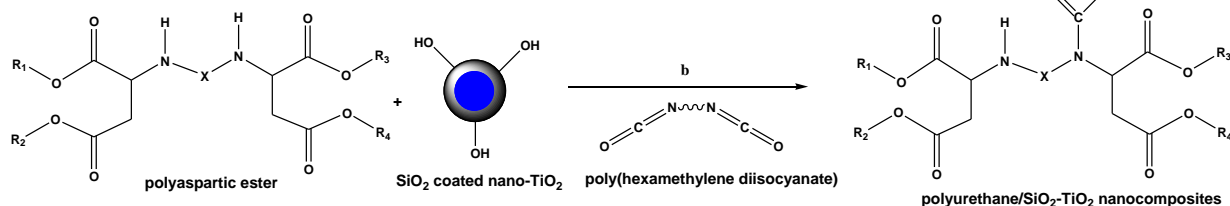
R_1, R_2, R_3, R_4 are the same or different and represent an alkyl group having at least two carbon atoms.

X:
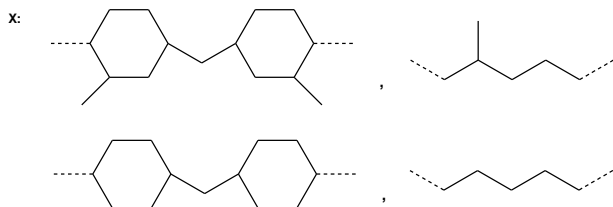
Scheme 3.1. Schematic diagram of the synthesis of SiO₂-coated TiO₂ nanoparticles and the preparation of polyurethane/SiO₂-TiO₂ nanocomposites; (a) room temperature in methanol solution; (b) room temperature with catalyst.

2.3 Characterization.   Photoactivity of polyurethane coatings was studied following a standard method developed by the International Organization of Standardization (i.e. ISO/DIS 10678). The photoactivity of the as-prepared SiO2-TiO2 particles were tested in 20ml 1ppm methylene blue solution with 100mg of nanoparticles under UV irradiation in a light simulator (Luzchen ICH1) with a light intensity of 0.635 w/m2. The methylene blue concentration was measured after 5, 10, 15, 20, 30, 40, and 60 minutes of irradiation. To examine the production of hydroxyl radicals during the photocatalytic reaction, the SiO2-TiO2 particles were mixed with a solution containing 3×10-4M terephthalic acid and 2×10-3M sodium hydroxide [221] under the

45

illumination of full light (1 Sun). Then the photoluminescense emission at 425 nm was observed using an excitation wavelength of 315 nm[222]. Brunauer– Emmett–Teller (BET) surface area data was obtained using a Micromeritics TriStar II 3020 instrument at 77 K. Prior to the N2 physisorption, the sample was degassed at 100 °C under vacuum for 5 hours. FTIR analysis was performed using a Nicolet 6700 spectrometer in the range of 400-4000 cm-1 and was operated using 32 scans at 4cm-1 resolution for each sample. The absorbance in the ultraviolet range and band gap energy was tested and calculated through UV-Vis measurements which were conducted using a Shimadzu UV-3600. Scanning Electron Microscopy (SEM) was performed on the experimental nanoparticles using a Hitachi S-4500 field emission SEM. All samples were taken at 10 kV at varying magnifications for different views. Energy Dispersive X-ray (EDX) was taken using a LEO (Zeiss) 1540XB. Contact angles were measured using a PGX Measuring Head at room temperature with 4μL distilled water. Young's modulus was taken follow ASTM D882 method using an Instron 5943. Thermal conductivity was measured by a transient temperature system based on the method from previous studies [223]. Thermo-gravimetric analysis (TGA) was performed to measure the prepared xerogel nanofibers using a TA Instruments® Q-series SDT Q600 analyzer. Thermogravimetric curves were measured in the temperature range of 25-800℃ (heating rate: 20□/min; under air) and analyzed using the TA Instruments® Universal Analysis 2000 software.

3. Results and Discussions

3.1 SiO_2 Encapsulated TiO_2 (A,R) Synthesis

Silica encapsulated TiO_2 nanoparticles were firstly prepared using a modified Stöber process

in which TEOS was reacted with anatase or rutile TiO_2 nanoparticles (see Scheme 3.1). Table 3.1 lists the calculated weight ratio of SiO_2:TiO_2 for the various synthesized samples and the average resulting (Si:Ti) values as measured using EDX, which gave values similar to the stochiometric ratio. The SEM images show (see Figure 3.1 and 3.2), that when using anatase TiO_2 (diameter = 25 nm, surface area = 49.3 m^2/g), increasing the loading of TEOS did not significantly increase the resulting particle size, although the SiO_2 layer is evident on the surface of anatase TiO_2. When using rutile TiO_2 (diameter = 100 nm, surface area =2.26 m^2/g), as the loading of TEOS was increased, the thickness of the silica layer on the TiO_2 surface also increased from 15nm, 29nm, 41nm, to 58nm respectively (see Support information 3.2). When the weight ratio of SiO_2:TiO_2 was beyond 9.75:100, the excess TEOS began to form individual SiO_2 nanoparticles, which are observed as small round particles in the electron micrographs. Also from the EDX analysis (Table 3.1), the weight ratio of SiO_2 to TiO_2 is quite close to that based on the stochiometric weight ratio indicating quantitative reaction.

Table 3.1. Calculated and EDX measured SiO_2:TiO_2 weight ratio

SiO_2:TiO_2	Anatase TiO_2			
Stoichiometric Ratio	3.25:100	6.50:100	9.75:100	13.0:100
Average EDX ratio	2.32±0.11:100	6.22±0.15:100	8.14±0.23:100	12.1±0.08:100
Sample Name	A1	A2	A3	A4
SiO_2:TiO_2	Rutile TiO_2			
Stoichiometric Ratio	3.25:100	6.50:100	9.75:100	13.0:100

Average EDX ratio	2.14 ± 0.05:100	5.90 ± 0.17:100	7.25 ± 0.14:100	10.6 ± 0.35:100
Sample Name	R1	R2	R3	R4

Dynamic light scattering (DLS) was used to determine the effect of SiO_2 encapsulation on anatase TiO_2 agglomeration. As Table 3.2 shows, the anatase TiO_2 nanoparticles have the largest size due to agglomeration. With the SiO_2 coated onto the titania surface, the particle size was reduced with increasing of SiO_2 content, indicating a lowered agglomeration effect. This SiO_2 limiting agglomeration effect has also been confirmed by other studies [224, 225]. After a utilized ratio of 9.75:100, the size starts to increase which might be due to some of the nanoparticles forming clusters during the encapsulation reaction, leading to the observed experimental results. When the SiO_2 encapsulated TiO_2 nanoparticles were integrated into polyurethane nanocomposites as shown in scheme 3.1, the nanoparticles with less agglomeration gave smaller particle size (Figure 3.3), indicating better distribution and less agglomeration in the polyurethane nanocomposites.

Table 3.2. The size of SiO_2-TiO_2 (A) nanoparticles obtained from DLS in H_2O.

Sample:	A0	A1	A2	A3	A4
Size (d. nm)	365	294	266	281	312
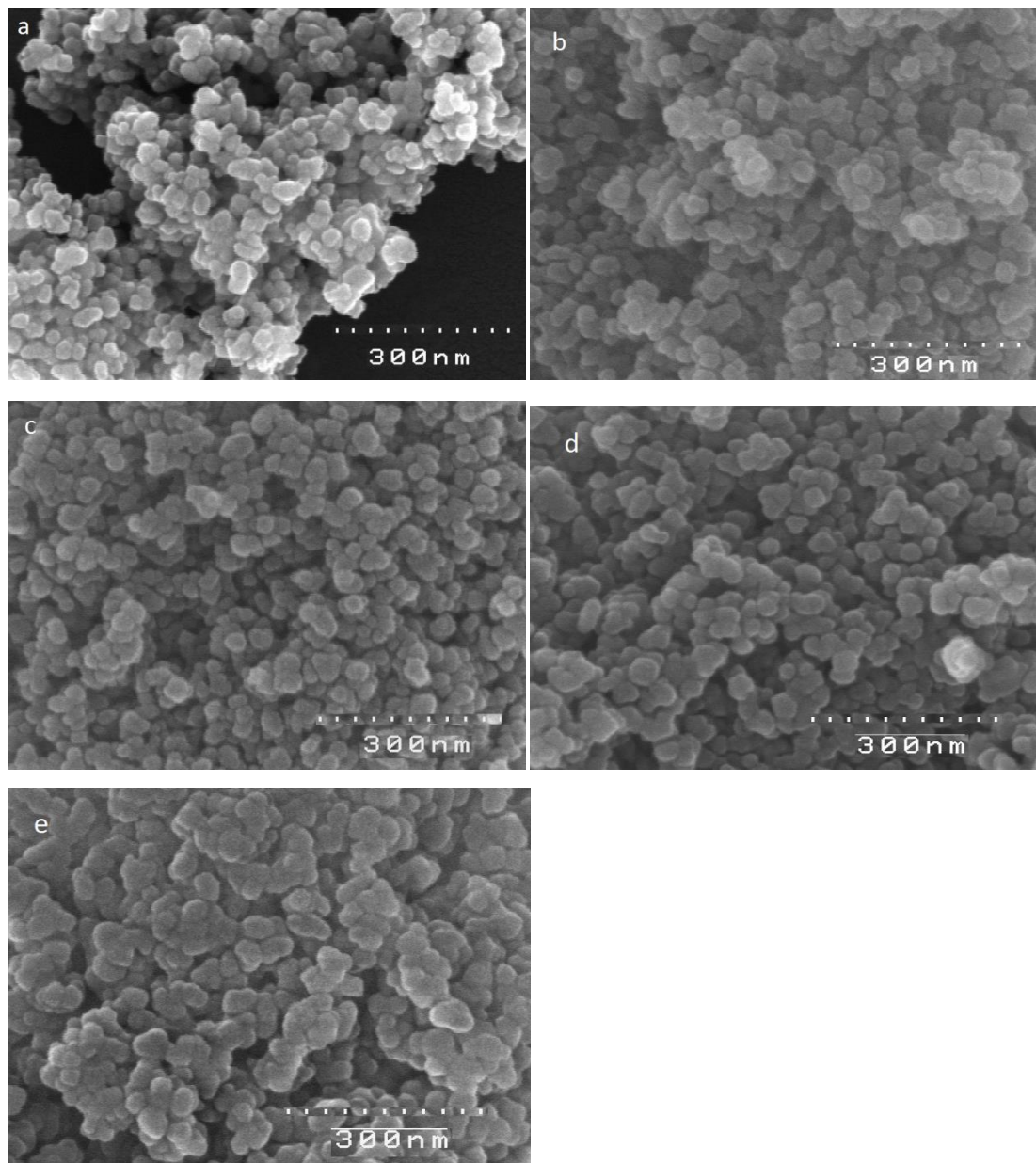
Figure 3.1. SEM images of surface morphology of SiO_2-TiO_2(A) nanoparticles. a: A0 (before

SiO_2 encapsulation). b: A1. c: A2. d: A3. e: A4.
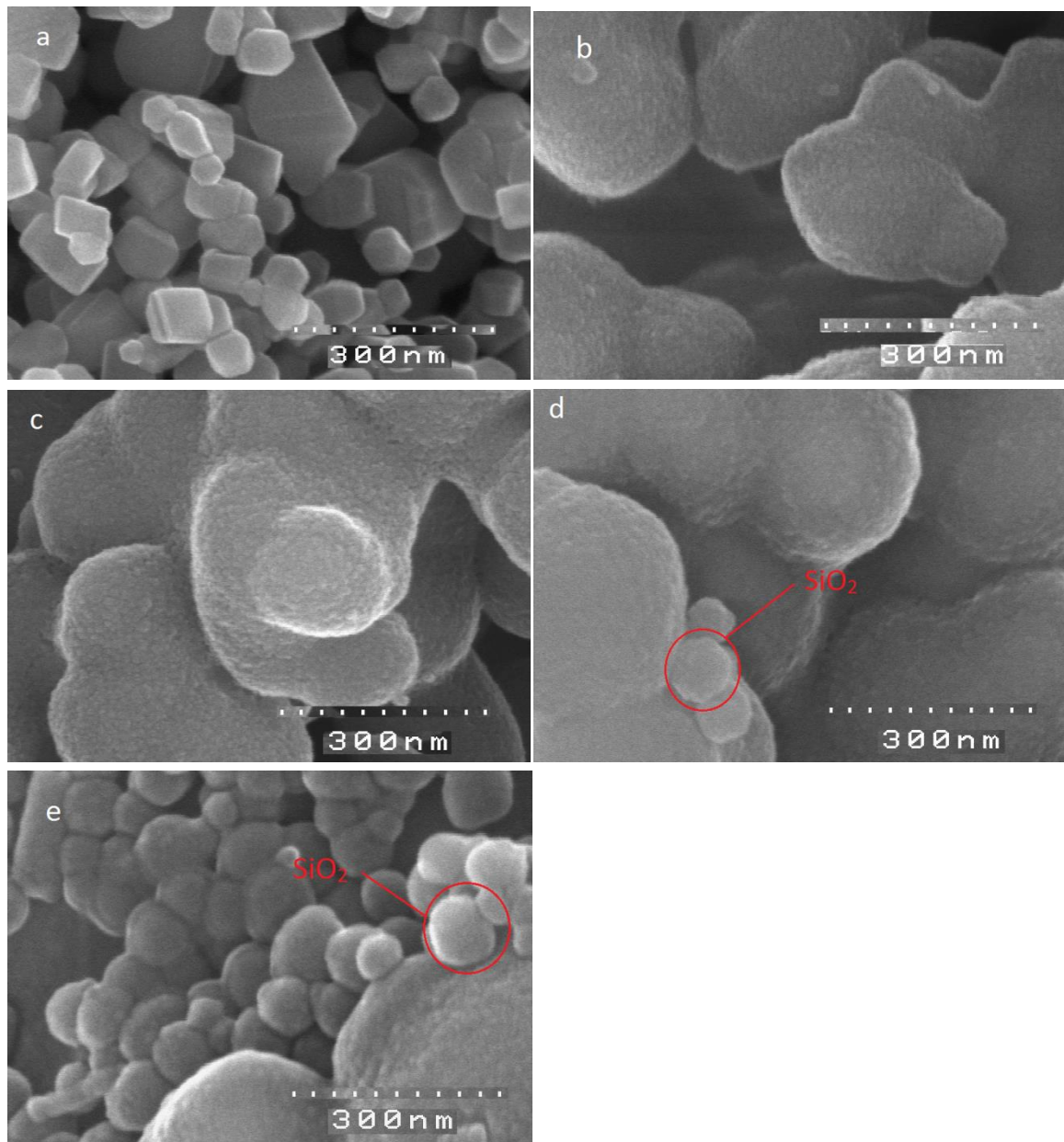
Figure 3.2. SEM images of surface morphology of SiO_2-TiO_2(R) nanoparticles. a: R0 (before

SiO_2 encapsulation). b: R1. c: R2. d: R3. e: R4.
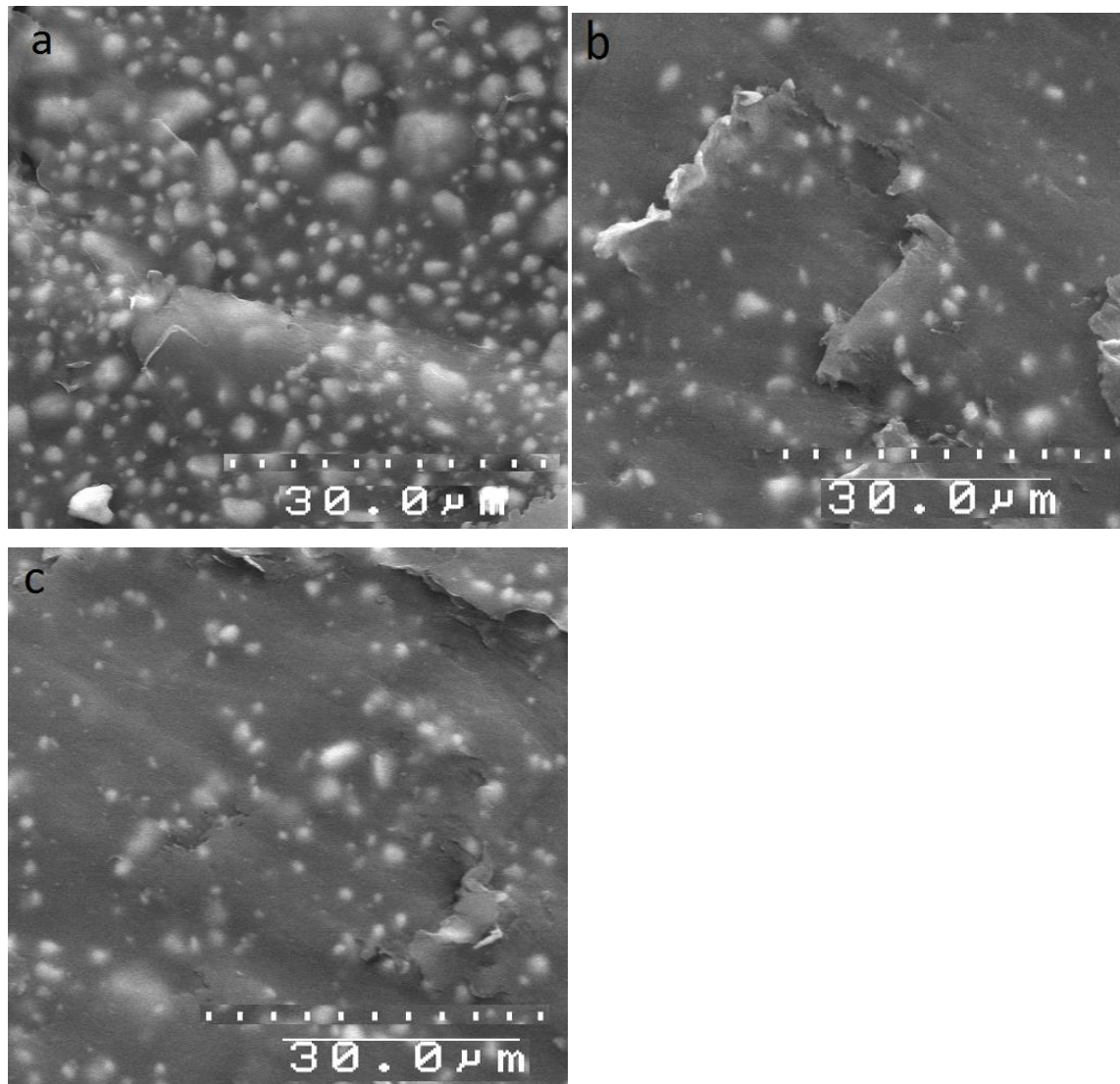
Figure 3.3. SEM image of nanoparticle distribution in polyurethane nanocomposites. a: A0; b: A1; c: A2.

For the FTIR spectra of the silica/titania NPs (Figure 3.4), when increasing the silica ratio from 3.25 to 13.0 %, a significant peak appears at 1060 cm^{-1} which increased with increasing silica content and is attributed to the stretching of the Si-O bond [156]. The peaks at 954 cm^{-1} and 962 cm^{-1} indicate the formation of Ti-O-Si according to previous studies [156]. Additional

loading of TEOS leads to higher $SiO_2:TiO_2$ ratios, as observed by the height of the significant

peaks increasing, indicating higher SiO_2 concentrations depositing onto the surface of the TiO_2
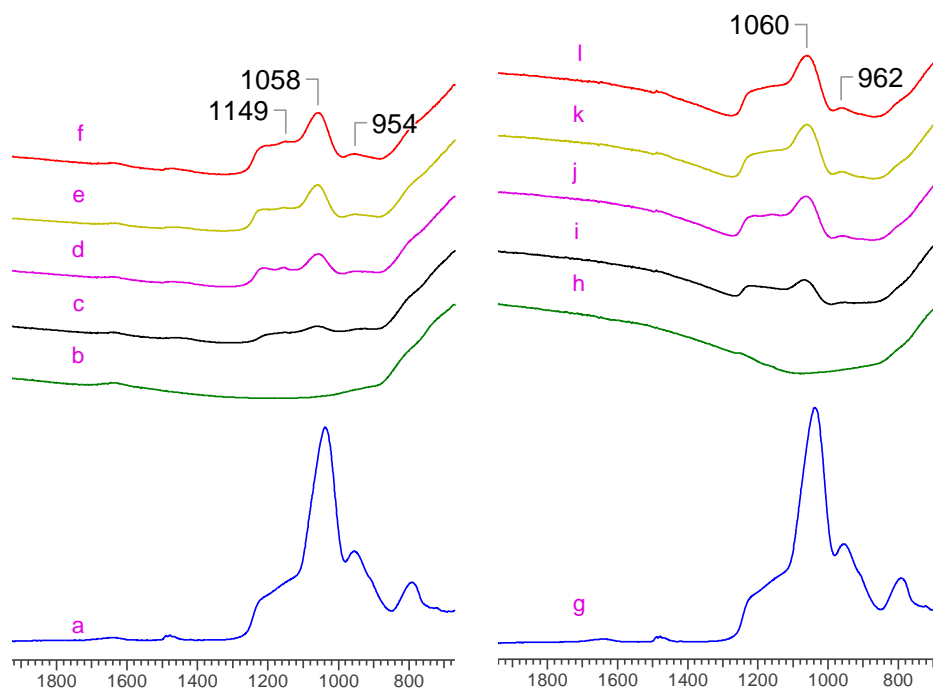
nanoparticles.

Figure 3.4. FTIR spectra of SiO_2-TiO_2 nanoparticles. Anatse TiO_2 (a: SiO_2. b: A0. c: A1. d: A2. e:

A3. f: A4.) Rutile TiO_2 (g: SiO_2. h: R0. i: R1. j: R2. k: R3. l: R4.)

The FTIR spectra of polyurethane nanocomposites shown in Figure 3.5, shows no stretching

of the isocyanate group NCO peak 2260 cm^{-1} on the nanocomposites which appears on poly

(hexamethylene diisocyanate), indicating complete reaction [226], while the absorbance at 1685

cm^{-1} is the urea –C=O vibration, and the absorbance at 1724cm^{-1} is the urethane –C=O vibration.

Both of these spectra indicate no polyisocyanate residue and complete formation of polyurethane

structure.
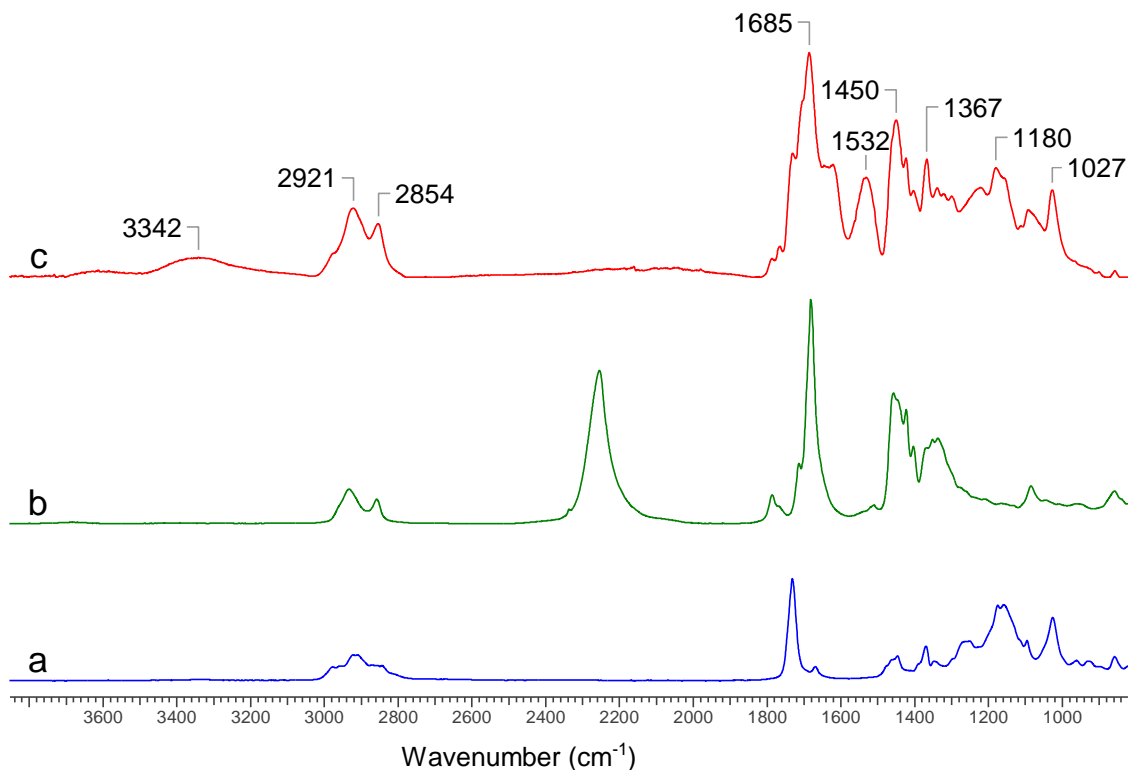
Figure 3.5. FTIR spectra of PU nanocomposite. (a) poly aspartic ester; (b) poly hexamethylene diisocyanate; (c) PU with 15mg A1(2.25 wt% in PU).

3.2 Photoactivity of SiO_2-TiO_2 NP and PU Nanocomposite

Photoactivity of the SiO_2-TiO_2 NPs (before integration into PU coatings) was measured using methylene blue degradation in water at room temperature according to ISO/DIS10678 (Figure 3.6). With a ratio of SiO_2:$TiO_2 < 3.25$:100, the photocatalytic activity is higher than from the virgin anatase form of TiO_2. This is attributed to the coated SiO_2 on the surface decreasing the agglomeration of TiO_2 and enhancing the photocatalytic effect. N.B. the amount of SiO_2 in this sample is insufficient to cover the entire surface of anatase TiO_2 (theoretically, assuming the

SiO$_2$ layers on the surface are thick enough to be considered as bulk material, with SiO$_2$:TiO$_2$ weight ratio of 3.25:100 and anatase form of TiO$_2$ surface area to be about 50 m^2/g, the average thickness of silica layers will be 0.25 nm. Assuming spherical structure, the average thickness of silica layers can be calculated to be 0.48 nm. In the amorphous SiO$_2$ structure, the distance between Si atoms is 0.31nm while the diameter of an individual Si atom is 0.27nm [227].) With a higher SiO$_2$:TiO$_2$ weight ratio utilized, there was sufficient SiO$_2$ to cover the surface. The reduced photoactivity is attributed to SiO$_2$ blocking the electron hole-pairs contacting the aqueous solution [228], which leads to higher photocatalytic activity than the blank. Similarly, the SiO$_2$ coated rutile form of TiO$_2$ (Figure 3.7) is also affected by the SiO$_2$ ratio. Since the thickness of SiO$_2$ layers on the surface of rutile form of TiO$_2$ ranged from 15nm to 58nm, not only will some blocking of UV radiation occur, also the electron hole-pairs will be blocked from contacting the aqueous solution. The photosensitizing effect of rutile TiO$_2$ is disabled and these SiO$_2$-TiO$_2$ nanoparticles no longer protect the methylene blue degradation from UV light. In contrast, due to the diffraction effect of coated SiO$_2$ [159], more of the UV light was diffracted and make contact with the methylene blue. Therefore, the degradation of methylene blue is observed to be accelerated.
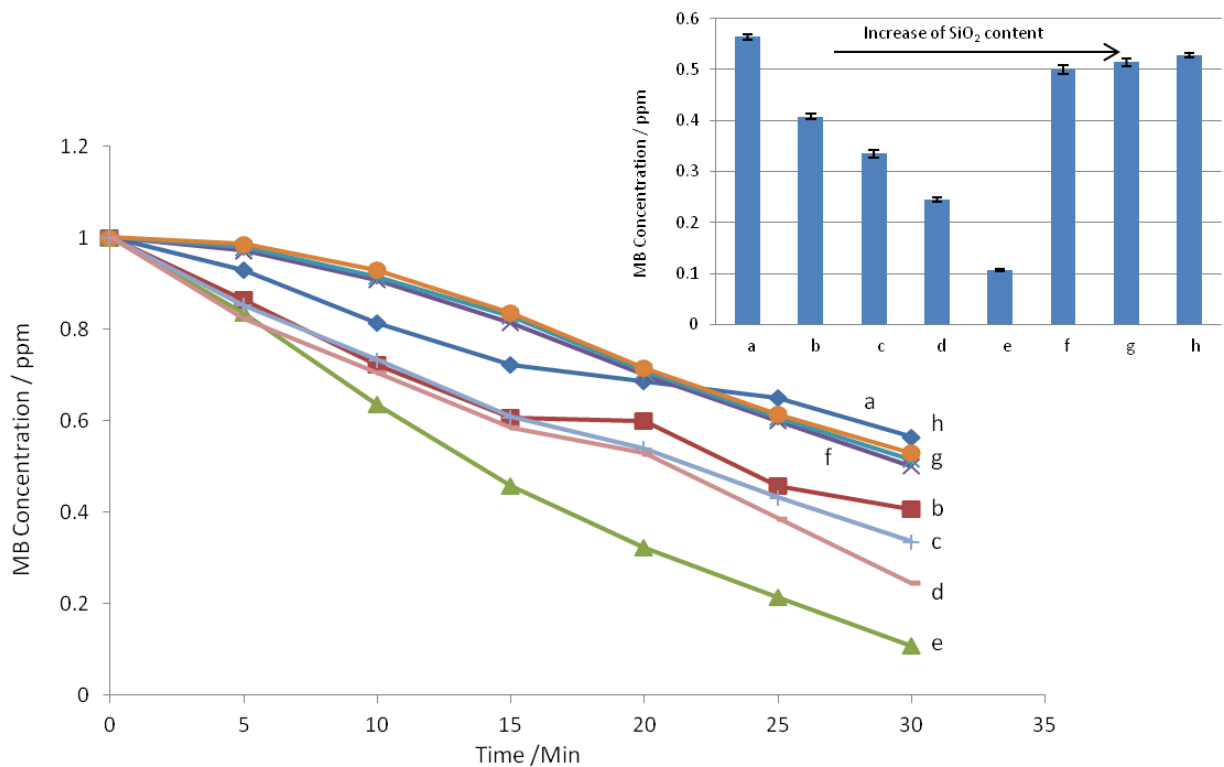
Figure 3.6. The photoactivity of SiO_2-TiO_2(A) nanoparticles varying SiO_2 content (wt. %) (1ppm methylene blue solution with light intensity of 0.635 W/m^2). a: blank (no TiO_2), b: 0. c: 0.81. d: 1.62. e: 3.25. f: 6.50. g: 9.75. h: 13.0.
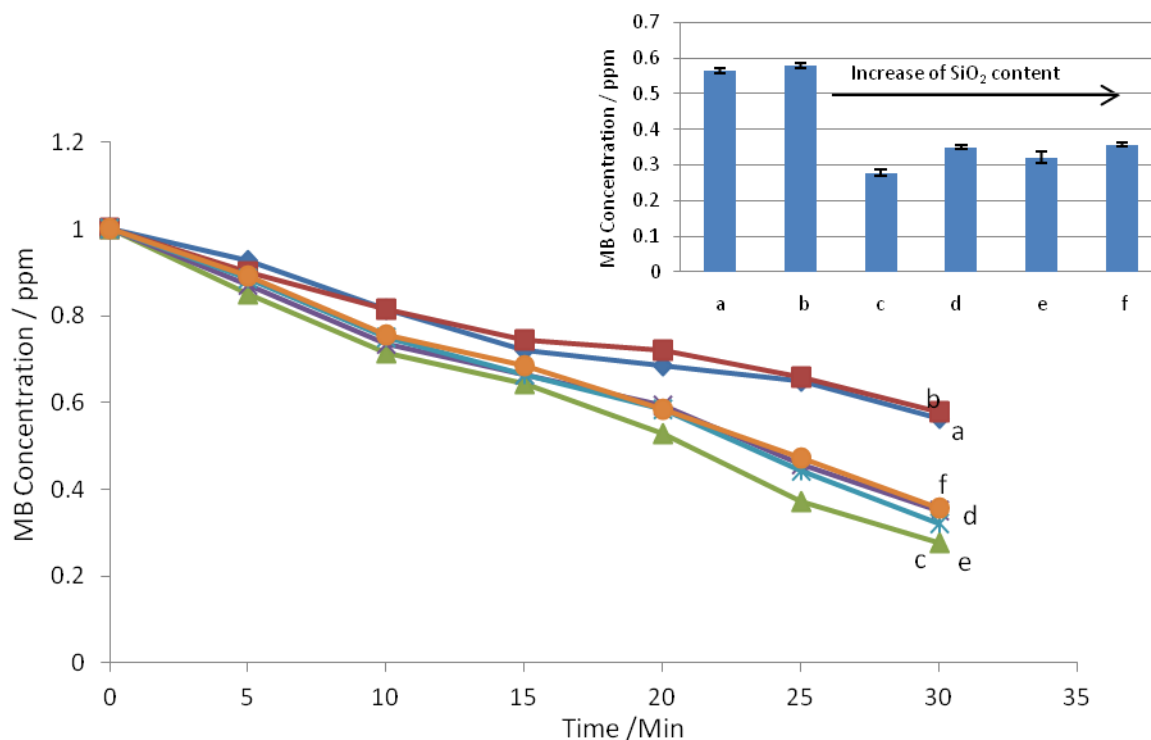
Figure 3.7. The photoactivity of SiO_2-TiO_2(R) nanoparticles varying SiO_2 content (wt. %) (1ppm methylene blue solution with light intensity of 0.635 W/m^2). a: blank (no TiO_2), b: 0. c: 3.25. d: 6.50. e: 9.75. f: 13.0.

The experimental SiO_2-TiO_2(A) nanoparticles were examined in polyurethane coatings and their subsequent physical/mechanical properties measured. As the photoactivity of SiO_2 encapsulated rutile form TiO_2 was not influenced by the SiO_2 weight ratio (data not shown), the photoactivity of polyurethane coatings was only examined with the anatase form of SiO_2-TiO_2 (Figure 3.8). Corresponding to the photoactivity property of the examined nanoparticles, the polyurethane coatings embedded with anatase SiO_2-TiO_2 nanoparticles exhibit the same photocatalytic activity trend. The coatings embedded with higher photocatalytic activity nanoparticles A3 showed the highest photoactivity. Moreover, with increasing loading of A3

nanoparticles into the coatings, the photoactivity of polyurethane coatings also increased. Comparing with a previous study regarding polyurethane/TiO$_2$ hybrid films, when using higher photocatalytic activity nanoparticles such as anatase TiO$_2$, the coatings provided higher photocatalytic ability [229].
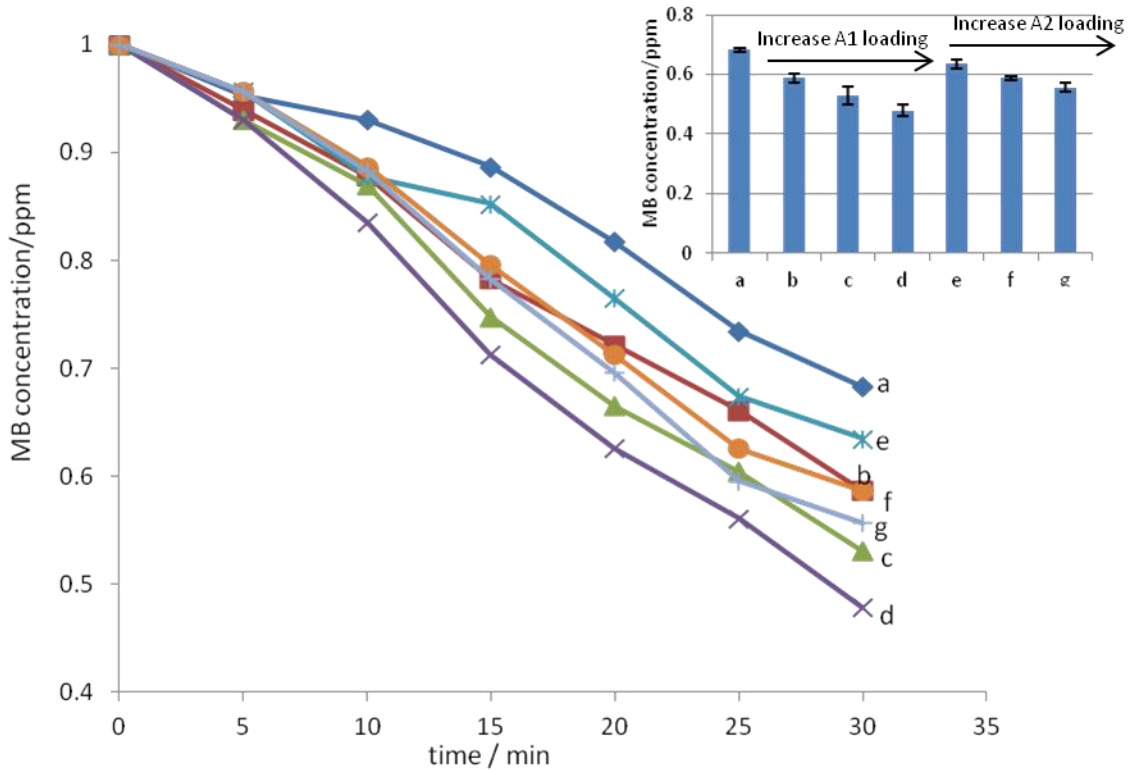
Figure 3.8. The photoactivity of polyurethane coatings in 1ppm methylene blue solution with light intensity of 0.635 W/m^2 after 30 mins. a: polyurethane coating. b: polyurethane coating with 5mg (0.75 wt%) A1. c: polyurethane coating with 10mg (1.50 wt%) A1. d: polyurethane coating with 15mg (2.25 wt%) A1. e: polyurethane coating with 5mg (0.75 wt%) A2. f: polyurethane coating with 10mg (1.50 wt%) A2. g: polyurethane coating with 15mg (2.25 wt%) A2.

3.3 Further investigation of photocatalytic activity

In order to better understand the effect of SiO_2 on the photoactivity of the anatase form of SiO_2 to $TiO_2(A)$ nanoparticles, UV-Vis spectra were examined (Figure 3.9). With the SiO_2:TiO_2 weight ratio equal to 3.25:100, the A3 sample has a higher UV absorbance than the unmodified anatase form of TiO_2 due to the decrease of agglomeration (as observed by DLS). When the SiO_2:TiO_2 weight ratio was increased to 6.50:100, most of the surface of TiO_2 is covered by SiO_2 and few electron-hole pairs are able to contact with the aqueous solution, leading to the observed decreasing of photocatalytic activity. Moreover, with almost all the TiO_2 surface is covered, the agglomeration effect became lowest which was confirmed in Table 3.2. Meanwhile, without the blockage of UV light due to the thin layer, the nanoparticle A2 shows the highest UV absorbance. With higher SiO_2:TiO_2 weight ratios, the thickness of the SiO_2 layer became higher. This thicker layer led to some of the UV radiation being diffracted [159], leading to the observed lower UV absorbance and resulting in a lower observed photocatalytic activity. Other studies have also shown that a thicker SiO_2 layer lowers the photocatalytic activity, which is similar to the results found in this study [159, 228].
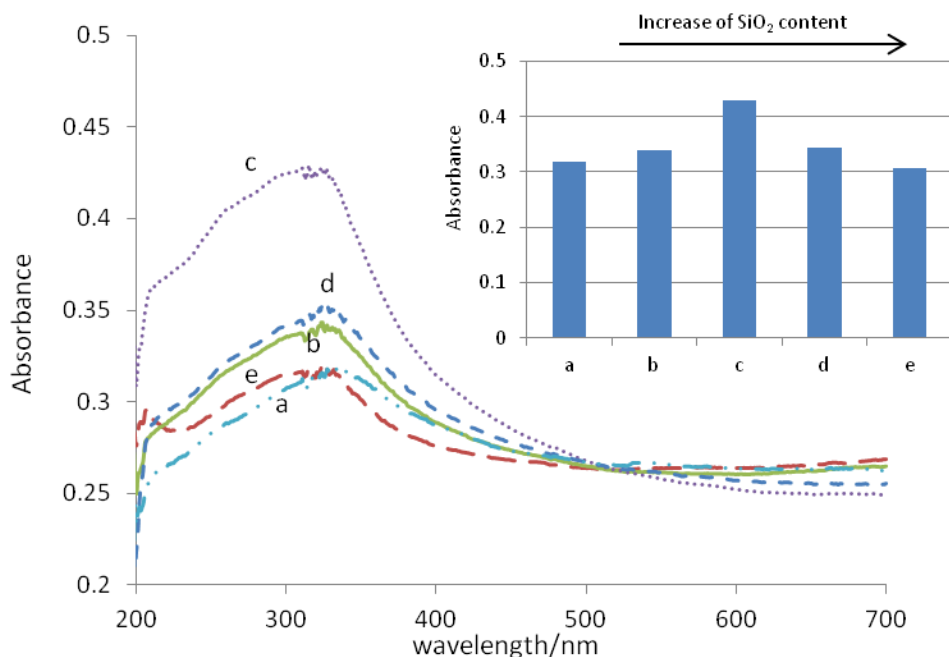
Figure 3.9. UV-Vis spectra of varying SiO_2 (wt. %) coated TiO_2 (A). a: 0. b: 3.25. c: 6.50. d: 9.75. e: 13.0.

The photoluminescence emission spectra were further studied to examine the formation of hydroxyl radicals during the photochemical reactions to provide insight into the photocatalytic mechanism [132]. Figure 3.10 and 3.11 demonstrate the formation of hydroxyl radicals using the experimental SiO_2 coated TiO_2 photocatalysts with terephthalic acid as the fluorescent probe. The highly fluorescent product 2-hydroxyterephthalic acid is formed when terephthalic acid and hydroxyl radicals react. Without the presence of photocatalyst, no peak was observed indicating no hydroxyl radicals were formed [132]. With the photocatalysts containing TiO_2 (A), a peak at 425nm was observed indicating the formation of hydroxyl radicals [132]. The increased emission count from the prepared photocatalysts corresponds to the enhanced photocatalytic testing results. However, the emission counts difference is rather low as the photodegradation data between

sample A0 and A3, which is because of the terephthalic acid being photodegradable and has a higher degradation rate in the presence of higher photoactivity catalyst which is A3 compared to A0 [230]. This can be confirmed by the spectra of catalysts with rutile form TiO_2 (SI 3.6). During illumination, the rutile TiO_2 produce hydroxyl radicals without performing degradation reaction, which generally observed as photoprotection behavior, leading to the highest counts compared to all other photocatalysts containing anatase TiO_2. When the SiO_2-TiO_2 nanoparticles were embeded into the polyurethane coatings, the photoluminisence results of these coatings show a similar trend to the nanoparticles themselves (Figure 3.11), which was confirmed by the methylene blue decomposition data.
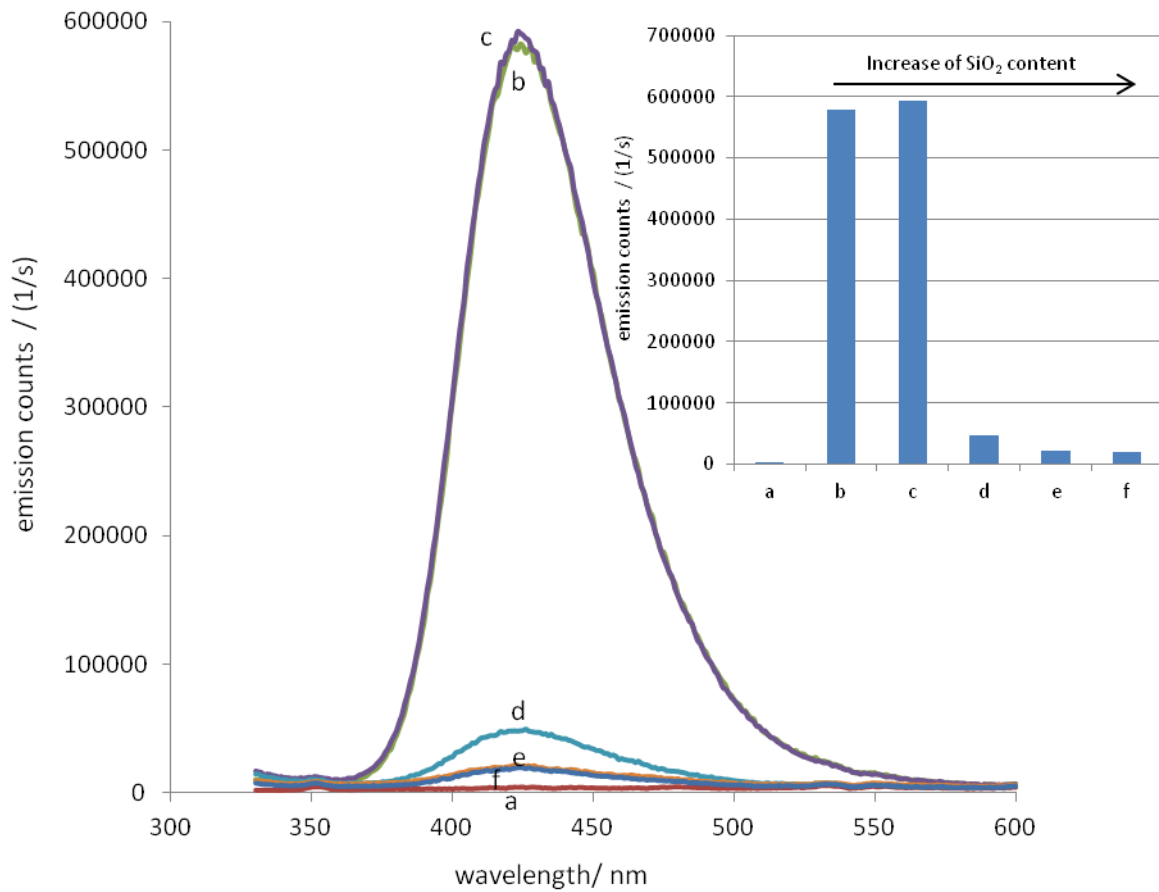
Figure 3.10. Photoluminescence spectra of SiO_2-TiO_2(A) nanoparticles varying SiO_2 content (wt. %) (basic solution under full light illumination of 1 sun for 10 min). a: blank. b: 0. c: 3.25. d: 6.50. e: 9.75. f: 13.0.
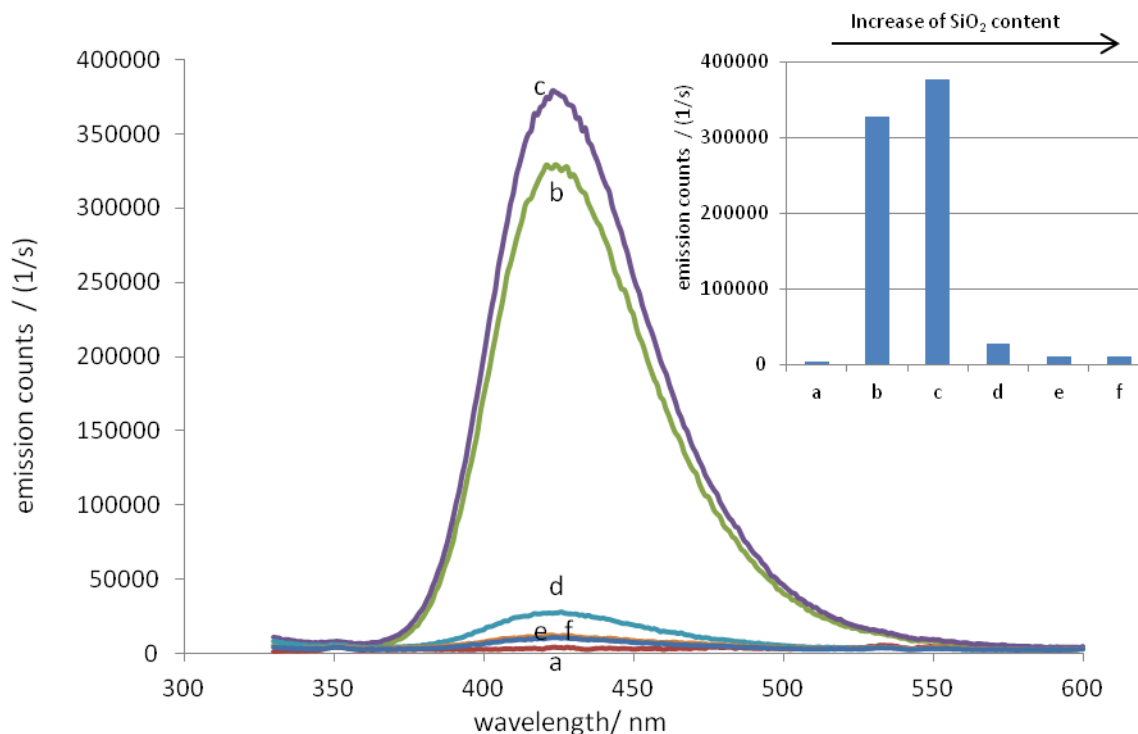
Figure 3.11. Photoluminescence spectra of polyurethane /SiO_2-TiO_2(A) nanocomposites varying nanoparticles (basic solution under full light illumination of 1 sun for 10 min). a: blank. b: A0. c: A1. d: A2. e: A3. f: A4.

3.4 Physical and Mechanical Properties of SiO_2-TiO_2 polyurethane coatings

The hydrophobicity of SiO_2-TiO_2 nanoparticles embedded into the polyurethane coatings was studied in order to better understand how the NPS are dispersed into the PU matrix. The contact angle was examined both before and after 10 min of $0.04W/cm^2$ UV light irradiation at 365nm wavelength. Before UV irradiation, the polyurethane blank sample is the most

hydrophobic (Figure 3.12 A and B) compared to the other experimental coatings. This is attributed to the additional hydroxyl groups introduced by silica on the titania NP surface as confirmed by FTIR (see SI 3.5). These hydrophilic nanoparticles being hydrophilic will have a tendency to phase separate to the surface. As previously shown, anatase TiO_2 is more hydrophilic than rutile TiO_2 [231], which is because in the anatase TiO_2 structure, H_2O molecules tend to coordinate to Ti^{4+} rather than H-bond to titanol (Ti-OH) [231]. The contact angle of polyurethane samples with anatase TiO_2 was lower than those with rutile TiO_2, confirming this effect was maintained when the nanoparticles were integrated into the polyurethane structure. When SiO_2 was coated onto the surface of anatase TiO_2, the strong coordination of H_2O and coordinatively unsaturated Ti^{4+} are decreased and the coating becomes more hydrophobic. However, when SiO_2 was coated onto the surface of rutile TiO_2, the contact angle first drops then increases, which is attributed to the additional hydroxyl groups on the surface of SiO_2. After UV irradiation, the contact angles of all samples decreases due to the formation of oxides during the UV degradation of the PU. As the anatase TiO_2 is working as photocatalyst, the contact angle decreases more significantly than that of rutile TiO_2, which is contributed from the formation of oxides [232]. Compared with polyurethane coatings with no nanoparticles, the embedded nanoparticles maintained the hydrophobicity of the polyurethane film after UV irradiation. Moreover, with an increased loading of nanoparticles in the coatings, the contact angle increased both before and after the UV irradiation (Figure 3.12 C, D).
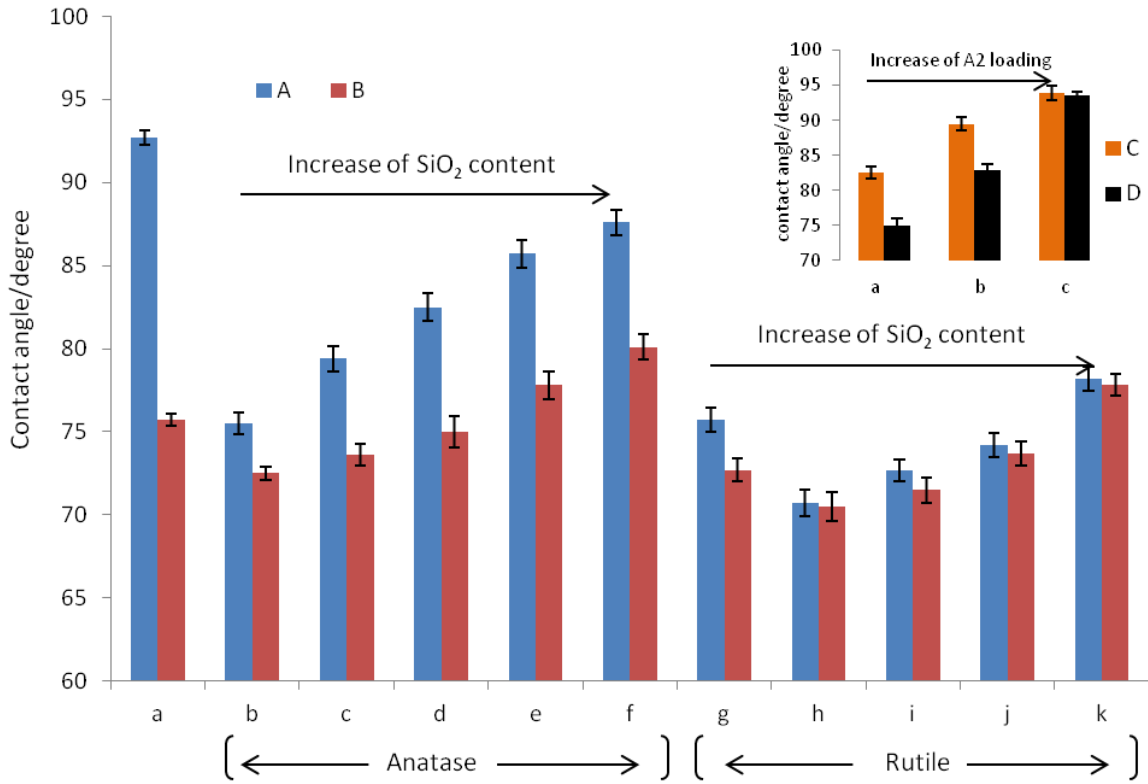
Figure 3.12. Comparison of contact angle of polyurethane coatings embedded with different SiO$_2$-TiO$_2$ nanoparticles before (A) and after (B) 10 min UV irradiation. Anatse TiO$_2$ (a: blank. b: A0. c: A1. d: A2. e: A3. f: A4.) Rutile TiO$_2$ (g: R0. h: R1. i: R2. j: R3. k: R4.) Comparison of contact angle of polyurethane coatings embedded with varying loadings of A2 before (C) and after (D) 10 min UV irradiation. a: 5mg (0.75 wt%). b: 10mg (1.50wt%). c: 15mg (2.25wt%).

In order to examine the mechanical strength of the prepared composites for potential applications in coatings, ASTM D882 method was used. The results (Figure 3.13) indicate that by adding anatase TiO$_2$ or rutile TiO$_2$, the Young's Modulus is initially lower than that of the PU raw coating. This is attributed to the anatase TiO$_2$ or rutile TiO$_2$ decreasing the adhesion between

the nanofillers and the polyurethane matrix as previously described[233]. Since the rutile TiO_2

tends to agglomerate more than anatase TiO_2, the weakened effect appears to be more obvious.

However, with an increasing amount of SiO_2 introduced into the system, the chemical linkage

between silica and the PU polymer becomes stronger, leading to a higher Young's Modulus [234].

Meanwhile, with increased loading of nanoparticles into the coatings, due to the additional

chemical linkage between the nanoparticles and polymer matrix, the Young's Modulus was found

to subsequently increase (Table 3.3).
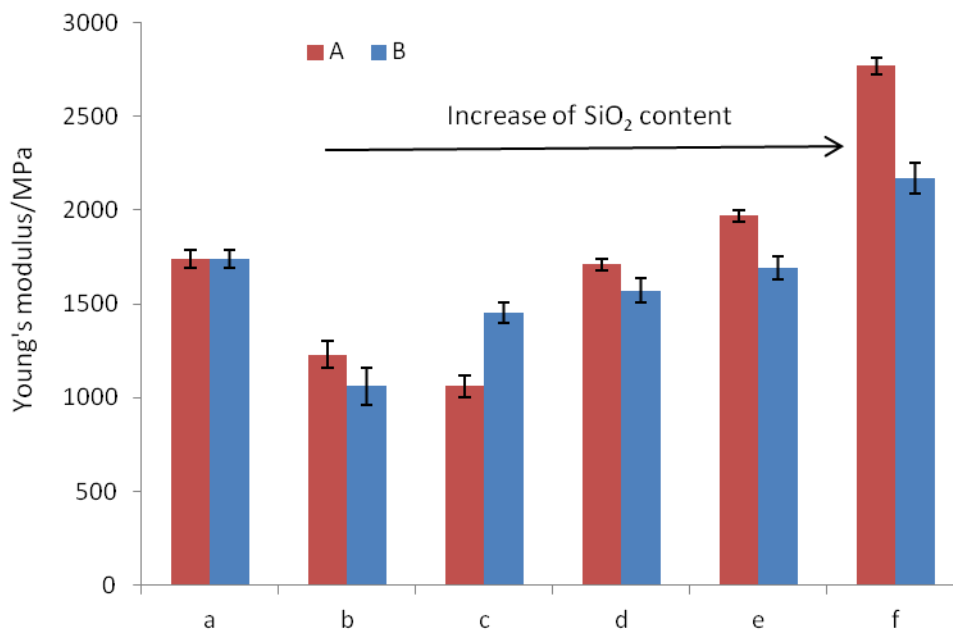
Figure 3.13. The comparison of Young's Modulus of polyurethane films with varying (A)

SiO_2-TiO_2 (A) nanoparticles. a: blank. b: A0. c: A1. d: A2. e: A3. f: A4. (B) SiO_2-TiO_2 (R)

nanoparticles. a: blank. b: R0. c: R1. d: R2. e: R3. f: R4.

Table 3.3. The comparison of Young's Modulus of polyurethane films with varying loadings of

A2.

Varying loading A2	0.75 wt%	1.50 wt%	2.25 wt%
Young's Modulus / MPa	1710±30	1870±42	2220±33

3.5 Thermal behavior of SiO_2-TiO_2 polyurethane coatings

As previous work with SiO_2 encapsulated quantum dots showed, SiO_2 encapsulation can influence thermal conductivity and vary with the amount of SiO_2 integrated into the polymer system[235]. The thermal conductivity of polymer films can be measured according to Hoosung Lee's work[236]. The thermal conductivity results (Figure 3.14) show that integrating TiO_2 based nanoparticles into the polyurethane matrix generally increases the thermal conductivity due to increase heat transfer through the solid nanoparticles[154]. However, due to the size of the anatase TiO_2 nanoparticles being smaller than that of rutile TiO_2 nanoparticles, the polyurethane coatings possess higher thermal conductivity because of their smaller size[237]. Moreover, the SiO_2 will significantly decrease the thermal conductivity with an increasing amount on the surface of TiO_2, which has the same result with previous studies about doping TiO_2 into silica[238]. These results by varying the SiO_2 layer thickness on the titania surface likely provide increased void space and increased porosity in the polyurethane coatings[154]. Moreover, when the SiO_2:TiO_2 ratio was beyond the 13.0:100, the thermal conductivity of polyurethane coatings is even lower than the polyurethane raw materials. In addition, after 10 min of 0.04W/cm^2 UV light irradiation at 365nm wavelength, the thermal conductivity stays the same.
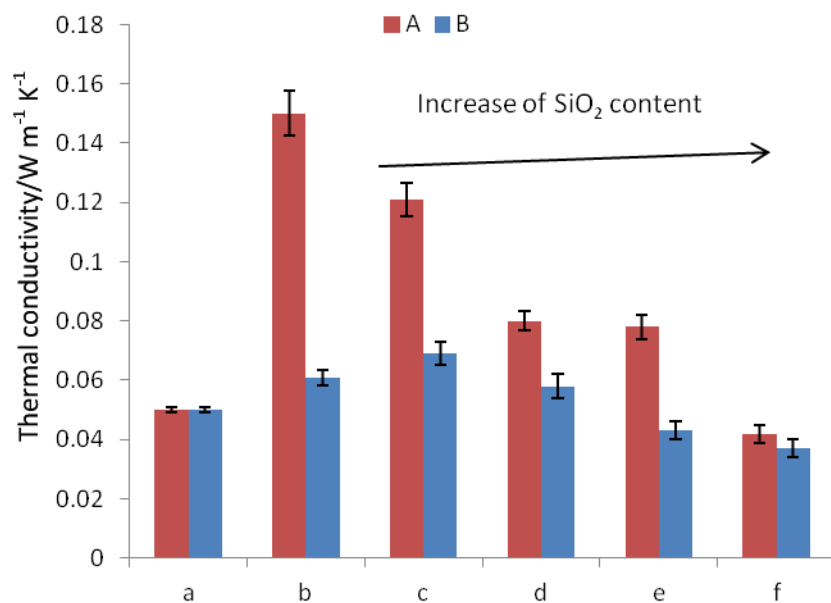
Figure 3.14. The thermal conductivity of polyurethane films with varying (A) Anatase based

nanoparticles. a: blank. b: A0. c: A1. d: A2. e: A3. f: A4. (B) Rutile based nanoparticles. a: blank

PU. b: R0. c: R1. d: R2. e: R3. f: R4.

5% weight loss is a general method for determining the thermal stability of polymer [239,

240]. In this study, the thermal stability of polyurethane nanocomposites were determined via 5%

weight loss measured by TGA. With more of the SiO_2 coated onto the surface, the polyurethane

nanocomposites become more thermal stable until a certain point, then with more SiO_2 on the

surface, the polyurethane nanocomposites become less thermal stable. These changes are mainly

attributed to both the nanoparticle structure and how they are integrated into the polymer

composite. With less SiO_2 coated on the surface, the structure of SiO_2 layers tend to be more

close to the core TiO_2 crystal structure and be more stable with less heat transfer. Then with more

SiO_2 coated onto the surface, the structure of SiO_2 layers tend to form more amorphous structure

which would be less stable with more heat transfer.

Table 3.4. The temperature of 5% weight loss of polyurethane/SiO$_2$-TiO$_2$ nanocomposite

coatings under air.

Sample	PU	PU/A0	PU/A1	PU/A2	PU/A3	PU/A4
Temperature /°C	234.1	235.3	246.0	242.2	233.5	220.3
Sample	PU	PU/R0	PU/R1	PU/R2	PU/R3	PU/R4
Temperature /°C	234.1	234.9	240.1	252.0	238.8	221.1

4. Conclusions

SiO$_2$ was successfully coated onto the surface of anatase and rutile TiO$_2$ by using a modified

Stöber process. With different loadings of SiO$_2$ on the surface of TiO$_2$, the photoactivity of

anatase form and rutile form TiO$_2$ could be modified to control both photoactivity and

photosensitivity. With a loading weight of SiO$_2$ < 3.25 wt%, the photocatalytic activity of anatase

TiO$_2$ was enhanced with a reduction of agglomeration, while the rutile form TiO$_2$ was tuned to be

photocatalytic due to light diffraction from the full coverage of SiO$_2$ on the surface. For loadings

beyond 3.25wt%, the photocatalytic activity of anatase TiO$_2$ decreases and rutile TiO$_2$ stays the

same. When applied in polyurethane coatings, with an increasing amount of SiO$_2$ on the surface,

the contact angle was increased from 75° to 87° for anatase form and 70° to 78° for rutile form. The Young's Modulus was also increased from 1.06GPa to 2.77GPa for anatase form and 1060MPa to 2170MPa for rutile form. The thermal insulation property of polyurethane coatings is successfully enhanced by encapsulating SiO_2 on the surface of TiO_2 with the thermal conductivity from 0.15 to 0.042 $W \cdot m^{-1} K^{-1}$ for anatase form and 0.069 to 0.037 $W \cdot m^{-1} K^{-1}$ for rutile form.

Chapter 4. SiO$_2$ Encapsulated TiO$_2$ nanotubes and nanofibers for Self-Cleaning Polyurethane Coatings

Abstract: TiO$_2$ nanofibers and nanotubes are of great interest due to their high specific areas, defined dimensions and enhanced photocatalytic activity. In order to prevent the aging from weakening the mechanical strength of polymer coatings with self-cleaning ability, in this work, the effect of thin layers of SiO$_2$ deposited onto the surface of titania nanostructures, both before and after integration into polyurethane nanocomposites, is investigated. TiO$_2$ nanofibers were synthesized via an environmental friendly supercritical CO$_2$ method and the TiO$_2$ nanotubes were synthesized by a conventional hydrothermal reaction. SiO$_2$ was added using a modified Stöber approach. The results showed that with more SiO$_2$ coated onto the nanofibers' surface, the photocatalytic activity, UV absorbance, and hydroxyl radical formation decreased due to the shielding effect of the SiO$_2$ layers. Polyurethane coatings integrating these nanofibers and nanotubes exhibited similar photoactivity trends as the individual nanostructures. Moreover, the mechanical strength of the composites was enhanced and protected from aging under UV light. The hydrophobicity of coatings was prevented from changing under UV irradiation by addition of these silica encapsulated 1D titania structures.

Keywords: SiO$_2$, TiO$_2$, Nanofiber, Nanotube, Polyurethane

1. Introduction

Nanotubes and nanofibers are one-dimensional (1D) nanostructures which provide high specific surface areas and high mechanical strength[96, 101]. They have helped inspire the nanotechnology field and trigged many efforts in the field of physical, chemistry, and material science. Carbon is still the most common material in preparing 1D geometry nanomaterials[241, 242]. However, other materials such as transition metal oxides have been synthesized in 1D geometry[243, 244]. In recent years, 1D nanostructures based on TiO_2 have attracted much attention due to their often enhanced photocatalytic properties in specific crystal structures, i.e. anatase and rutile[102-104]. Shape-controlled synthesis is a method developed recently to enhance the catalytic effect of TiO_2 nanostructures[98]. Synthesizing TiO_2 nanotubes or nanofibers instead of TiO_2 nanoparticles is a promising method similar to shape-control to alter the photocatalytic activity [96, 97].

Generally, there are three common methods to synthesize TiO_2 nanotubes, i.e. template preparation[117, 118], anodic oxidation[119], and chemical processing[120]. In the template preparation method, the size and morphology of nanotubes are mainly dependent on the template, which are hard to maintain their shape when separated from the template. Anodic oxidation is able to synthesize nanotubes with similar sizes but relatively larger diameters-with smaller diameters being of more scientific interest. Chemical processing such as hydrothermal is the classic method for preparing nanotubes with the smallest size, with the hydrothermal conditions controlling the mesoporous structure of nanotubes[121].

TiO$_2$ nanofibers are commonly prepared via hydrothermal method[122], electrospinning[123, 124], and the sol-gel method[97, 125]. Using supercritical CO$_2$ as an environmentally functional solvent, our group has demonstrated the synthesis of TiO$_2$ nanofibers[97]. Supercritical CO$_2$ has attracted considerable attention recent years due to its lack of solvent residue, inexpensive nature, nontoxic, and negligible surface tension, which makes it an ideal for nanomaterial synthesis [97, 126, 127].

Titania can be modified by doping with various elements including N, C, Fe [128-130], and depositing with other metal oxides [131-133]. However, there is a lack of investigation of SiO$_2$'s effect on nanotubes and nanofibers. In our previous study, SiO$_2$ was successfully coated onto the surface of TiO$_2$ nanoparticles, reducing their agglomeration while enhancing their photocatalytic activity. Due to their high photocatalytic activity under UV light, TiO$_2$ is ideal for preparing self-cleaning coatings with polymer especially polyurethane [198, 245, 246]. In this study, TiO$_2$ nanofibers and nanotubes will be encapsulated with SiO$_2$ via the Stöber process [146, 148]. The self-cleaning property of the prepared nanostructures integrated polyurethane coatings and the effect of SiO$_2$ layers on these coatings is investigated while measuring the composites physical and mechanical properties.

2. Materials and Experiments

2.1 Materials. Alkyltrimethylammonium bromide (C16TAC) (Sigma Aldrich, $\geqq$95%), tetraethoxysilane (TEOS) (Sigma Aldrich), methanol (Caledon, Ontario, Canada), 28% aqueous ammonia solution (Caledon, Ontario, Canada), anatase TiO$_2$ (Sigma Aldrich, <25nm, 99.7%),

sodium hydroxide (ACP, 97%), titanium isopropoxide (Sigma Aldrich, 97%), acetic acid

(Caledon, Ontario, Canada, 99.7%), poly aspartic ester (Bayer MaterialScience), poly

hexamethylene diisocyanate (Bayer MaterialScience), isophorondiamine - isobutyraldimine

(Bayer MaterialScience), methylene blue (Caledon, Ontario, Canada).

2.2 Synthesis Procedure. The synthesis of TiO_2 nanotubes followed the classic hydrothermal

reaction[247]. 10 g of anatase TiO_2 was sonicated dispersed in a 250 mL round bottom flask

containing 100 mL of 10M NaOH solution. The solution was then stirred at 110°C in an oil bath

for 20 h. After that, the product was washed repeatedly with distilled water and 0.1M HCl

solution until the pH reached 7. The final product was then calcined at 200°C for 2h.

Synthesis of TiO_2 nanofibers were preparing in supercritical CO_2 as previously reported [97].

10.6g Titanium isopropoxide and 8.13 mL Acetic Acid (TIP to acetic acid molar ratio 1.5:6.1)

were mixed into the 25 mL autoclave reactor. The reaction was performed at 60°C at 6000psi

with continuous stirring for 3 h. Then the product was aged for 3 days followed by 3 days of

washing with 0.5 mL/min CO_2. The final product was then calcined at 400°C for 1 hour.

SiO_2 encapsulated TiO_2 nanostructures were performed using the classic Stöber process[146].

During this experiment, 0.1 g of TiO_2 nanotubes or nanofibers were dispersed in 5 mL of

methanol solution and sonicated for 30 minutes to form Solution A. Then in 10 mL of methanol

solution, 0.02g of C16TAC surfactant, 1.8g of deionized water, 0.7g of 28% aqueous ammonia

solution were mixed to form solution B. After that, different amounts (20mg, 40mg, 60mg) of

TEOS was added to solution B, and therefore the weight ratio of SiO_2 and TiO_2 were 5.40:100,

10.8:100, and 16.2:100 respectively. Finally, solution A was poured into solution B, followed by

continuous stirring for 24 h. The product was centrifuged and then washed with methanol

repeatedly, and dried in a vacuum oven at 50°C for 48 h. The polyurethane coatings were then

made with the weight ratio of SiO_2-TiO_2: polyol mixture (with weight ratio of poly aspartic ester

: isophorondiamine - isobutyraldimine equal to 4 : 1) : poly hexamethylene diisocyanate equal to

5 : 425 : 250. The SiO_2-TiO_2 nanoparticles were first physically mixed with polyol mixture and

then dispersed in acetone solution, then poly hexamethylene diisocyanate was mixed with the

solution and cured in Teflon plates. After complete evaporation of the acetone solution, thin

layers of coating were formed.

Step 1. Synthesis of SiO_2-TiO_2 nanostructures
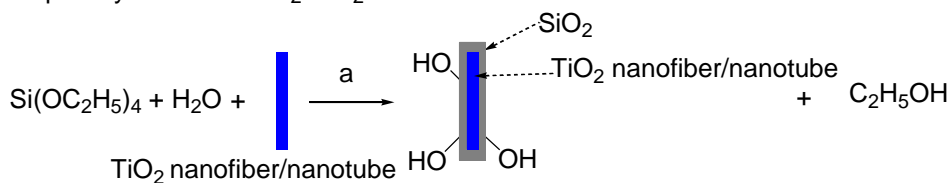
Step 2. Synthesis of PU/SiO_2-TiO_2 nanocomposites
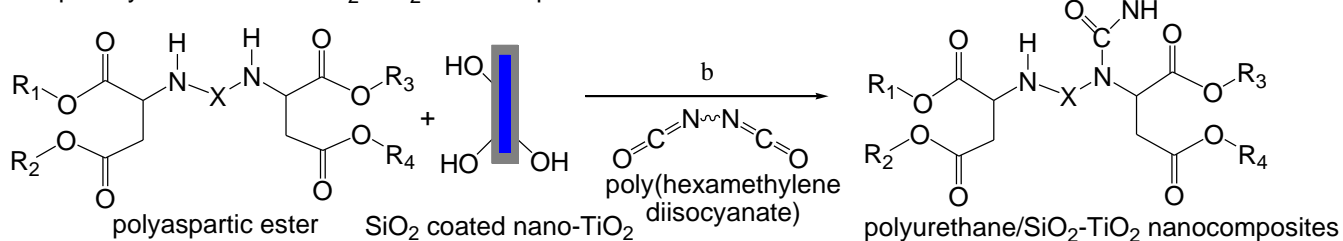
R_1, R_2, R_3, R_4 are the same or different and represent an alkyl group having at least two carbon atoms.

X:
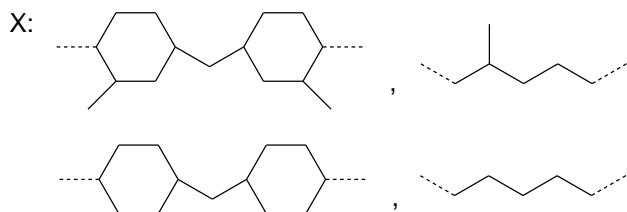
Scheme 4.1. Schematic diagram of the synthesis of SiO_2-coated TiO_2 nanostructures and the

preparation of polyurethane/SiO_2-TiO_2 nanocomposites. (a) room temperature in methanol

solution; (b) room temperature with catalyst.

2.3 Characterization. Photoactivity of polyurethane coatings were measured following a standard method developed by the International Organization of Standardization (i.e. ISO/DIS 10678). The photoactivity of the as-prepared SiO_2-TiO_2 nanostructures were tested in 20 mL 1ppm methylene blue solution with 10mg of catalyst in a light simulator (Luzchen ICH1) for 0.635 w/m^2 UV irradiation. The methylene blue concentration was measured after 5, 10, 15, 20, 25, and 30 minutes of irradiation. To examine the radicals formation during the photocatalytic reaction, 10mg SiO_2-TiO_2 nanostructures were mixed with 20 mL solution containing 3×10^{-4}M terephthalic acid and 2×10^{-3}M sodium hydroxide [221] under the illumination of full light (1 Sun). Then the photoluminescence emission at 425 nm excited with 315 nm was observed [222]. Brunauer–Emmett–Teller (BET) surface area analysis was performed by a Micromeritics TriStar II 3020 instrument at 77 K. Prior to the N_2 physisorption, the sample was degassed at 100℃ under vacuum for 5 h. FTIR spectra were obtained using a Nicolet 6700 spectrometer in the range of 400-4000cm-1 and was operated using 32 scans at 4cm-1 resolution for each sample. The absorbance in the Ultraviolet range and band gap energy was tested and calculated through UV-Vis measurements which were conducted using a Shimadzu UV-3600. Scanning Electron Microscopy (SEM) was performed on the experimental nanoparticles using a Hitachi S-4500 field emission SEM. All samples were taken at 10 kV at varying magnifications for different views. Energy Dispersive X-ray (EDX) was taken using a LEO (Zeiss) 1540XB. Contact angles were measured using a PGX Measuring Head. Young's modulus was taken follow ASTM D882 method using an Instron 5943.

3. Results and Discussions

3.1 SiO_2 Encapsulation of TiO_2 nanofibers and nanotubes

In order to determine the morphology change after the SiO_2 encapsulation on the surface of TiO_2 nanofibers and nanotubes, SEM imaging was performed. Through Figures 4.1 and 4.2, there are significant SiO_2 layers appearing on the surface of TiO_2 nanofibers while they are not so significant on the surface of TiO_2 nanotubes, attributed to the relevantly high surface area of nanotube comparing with nanofiber (BET analysis revealing that the surface area of TiO_2 nanofiber is 85.8 m^2/g while the surface area of TiO_2 nanotube is 358 m^2/g). With the increasing loading of TEOS, the SiO_2 on surface become more and more obvious, and with the highest loading amount, nanotubes are observed to be covered by SiO_2. Also from the EDX analysis (Table 4.1), the ratio of SiO_2 to TiO_2 which calculated from the EDX data is quite close to what we introduced based on the stochiometric ratio.

Table 4.1. SiO_2:TiO_2 weight ratio stoichiometric and calculated through EDX data.

Type of Material	TiO_2 nanofiber		
Stoichiometric Ratio	5.40:100	10.8:100	16.2:100
EDX Ratio	5.36:100	10.7:100	14.1:100
Sample name	F1	F2	F3
Type of Material	TiO_2 nanotube		
Stoichiometric Ratio	5.40:100	10.8:100	16.2:100
EDX Ratio	4.81:100	10.5:100	16.1:100

Sample name	T1	T2	T3
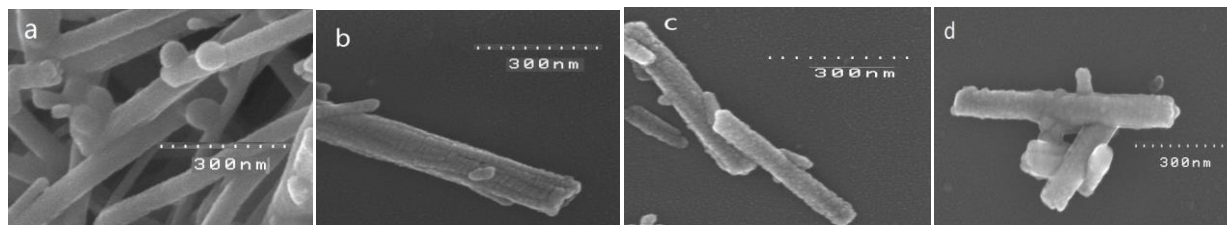
Figure 4.1. SEM images of surface morphology of SiO_2-TiO_2 nanofibers. (a) F0 (TiO_2 nanofiber); (b) F1; (c) F2; (d) F3.
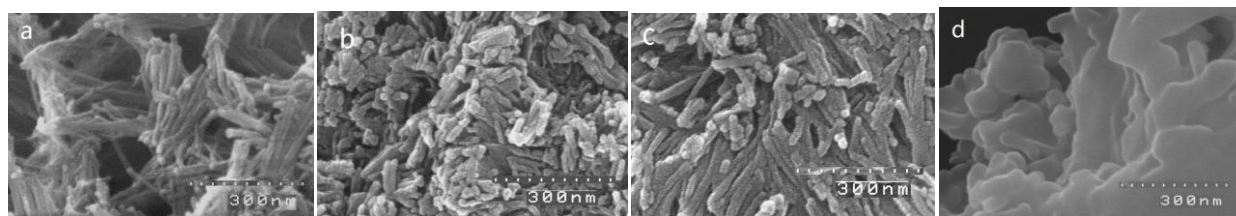
Figure 4.2. SEM images of surface morphology of SiO_2-TiO_2 nanotubes. (a) T0 (TiO_2 nanotube); (b) T1; (c) T2; (d) T3.

From the FTIR spectra (Fig. 4.3), the absorbance at 1058 cm^{-1} from the SiO_2 spectra is the significant peak of stretching bond Si-O [156]. There is a significant peak appearing in the spectrum of SiO_2-TiO_2 at 1062 cm^{-1} for TiO_2 nanofibers and at 1041 cm^{-1} for the TiO_2 nanotubes. With increasing loading of TEOS, the height of this peak increased indicating increased SiO_2 coating onto the surface of TiO_2. The significant peaks at 953 cm^{-1} for TiO_2 nanofibers and 918 cm^{-1} for TiO_2 nanotubes suggested that on the surface of TiO_2, there is chemical bonding between SiO_2 and TiO_2 which appears to be Ti-O-Si [156]. With more loading of TEOS on the surface, leading to higher SiO_2:TiO_2 ratio's (Table 4.1), the height of the significant peak is

increasing, indicating more SiO_2 depositing on the surface of TiO_2.
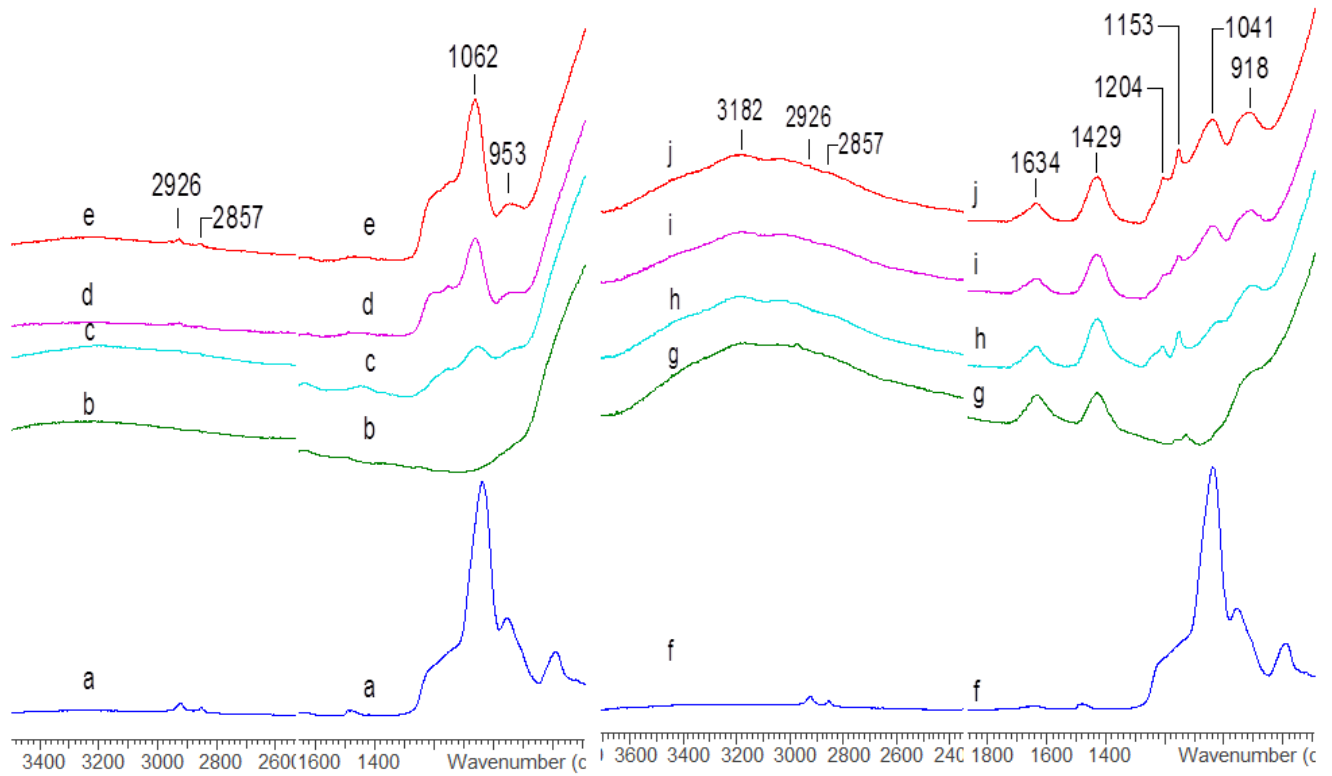
Figure 4.3. FTIR spectra of SiO_2-TiO_2 nanofiber & nanotube. (a) SiO_2; (b) F0; (c) F1; (d) F2; (e) F3; (f) SiO_2; (g) T0; (h) T1; (i) T2; (j) T3.

Through the XRD images (Figure 4.4a), peaks from both the anatase and the rutile phases were observed in the TiO_2 nanofiber. However, the peaks related to anatase phase are much higher than that of rutile phase due to the utilized calcination temperature of 400°C we performed, since at 400°C TiO_2 tends to form anatase structure. Previous study shows that with calcinations temperature higher than 380 °C, TiO_2 nanofiber will form anatase structure [97], enhancing photocatalytic activity. From Figure 4.4b, several significant peaks of TiO_2 nanotubes are confirmed to be the same as previous studies[248], which complied with the trititanate

nanotube model, $Na_2Ti_3O_7$ or $H_2Ti_3O_7$. Since the nanotubes were washed with 0.1M HCl solution and Na^+ was replaced with H^+, the basic structure of nanotube would be $H_2Ti_3O_7$. As the SiO_2 percent is fairly small compared with TiO_2, individual peaks amorphous SiO_2 which indicated in Figure 4.4c are not observed from XRD patterns of SiO_2-TiO_2 nanofibers and nanotubes.
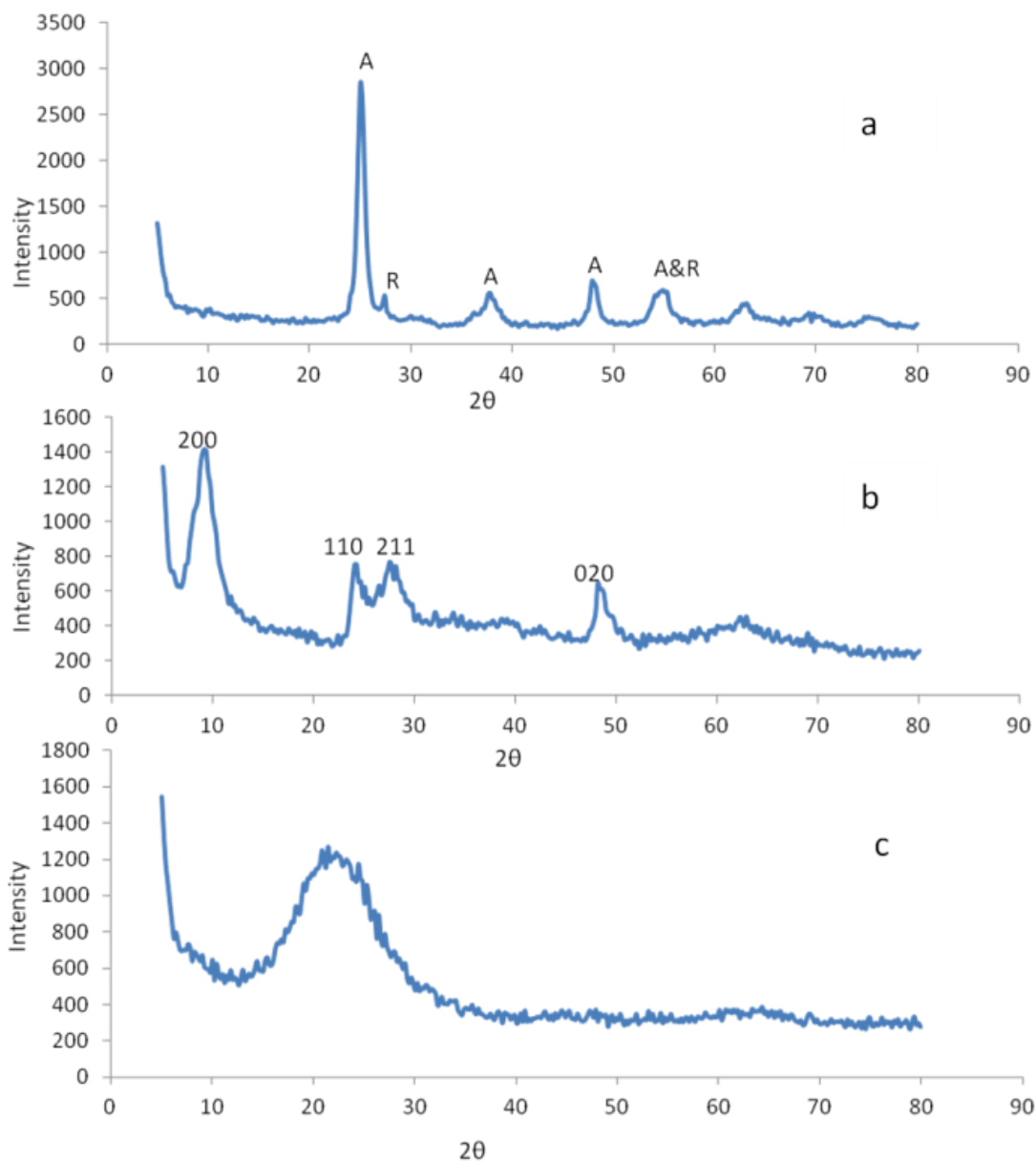
Figure 4.4. XRD patterns of (a) TiO_2 nanofibers; (b) TiO_2 nanotubes; (c) SiO_2.

When the SiO_2 encapsulated titania nanostructures were reacted with monomer to form

the polymer coatings as shown in Scheme 4.1, the coatings were also examined by FTIR.

According to the FTIR spectra of polyurethane nanocomposites shown in Figure 4.5, there is no

stretching of isocyanate group NCO peak at 2270 cm^{-1} [226] which appears on poly

hexamethylene diisocyanate (4.5b). This indicates complete reaction of the isocyanate

component. In addition, the absorbance at 1686cm^{-1} is the urea –C=O vibration, which indicates

no polyisocyanate residue and a complete formation of polyurethane structure using the

described reaction conditions. Figure 4.6 demonstrates the distribution of nanoparticles in

polyurethane matrix using SEM microscopy. It clearly shows that with the SiO_2 coated onto the

surface, the nanoparticles are distributed better throughout the polyurethane matrix. We attribute

this to both enhanced compatibility between SiO_2 and the polyurethane matrix and to chemical

bonding between the silica shell and the polyurethane as shown in Scheme 4.1.
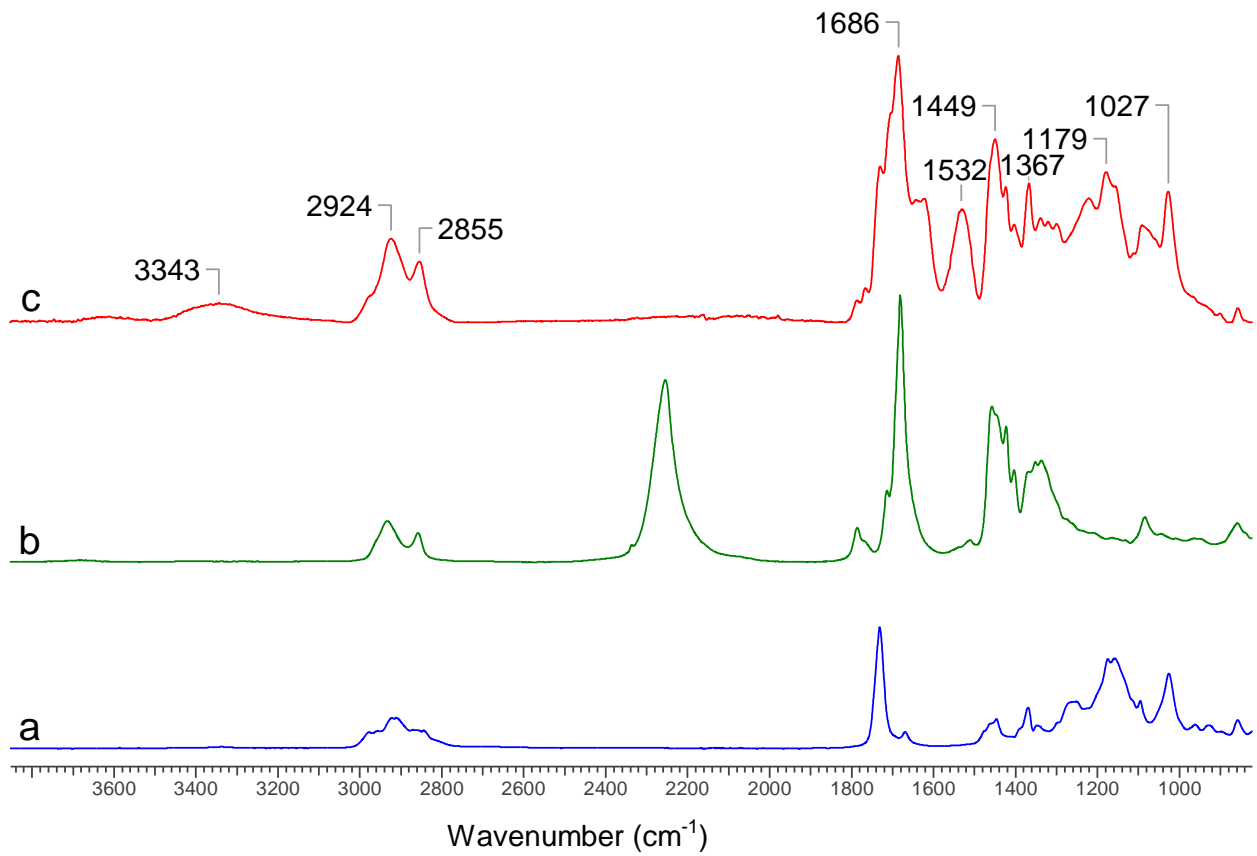
Figure 4.5. FTIR spectra of (a) poly aspartic ester; (b) poly hexamethylene diisocyanate; (c) polyurethane with 15 mg F1.
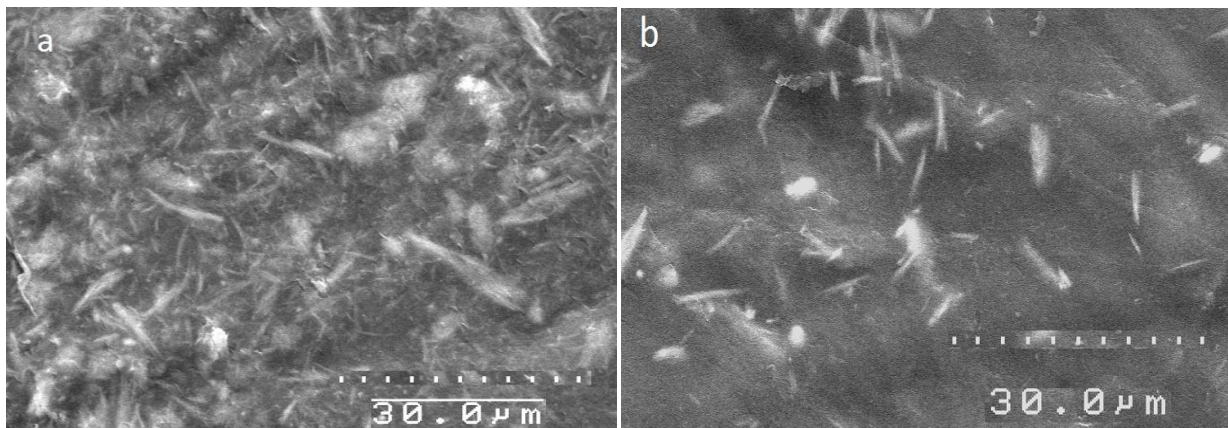
Figure 4.6. SEM images of PU nanocomposites with different nanoparticles. (a) F0; (b) F2.

3.2 Photocatalytic activity of SiO_2-TiO_2 nanostructures and polyurethane nanocomposites

With the SiO_2 coated onto the 1D titania's surface, the photoactivity will be affected. From the photoactivity tests performed through the methylene blue solution, the photoactivity of SiO_2-TiO_2 nanofibers is less active with increased amounts of SiO_2 addition (Figure 4.7). The TiO_2 nanofibers without SiO_2 coating possessed the highest photoactivity, with the photoactivity becoming lower due to the increased amounts of silica. This is attributed to the shielding effect of SiO_2 which blocks the UV irradiation and transfer of electrons to the coating surface to form hydroxyl radicals. These effects are confirmed as later discussed for UV-Vis spectra (Figure 4.10) and photoluminescence spectra (Figure 4.11). Due to the low calcination temperature (200°C, higher calcination temperatures were found to lead to nanotube structure collapse, see SI 4.3), the photoactivity of TiO_2 nanotubes is lower than that of the TiO_2 nanofibers and exhibits weak photocatalytic activity, which has been confirmed by other studies [249, 250]. With SiO2 coated onto the surface, the photoactivity is slightly more active at first (Figure 4.8) which is attributed to the SiO_2 thin coatings diffracting and absorbing more UV light due to the high specific surface area of nanotubes. However, for the SiO_2-TiO_2 nanostructures with ratio's higher than 5.4:100, the photoactivity turned to be lower than previous ones, which is attributed to enhanced coverage of SiO_2 preventing the absorbance of UV light.
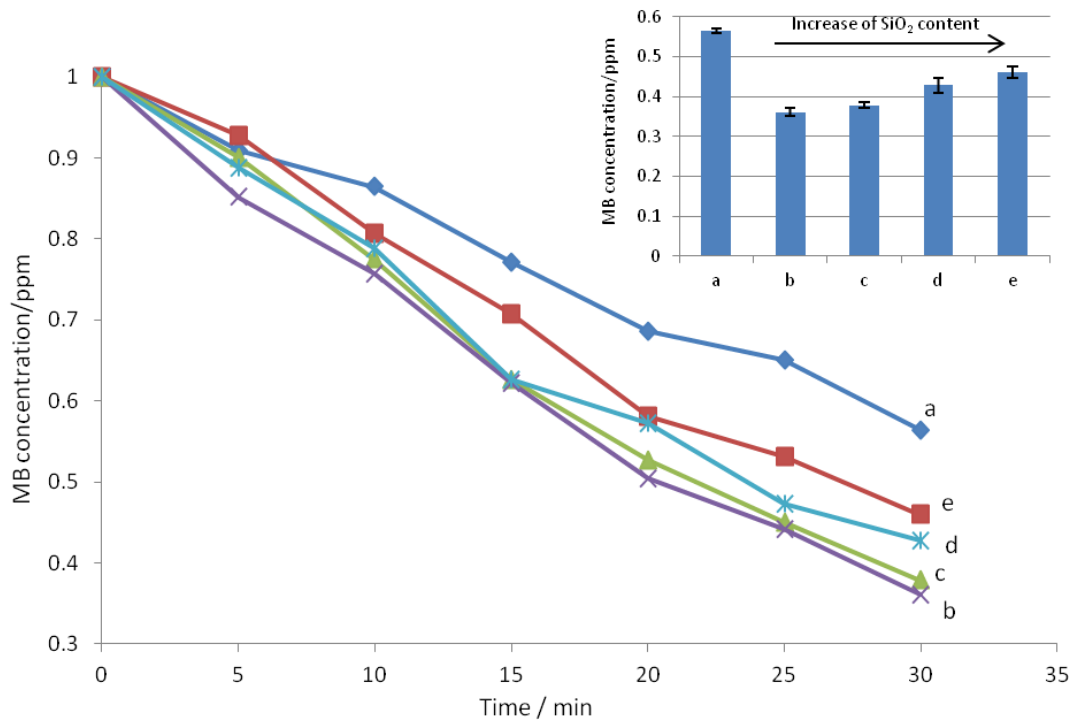
Figure 4.7. The photoactivity of SiO_2-TiO_2 nanofibers of varying SiO_2 content (wt. %) (1 ppm methylene blue solution with light intensity of 0.635 W/m^2). (a) blank (no TiO_2); (b) 0; (c) 5.40; (d) 10.8; (e) 16.2.
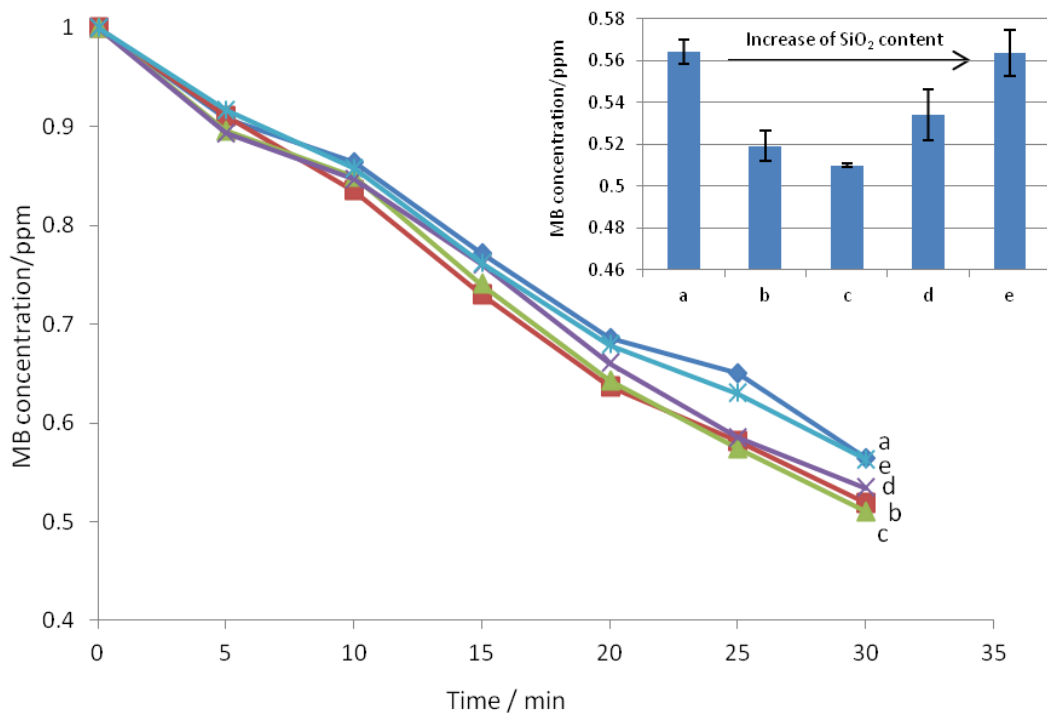
Figure 4.8. The photoactivity of SiO_2-TiO_2 nanotubes varying SiO_2 content (wt. %) (1 ppm methylene blue solution with light intensity of 0.635 W/m^2). (a) blank (no TiO_2); (b) 0; (c) 5.40; (d) 10.8; (e) 16.2.

The photoactivity of polyurethane coatings with SiO_2–TiO_2 nanofibers are investigated as shown in Figure 4.9. Corresponding to the photoactivity property of nanofibers, the polyurethane coatings embedded with SiO_2-TiO_2 nanofibers exhibit the same photocatalytic activity trend as the pre-reacted nanostructures. The polyurethane coating with higher photocatalytic activity nanostructure which is nanofibers, exhibits higher photoactivity. With increased loading of nanostructure into the coatings, the photoactivity of polyurethane coatings also increased which works as expected and is consistent with our previous study regarding the polyurethane coatings with photocatalysts. According to other studies[251], more of the photocatalyst in the coating, will lead to higher catalytic activity. However, comparing with our previous studies regarding the

SiO$_2$ coated anatase TiO$_2$ which significantly enhanced the photoactivity due to the reduction of agglomeration effect, there is barely any agglomeration of TiO$_2$ nanofibes than that of anatase TiO$_2$. Therefore, no enhanced photoactivity could be observed from the SiO$_2$ encapsulation of TiO$_2$ nanofibers.
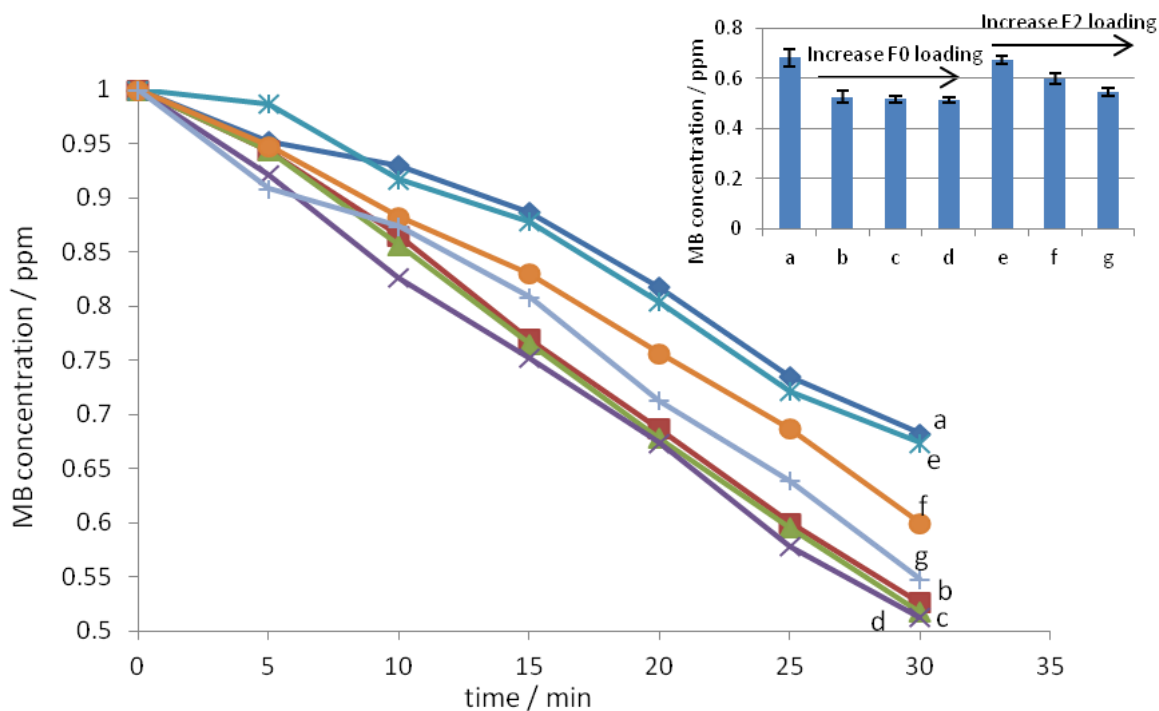
Figure 4.9. The photoactivity of polyurethane (PU) nanocomposite varying nanostructures (1 ppm methylene blue solution with light intensity of 0.635 W/m^2 after 30 min). (a) PU. (b) PU with 2.5 mg F0. (c) PU with 5.0 mg T0. (d) PU with 7.5mg F0. (e) PU with 2.5 mg F2. (f) PU with 5.0 mg F2. (g) PU with 7.5 mg F2.

3.3 Further investigation of photocatalytic activity

In order to better determine the effect on photoactivity of SiO$_2$ to TiO$_2$, UV-Vis spectra of SiO$_2$ coated TiO$_2$ nanofibers were measured and are shown in Figure 4.10. With the SiO$_2$:TiO$_2$

weight ratio increased, the UV absorbance decreases. The SiO_2 on the surface of nanofiber works as a blockage of UV absorbance of nanofibers and prevent the radicals transferring to solution, which is similar to the results from other studies[228]. In order to confirm the photoactivity of nanostructures, photoluminescence emission is performed (Figure 4.11 and 4.12). Figure 4.11 and 4.12 demonstrate the formation of hydroxyl radicals by the experimental catalysts with terephthalic acid as a fluorescent probe due the formation of high fluorescent product 2-hydroxyterephthalic acid from the reaction of terephthalic acid and hydroxyl radicals. Without the presence of photocatalyst, no peak was observed meaning that no hydroxyl radicals were formed according to previous studies [132]. With the utilized TiO_2 photocatalysts, the peak at 425nm was observed indicating the formation of hydroxyl radicals. The gradual decrease of emission counts are complied with the photocatalytic results of methylene blue tests. The photoluminescence of polyurethane nanocomposite coatings has the similar trend of nanostructures and complied with the photocatalytic activity in Figure 8 as well.
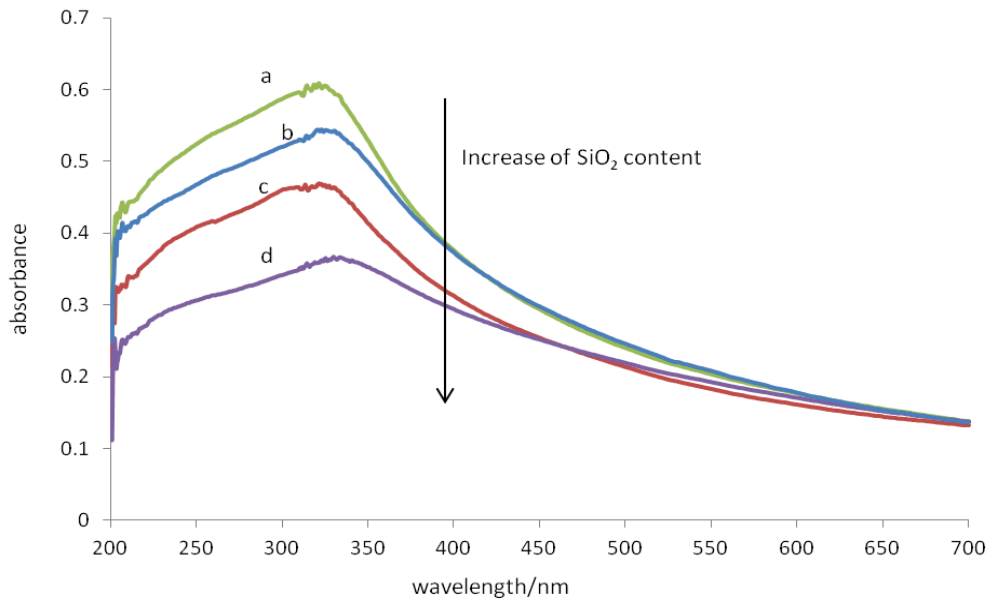
Figure 4.10. UV-vis spectra of SiO_2-TiO_2 nanofiber varying SiO_2 content (wt. %). (a) 0; (b) 5.40;

(c) 10.8; (d) 16.2.
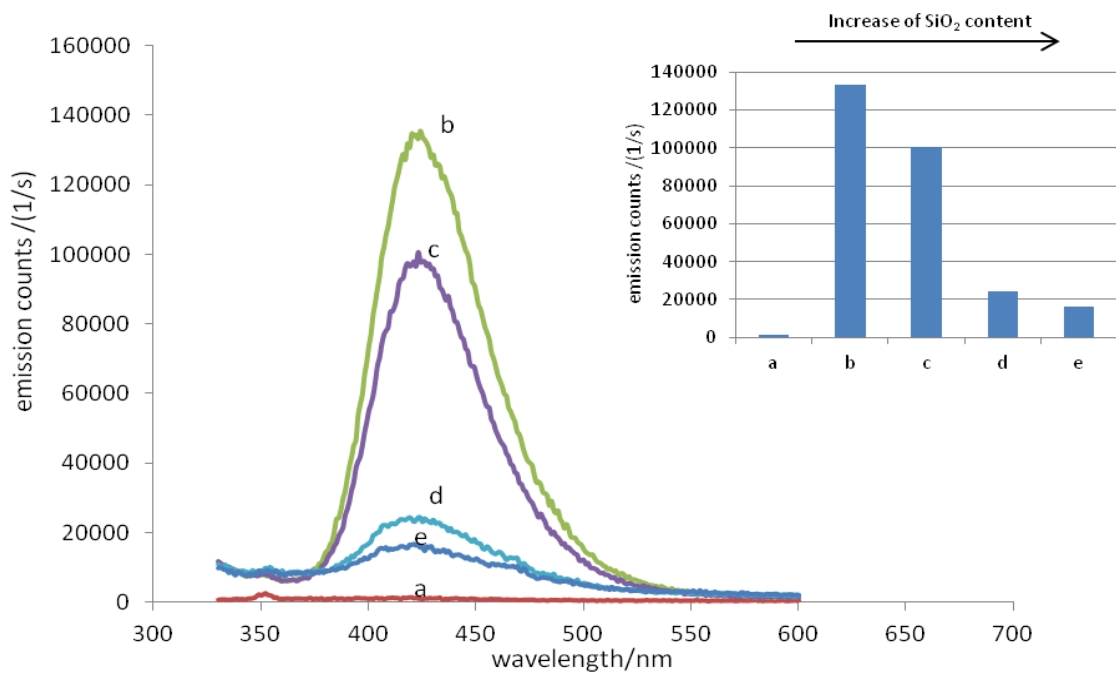
Figure 4.11. Photoluminescence spectra of SiO_2-TiO_2 nanofibers varying SiO_2 content (wt. %)

(full light illumination of 1 sun for 10 min). (a) blank (no TiO_2); (b) 0; (c) 5.40; (d) 10.8; (e)

16.2.
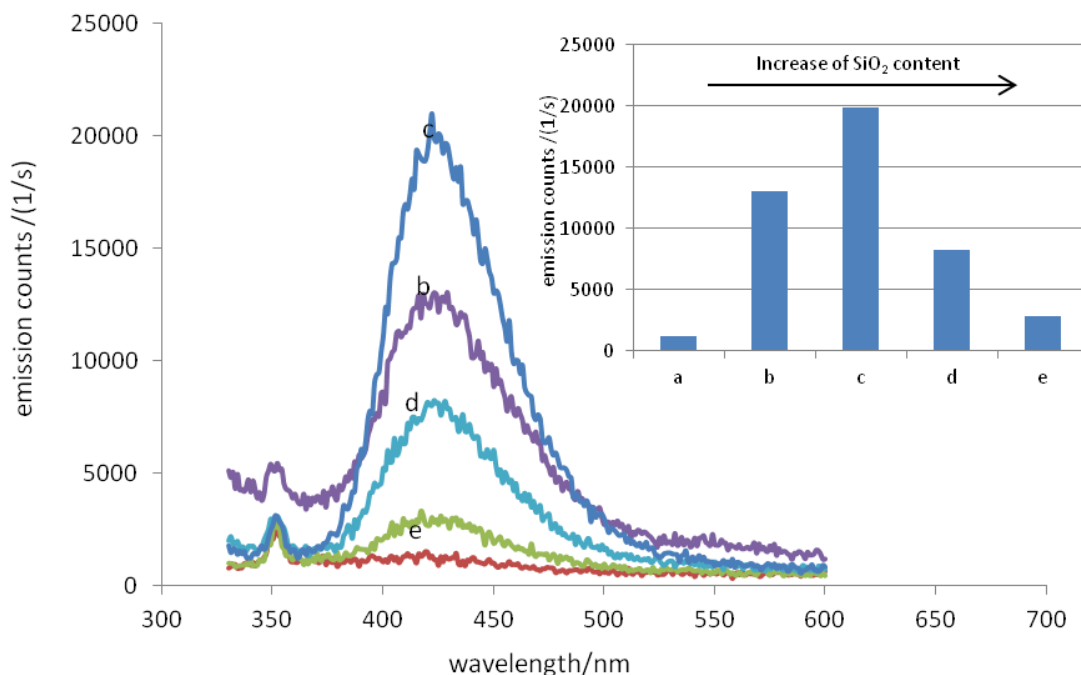
Figure 4.12. Photoluminescence spectra of SiO_2-TiO_2 nanotube varying SiO_2 content (wt. %) (full light illumination of 1 sun for 10 min). (a) blank (no TiO_2); (b) 0; (c) 5.40; (d) 10.8; (e) 16.2.

3.4 Mechanical Properties of SiO_2-TiO_2 Modified Polyurethane Coatings

Silica aerogels can be either hydrophobic or hydrophilic[252], therefore it is fairly important to investigate the hydrophobicity of SiO_2-TiO_2 nanostructures embedded polyurethane coatings. The contact angle measurements were performed for the samples before and after 10 min of $0.04W/cm^2$ UV light at 365nm wavelength (Figure 4.13 A&B). The TiO_2 nanofibers exhibit increased hydrophilic behavior compared to the nanotubes due to increased amounts of hydroxyl groups on the surface, which remain when embedded into the polyurethane coatings. Therefore, the contact angle of the embed coatings reduced. However, with the increased SiO_2

content on the surface, the nanofibers become more hydrophobic because of the decreased

amount of hydroxyl groups and hydrophobic behavior of silica. As the nanotubes exhibit more

hydrophobic behaviour, the contact angle increased with increasing SiO_2 content on the surface.

However, when the ratio of SiO_2 to TiO_2 is 16.2:100, both of the nanofiber and nanotube

becomes more hydrophilic. The embedded nanostructures will protect the coatings from the

hydrophobicity change after UV irradiation. Moreover, with increased loading of nanostructures,

the coatings will become more hydrophobic (Figure 4.13 C&D).
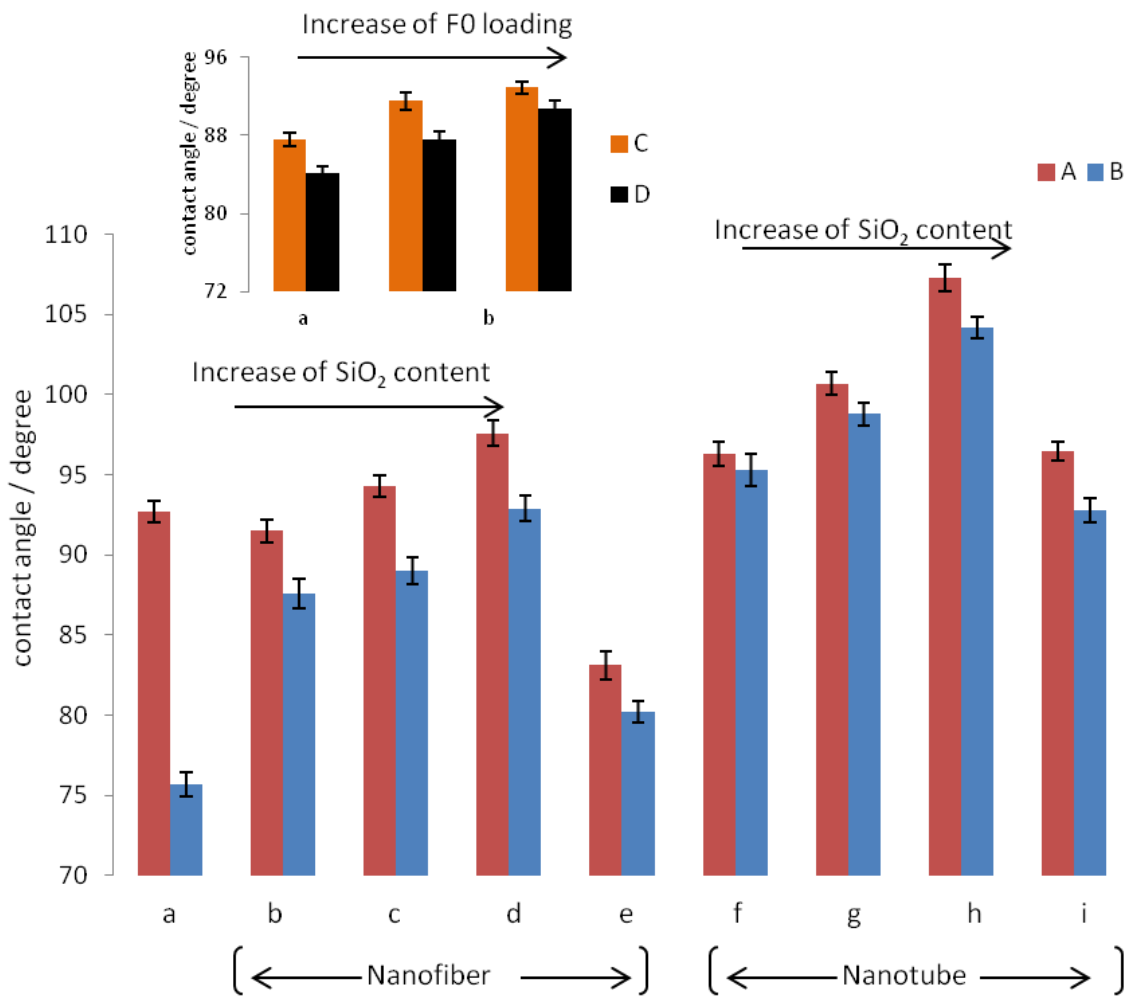
Figure 4.13. Comparison of contact angle of polyurethane coatings embedded with 5.0 mg

SiO$_2$-TiO$_2$ nanostructures before (A) and after (B) 10 min UV irradiation. TiO$_2$ nanofiber (a: blank. b: F0. c: F1. d: F2. e: F3.) TiO$_2$ nanotube (f: T0. g: T1. h: T2. i: T3.) Comparison of contact angle of polyurethane coatings embedded with different loadings of F0 before (C) and after (D) 10 min UV irradiation. a: 2.5 mg. b: 5.0 mg. c: 7.5 mg.
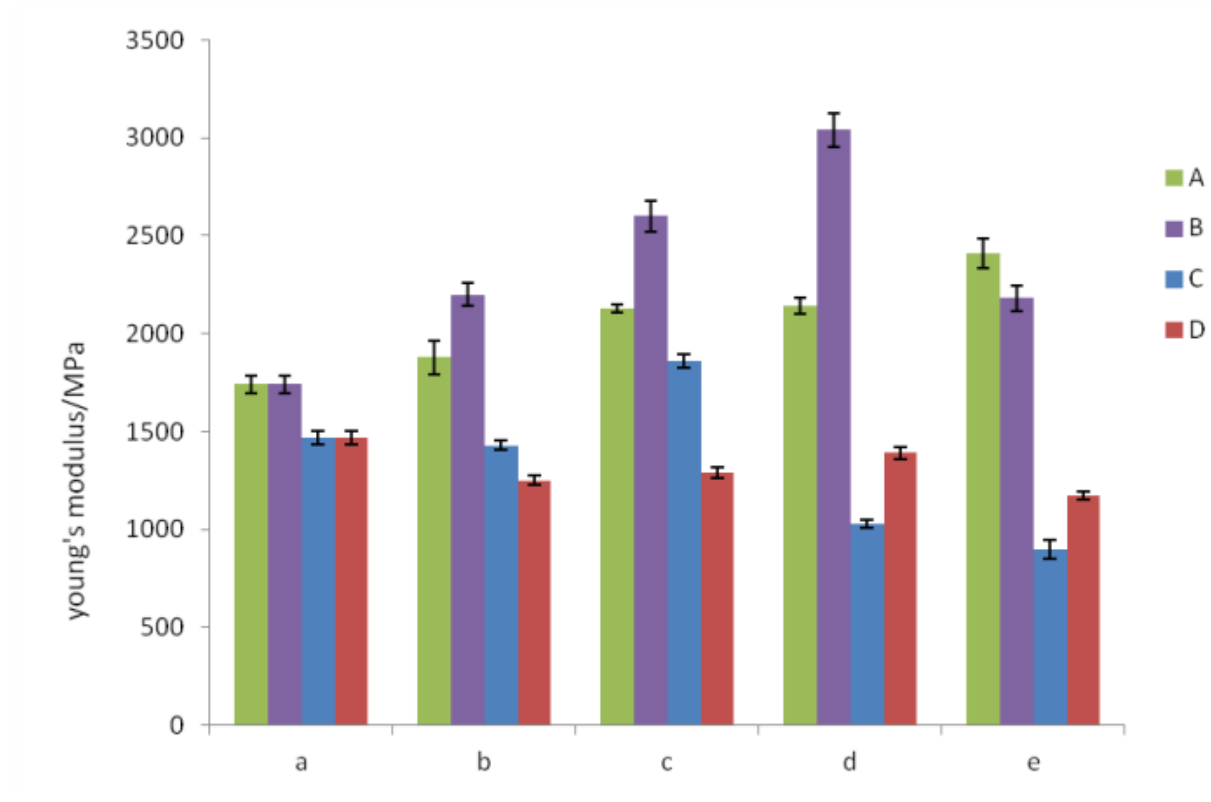
Figure 4.14. The comparison of Young's modulus of polyurethane films before UV irradiation (365nm, 36W, 120h) (A) SiO$_2$-TiO$_2$ nanofibers. (a) blank. (b) F0. (c) F1. (d) F2. (e) F3. (B) SiO$_2$-TiO$_2$ nanotubes. (a) blank. (b) T0. (c) T1. (d) T2. (e) T3. After UV irradiation (365nm, 36W, 120h) (C) SiO$_2$-TiO$_2$ nanofibers. (a) blank. (b) F0. (c) F1. (d) F2. (e) F3. (D) SiO$_2$-TiO$_2$ nanotubes. (a) blank. (b) T0. (c) T1. (d) T2. (e) T3.

The tensile strength test followed the ASTM D882 method. The results (Figure 4.14) indicate that by adding TiO$_2$ nanofibers or TiO$_2$ nanotubes, the Young's Modulus is higher than

that of polyurethane raw coating (blank). This is attributed to strong adhesion from bridging or

chelating coordination between the titania nanofiller and the polyurethane matrix. Chen et al.

showed that nano-TiO_2/polyurethane composites gave higher Young's modulus due to the TiO_2

nanofibers or nanotubes strengthening the polyurethane matrix linkage[233]. With increasing

amount of SiO_2 introduced into our system, the adhesion became stronger leading to higher

Young's modulus, attributed to higher adhesion between SiO_2 and polymer matrix[234].

However, when the ratio of SiO_2 to titania nanotubes is 16.2:100, the Young's modulus suddenly

dropped, probably due to a morphology change as indicated in Figure 4.2. After UV irradiation

testing, all of the polyurethane coatings exhibited a loss in mechanical strength. Since the

photoactivity of SiO_2-TiO_2 nanotubes are fairly similar, the drop of Young's modulus has no

significant difference. However, as shown by sample F1, the SiO_2 coating provided decreased

photodegradation in the coating while maintaining UV absorbance. Meanwhile, with increased

loading of silica coated titania nanofibers into the coating, the Young's modulus increased

directly with wt. % (Table 4.2).

Table 4.2. The comparison of Young's modulus of polyurethane films with varying loadings of F2.

Varying loading F2	2.5 mg	5.0 mg	7.5 mg
Young's Modulus / MPa	1867±34	2140±60	2552±81

4. Conclusion

SiO$_2$ was coated onto TiO_2 nanofibers and nanotubes via the Stöber process. The TiO_2

nanofibers exhibited the highest photoactivity, with more SiO_2 on the nanofiber surface blocking

both the UV absorbance and electron transfer, leading lower photoactivy.   When these

nanostructures were added into polyurethane coatings, the photoactivity of coatings was found to

exhibit the same catalytic activity trend. They both strengthened the Young's modulus of coatings

while keep the hydrophobicity from changing. The SiO_2 encapsulation process was found

promising to enhance integration of titania into polyurethane coatings while prevent the coatings

from aging under UV light.

Chapter 5. TiO$_2$ xerogel nanofillers for Transparent UV proofing polyurethane coatings

Abstract: Supercritical CO$_2$ (ScCO$_2$) is an environmentally friendly approach for producing nanosized metal/organic composites such as xerogels. Comparing with the conventional sol-gel method, it reduces the chemical residue content and has negligible surface tension which is ideal for synthesizing nanosized xerogels. In the present work, TiO$_2$ xerogel nanofibers are successfully synthesized via supercritical CO$_2$. The coordination between Ti and the carboxylic acid group was investigated showing a bidentate coordination. The TiO$_2$ xerogel nanofibers are possessed high UV absorbance. In the present study, we have integrated the fibers into polyurethane coatings, which exhibited high UV shielding properties, and possess a negative effect in reducing the thermicity and increasing reflective index, which allows enhanced IR transfer through the coatings faster.

Keywords: TiO$_2$, xerogel, nanofiber, supercritical CO$_2$, Polyurethane

1. Introduction

Polymer/nanostructured composites have had great successes in the development of advanced materials, particularly with unique properties and combination of properties including optical [253-255]. However, they suffer from the agglomeration of nanoparticles which causes significant light scattering and reduces the transparency of the polymer composites [256]. There are four methods for reducing the agglomeration effect and enhancing the transparency of polymer nanocomposites, including: melt compounding such as extrusion [19, 20], film casting [21, 22], *in situ* polymerization [23, 24], and *in situ* particle generation [25, 26].

Transparent polyurethane coatings have been investigated in other studies via *in situ* sol-gel process [145]. However, in this study, the film casting method is utilized for the synthesis of transparent polyurethane coatings. The nanofiller involved here are TiO_2 xerogel which possesses both solvent solubility and UV absorbance [257]. Therefore, it will introduce the UV shielding property into the transparent polyurethane coatings. The conventional method to synthesize TiO_2 xerogels is sol-gel process in which titanium isopropoxide and acetic acid are reacted in pure methanol solution[141]. However, this method is not an environmentally friendly way to go, and the resulted xerogel is more like bulk material instead of nanosized. In the present work, we have, therefore, chosen to synthesize nanosized TiO_2 xerogel via a green approach using supercritical CO_2.

Supercritical CO_2 ($scCO_2$) is a fluid state of carbon dioxide where it is held at or above its critical temperature and critical pressure. $ScCO_2$ has attracted considerable attention in recent years as it is inexpensive, nontoxic, lacks any solvent residues, and shows only negligible surface

tensions, a fact which makes the solvent ideal for e.g. chemical extraction and nanomaterial synthesis [97, 126, 127]. In this study, titanium isopropoxide and acetic acid are reacted in supercritical CO_2 and form TiO_2 xerogel and isopropanol (scheme 5.1), which is an environmental friendly approach. The as prepared xerogel are able to dissolve in solvent with similar polarity of Acetic acid such as methanol or ethanol due to the acetyl group linked with titania. When the nanofiber xerogel integrated into polyurethane coatings, due to the UV absorbance property of TiO_2 component [144] and the xerogel nanofiber structure, polyurethane nanocomposite transparent coatings could exhibits various modified properties including photoactivity, UV shielding, and thermicity.
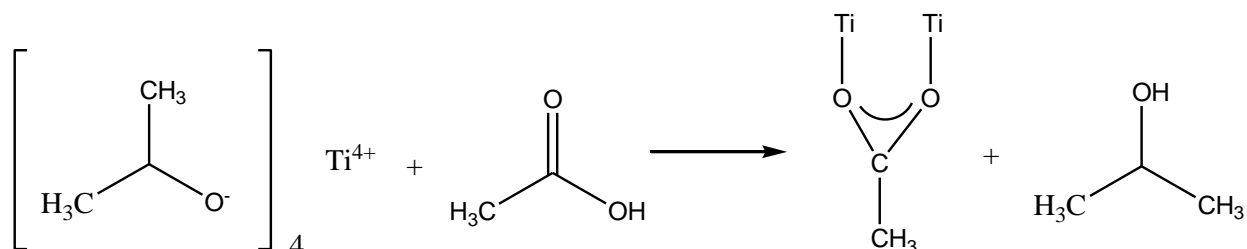
Scheme 5.1: The reaction of Titanium isopropoxide and Acetic acid in Supercritical CO_2.

2. Materials and Experiments

2.1 Materials.

For chemical synthesis, the following chemicals were used as supplied: titanium isopropoxide (97%, Sigma Aldrich), glacial acetic acid (99.7%, Caledon laboratory chemicals), methanol (Caledon laboratory chemicals), poly aspartic ester (Bayer MaterialScience), poly hexamethylene diisocyanate (Bayer MaterialScience), isophorondiamine - isobutyraldimine

(Bayer MaterialScience), methylene blue (Caledon laboratory chemicals), anatase TiO_2 (particle diameter < 25nm, 99.7%, Sigma Aldrich), rutile TiO_2 (particle diameter <100nm, 99.5%, Sigma Aldrich).

2.2 Xerogel synthesis and coating preparation

The synthesis of TiO_2 xerogel nanofibers is following a procedure described is a previous study[97]. The reaction took place in supercritical CO_2 (Figure 5.1) at 60° C and 6000 psi with 10.6g Titanium isopropoxide and 8.13ml Acetic Acid mixed into the 25ml autoclave reactor, and continues stirring for 3 hours, followed by the 3 days aging and 3 days washing with 0.5 mL/min CO_2. After that, the TiO_2 xerogel nanofiber was take out from the reactor. Different amount of TiO_2 xerogel (5 mg, 10 mg, or 15 mg) were dissolved in 1.0 ml of methanol. Then 1.5g of polyol mixture (with weight ratio of Poly Aspartic Ester : Isophorondiamine - isobutyraldimine equal to 4 : 1) and 2.0g of Poly Hexamethylene Diisocyanate were mixed one by one into the solution and shake for 15 seconds to form homogeneous solution which is used for preparation of coatings.

The polyurethane coatings were prepared by spin coating method with Model WS-200BZ -6NPP/LITE spin coater. The solution was spin coated onto the surface of 75mm x 25mm quartz plates with different coating speed (1000 rpm, 2000 rpm, 3000 rpm) to form different thickness of coatings, followed by curing at room temperature under 1 atm for 24 hours.
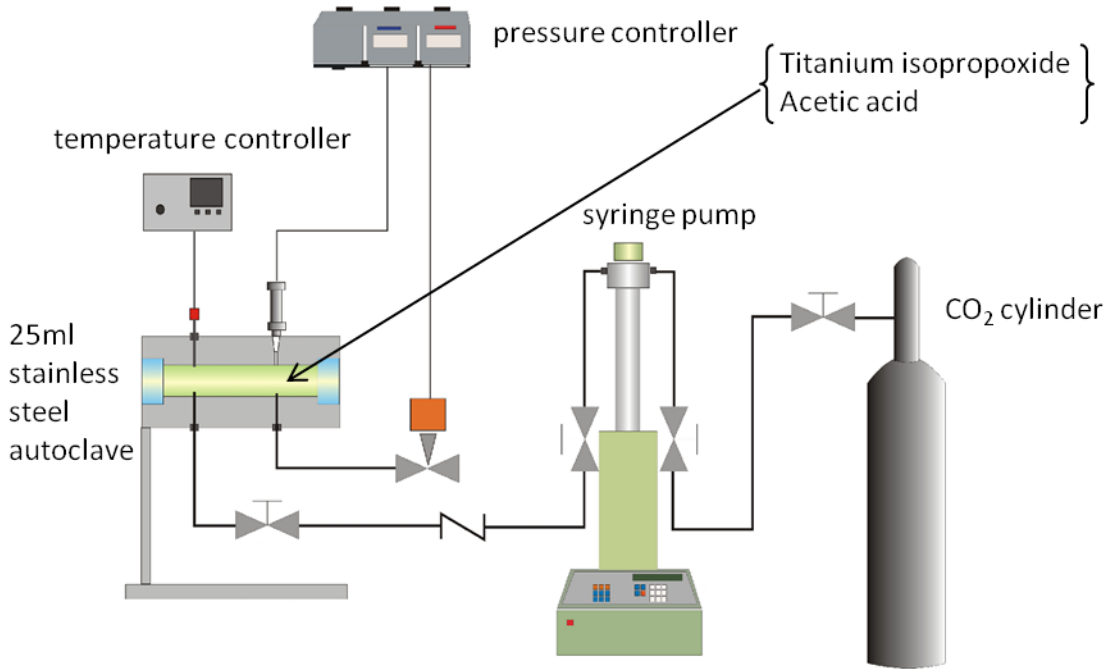
Figure 5.1: Scheme of the set-up to synthesize of TiO_2 xerogel nanofiber via supercritical CO_2.
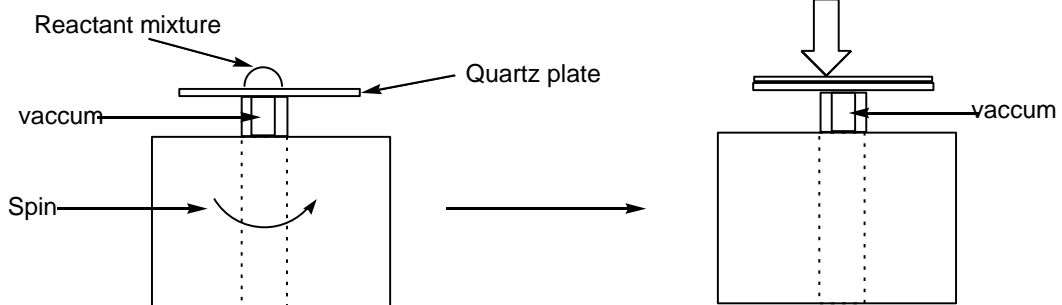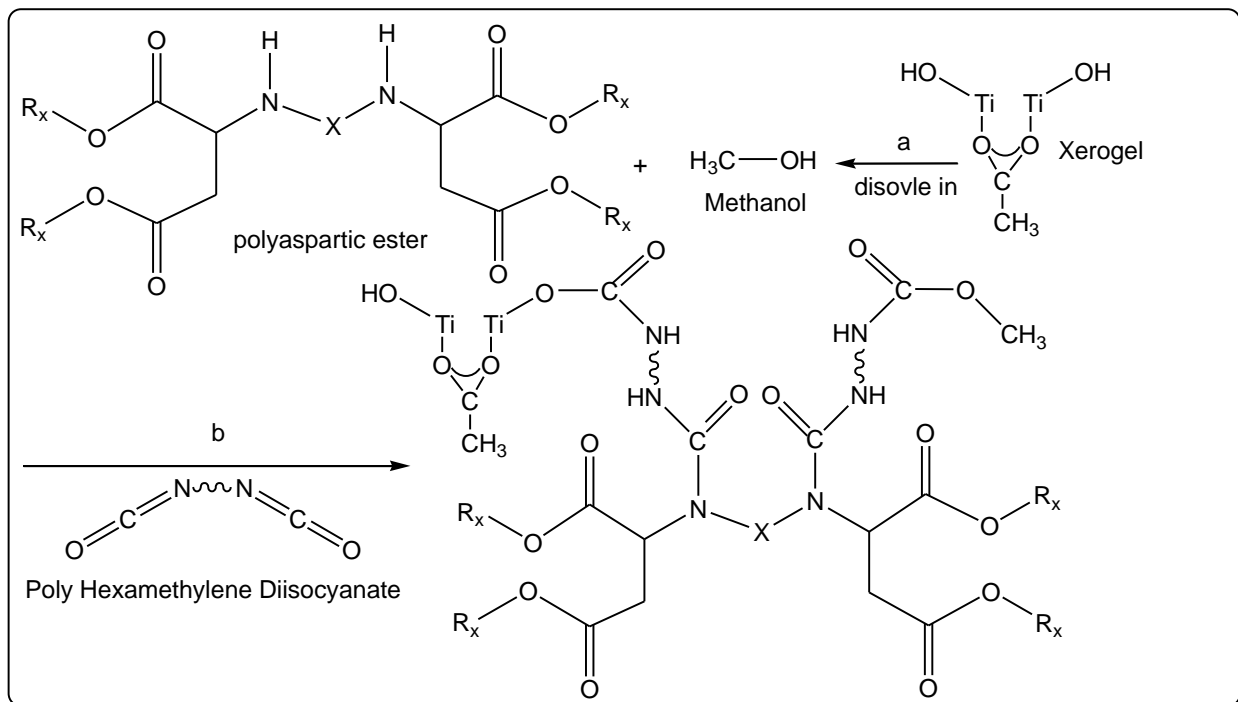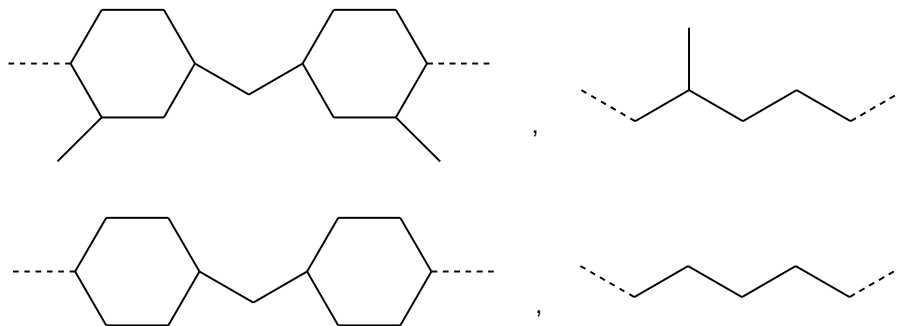
Scheme 5.2: Synthesizing polyurethane/TiO$_2$ nanofiber xerogel nanocomposites via spin coating.

(a) sonication at room temperature; (b) room temperature with catalyst.

2.3 Characterization

The photoactivity of the as prepared TiO_2 xerogel nanofibers was tested using 20ml methylene blue solution (1ppm) containing 10mg of xerogel nanofibers. UV irradiation of the solution was measured at an intensity of 0.635 W/m^2 after 5, 10, 15, 20, 30, 40, and 60 minutes. with a Luzchen ICH1light simulator.

Fourier transform infrared (FTIR) spectroscopy was used to identify the functional groups of the prepared xerogel nanofibers and polyurethane coatings. FTIR analysis was performed using a NICOLET 6700 spectrometer in the range of 600-4000cm^{-1} and was operated using 32 scans at 4cm^{-1} resolution.

Thermo-gravimetric analysis (TGA) was performed to measure the prepared xerogel nanofibers using a TA Instruments® Q-series SDT Q600 analyzer. Thermogravimetric curves were measured in the temperature range of 25-800 $^{\circ}$C (heating rate: 20℃/min; under air) and analyzed using the TA Instruments® Universal Analysis 2000 software.

The absorbance in the ultraviolet range was measured by a SHIMADZU UV-3600 from 200nm to 700nm. Transmission electron microscope (TEM, Philips CM10) was performed at an acceleration voltage of 80KV to determine the morphology of the prepared xerogel.

Scanning Electron Microscopy (SEM) was performed using a LEO(Zeiss) 1540XB SEM. All images were taken at an acceleration voltage of 10 kV.

The Thickness of the polyurethane coatings prepared via spin coating method on quartz plates (from VWR) are measured by TEMCOR® P-10 surface profiler.

3. Results and Discussions

3.1 TiO$_2$ xerogel Characterization
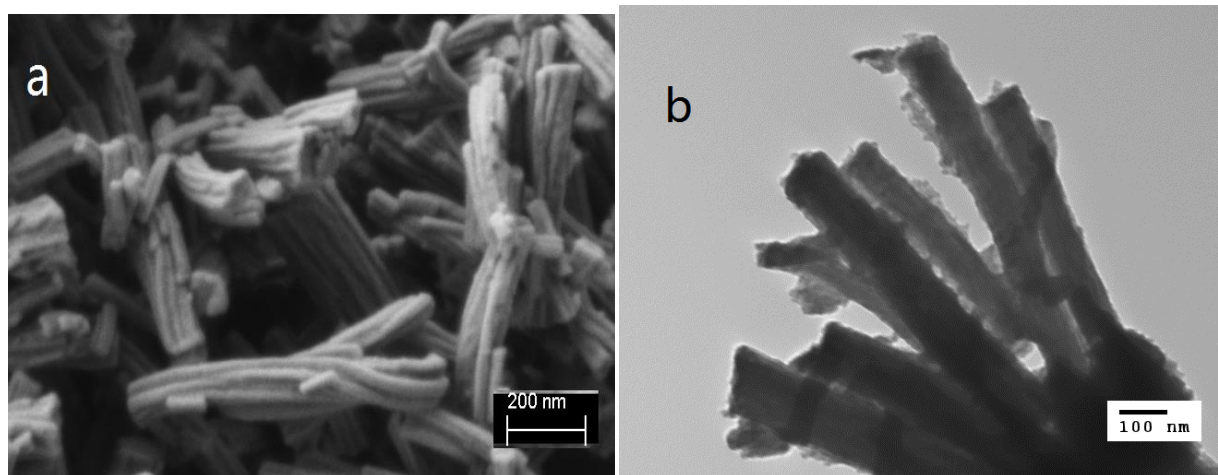
Figure 5.2: Morphology of TiO$_2$ xerogel nanofibers: (a) SEM and (b) TEM images.

The prepared xerogel shows the amorphous TiO$_2$ structure (SI 5.1), and in Figure 5.2 indicates nanofiber morphologies with individual fibers well separated from each other. The fibers exhibit diameters in a range from 50 nm to 100 nm. Around the nanofiber core, the components which are light gray in color can be seen from the TEM image, consisting as the titanium structure which linked with acetyl groups. By running thermo-gravimetric analysis of the xerogel, it was found that the acetyl groups completely decompose at about 400 $^{\circ}$C. The weight loss caused by decomposing the organic groups of the xerogel was calculated to be ~ 55 wt%. Comparing the experimental with the theoretical data which is calculated from the Scheme 1, we found that they are in good agreement and that the reaction in scCO$_2$ was complete leaving no residuals within the xerogel structure (Table 5.1).

Table 5.1: Comparison of stoichiometric and TGA measured composition (acetyl groups / TiO$_2$)

of the TiO$_2$ xerogel.

	Organic Group	TiO$_2$
TGA measured Ratio	55	45
Stoichiometric Ratio	58	42

The FTIR spectra shown in Figure 5.3 demonstrates the chemical structure of TiO$_2$ xerogel.

The C=O at peak 1718 cm^{-1} and C-O at peak 1258 cm^{-1} of carboxylic acid group are almost

disappeared after the reaction, which confirmed that the coordination of Ti and acetic acid is a

bridging bidentate coordination instead of a simple ring [202]. This result is similar to other

metal-acid coordination studies[202] which confirms the existence of bidentate coordination

between TiO$_2$ and acid groups.
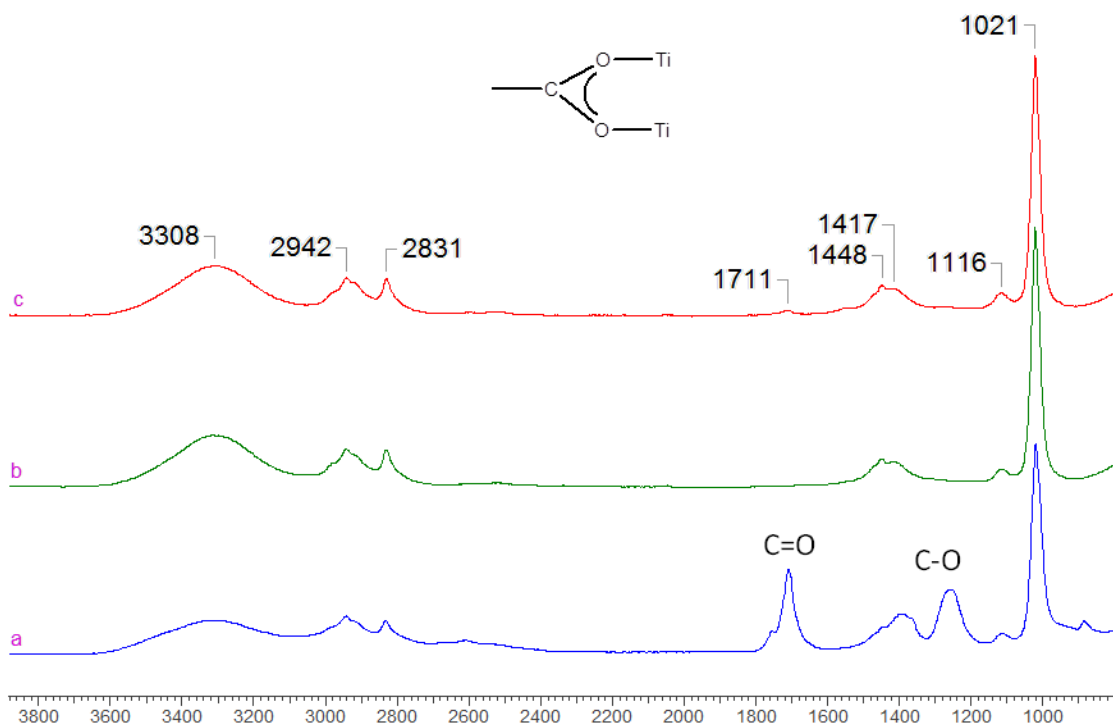
Figure 5.3: FTIR spectra of (a) acetic acid in methanol with concentration 5 g/L; (b) methanol; and (c) TiO$_2$ xerogel in methanol with concentration 5 g/L.

The TiO$_2$ structure is a xerogel structure in neither anatase phase nor rutile phase as confirmed from the XRD results (see SI 5.1), the UV absorbance is always an important factor to investigate. The methylene blue test was performed with 10 mg of TiO$_2$ xerogel in 20ml solution. The results (Figure 5.4A) demonstrate that the TiO$_2$ xerogel absorbed a promising amount of UV radiation and prevented the photodegradation of methylene blue significantly. And comparing with the xerogel from concentional method, the xerogel nanofiber clearly has higher UV absorbance and provides a better protection. In 60 minutes, about 75% of the methylene blue was decomposed in the blank sample, while only 40% of the methylene blue was decomposed in the sample with TiO$_2$ xerogel. This result is in contrast with previous studies regarding TiO$_2$ xerogel, in which the photoactivity was enhanced [258, 259]. It is mainly because of their xerogels were

treated by calcination so partially exhibited anatase crystal structure.

From the UV-vis spectra (Figure 5.4B), TiO_2 xerogel nanofiber has a high UV absorbance at the range from 200 to 300nm, some of which comes from the acetyl group whose UV absorbance could be seen from the UV-vis spetra (Figure 4B), and others of which are from the TiO_2 structure inside the xerogel nanofiber. Compare to the xerogel synthesized from comventional method, xerogel nanofiber has higher UV absorbance. Meanwhile, there is no absorbance in the visible range, which is encouraging for subsequently producing a transparent coating with UV absorbance TiO_2 structure inside.
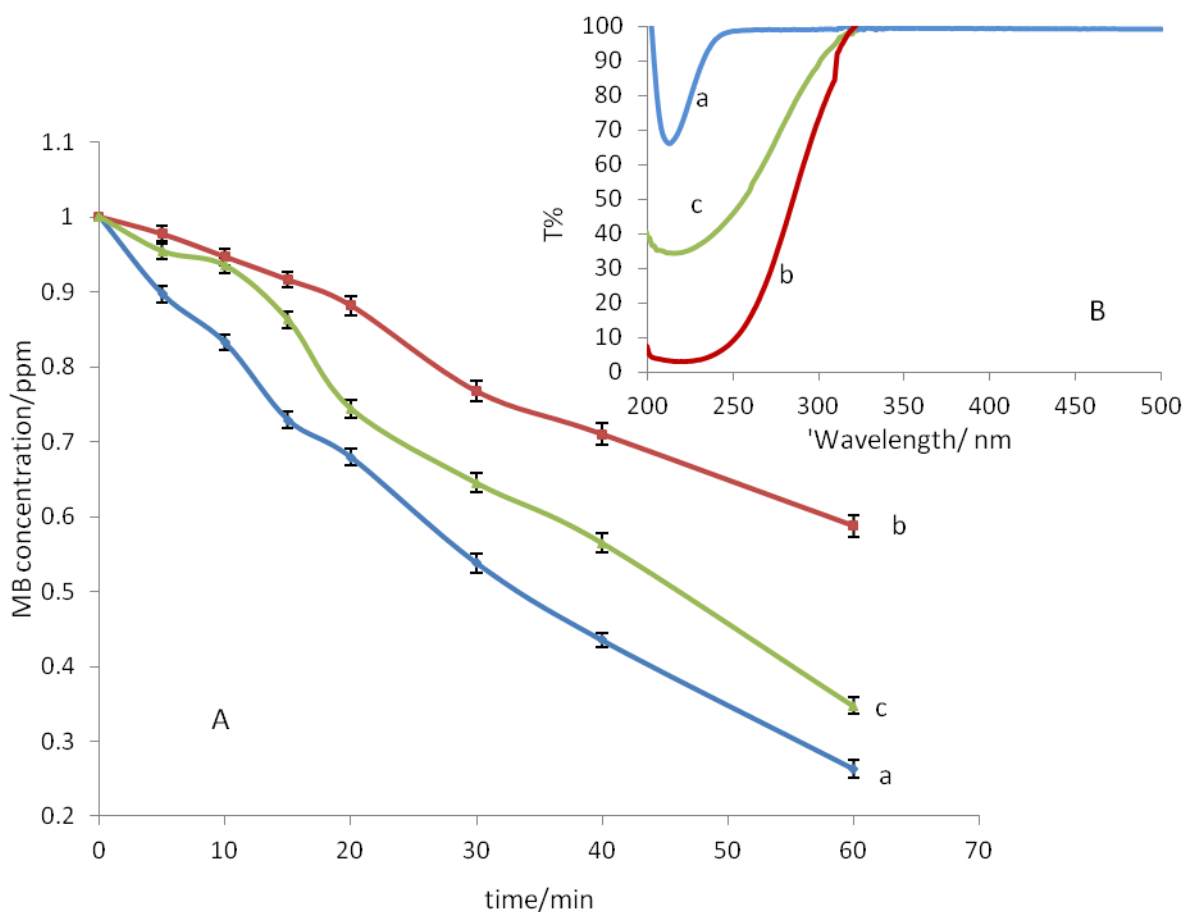
Figure 5.4: (A): The photoprotection effects of TiO_2 xerogel in 1 ppm methylene blue solution

with light intensity of 0.635 W/m^2. (a) blank; (b) TiO$_2$ xerogel nanofiber; (c) TiO$_2$ xerogel obtained via conventional method. (B): UV-Vis spectra of TiO$_2$ xerogel in methanol with concentration 3×10^{-4} mol/L. (a) acetic acid; (b) TiO$_2$ xerogel nanofiber; (c) TiO$_2$ xerogel obtained via conventional method.

3.2 TiO$_2$ xerogel and transparent polyurethane coatings

Table 5.2: Different thickness of polyurethane coatings with different spinning coating speed.

Spin speed (rpm)	1000	2000	3000
Average Thickness (μm)	27.0±0.3	23.2±0.1	13.6±0.1

Figure 5.5. Photo of transparency of quartz plate (a) blank; (b) coated with polyurethane coating

with 15mg (0.36wt%) TiO_2 xerogel.

Due to the different speeds of spin coating, different thicknesses of polyurethane coatings

are formed on the surface of the quartz plates (Table 5.2). As the studies regarding the

relationship between spin speed and film thickness [260, 261], with higher spin coating speeds,

the thickness of the coating is become lower. Moreover, with different spinning speeds leading to

different layer thicknesses, the resulting samples were found to exhibit good transparency in the

visible range 350-700 nm, as shown Figure 5.5 and in the UV-vis spectra (Figure 5.6A), despite

the different xerogel concentration in polyurethane coatings. From the spectra, there is barely

absorbance in the range of 250-300 nm of polyurethane coating. However, with the increasing of

xerogel amount, there is reducing transmittance in the UV region due to more UV absorbance

material was inside the structure which is similar to other studies regarding polyurethane/TiO_2

hybrid films [145], suggesting a promising coating improvement of UV shielding property

without decreasing transparency. With the increasing of coating thickness, the coating

transmittance in UV range is reduced as excepted (Figure 5.6B). However, after 10 days of 4.08

mW/cm^3 UVC lamp irradiation, there is no noticeable change of UV spectra indicating a stable

UV shielding property (Figure 5.6C). However, with an increase of temperature, the UV spectra

shows a slight difference in the visible range (Figure 5.6D). With an increase of temperature, the

absorbance of visible light increased gradually due to the decomposition of polymer at higher

temperature.
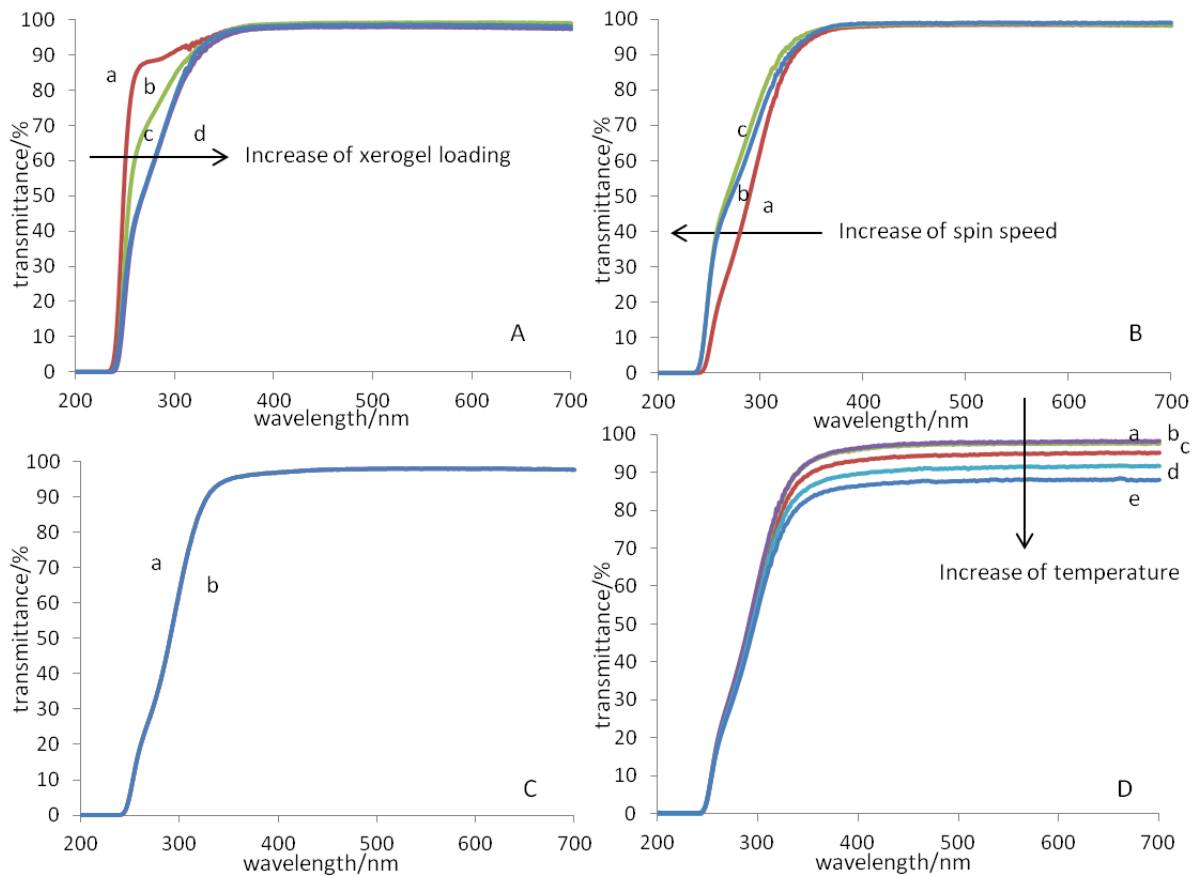
Figure 5.6. UV-Vis spectra of polyurethane coatings (A) prepared at 3000rpm with different loadings of TiO_2 xerogel. (a): 0 mg (0wt%). b: 5 mg (0.12wt%). c:10 mg (0.24wt%). d:15 mg (0.36wt%). (B) with 15 mg (0.36wt%) TiO_2 xerogel at different spin coating speed. a: 1000 rpm. b: 2000 rpm. c: 3000 rpm. (C) with 15 mg (0.36wt%) TiO_2 xerogel at 1000 rpm (a) before and (b) after 4.08 mW/cm^2 UVC lamp irradiation for 10 days. (D) with 15 mg (0.36wt%) TiO_2 xerogel at 1000 rpm at different temperatures. (a) 25.1℃. (b) 34.0℃. (c) 43.5℃. (d) 51.4℃. (e) 58.1℃.

Regarding to polymer coatings, thermicity is an essential factor to measure the heat transfer via irradiation. It is a measurement regarding long-wavelength IR transmittance of coatings. Lower thermicity means higher IR blocking and lower heat transfer through IR radiation. It was calculated by the following equation:

$$T = \frac{A_T}{A_{100}} \times 100\% \qquad (1)$$

where T is the thermicity of coatings, A_T is the area under the transmittance curve between 700

to 1400 cm^{-1}, A_{100} is the area in this region of 100% transmittance[262]. The calculated

thermicity results obtained from FTIR spectra are summarized in Table 5.3. With a reducing of

coating thickness, thermicity increased directly, which is expected according to

Bouguer-Lambert-Beer law [263, 264]. With an increasing xerogel amount, thermicity also

increased indicating that the TiO$_2$ xerogels possess the ability of enhancing the coating thermicity.

However, this is in contrast with other studies in which the thermicity decreased with increased

loading of nanofillers [223, 264]. This difference is mainly because of the nanofiller in this study

is xerogel structure which improves the infrared radiation transferring instead of crystal structure

which diffracts and reflects the infrared radiation [265].

Table 5.3: Thermicity of different polyurethane coatings.

Spin speed	Amount of Xerogel (mg)			
(rpm)	0	5	10	15
1000	20.2	22.6	24.0	24.3
2000	32.6	34.2	35.6	41.3
3000	35.4	38.7	39.4	53.3

Refractive index is an essential factor to investigate regarding polymer coatings [266, 267].

It is a factor describing the resistance of light traveling in a material. In this study, with more of

xerogel integrated into the polyurethane coatings, the refractive index is lower, which indicates the light is travels faster in the polyurethane coatings with more xerogel inside. Therefore, the xerogel fillers are reducing the light travel resistance resulting in slightly lowered refractive index. This is complied with other studies regarding xerogel nanofillers [268].

Table 5.4: Refractive index of different polyurethane coatings.

Amount of Xerogel (mg)	Refractive index (n)
0	1.534±0.003
5	1.525±0.002
10	1.515±0.001
15	1.509±0.001

4. Conclusion

TiO_2 xerogel nanofibers were successfully synthesized via an environmental friendly method in supercritical CO_2. Comparing with conventional sol-gel method, it reduces chemical residues and has negligible surface tension which is ideal for nanosized xerogel synthesis. The synthesized TiO_2 xerogel nanofibers exhibited high UV absorbance and UV protection property. When integrated into polyurethane coatings, more the amount of xerogel inside the system, higher the UV shielding property without the decreasing of transparency in visible range. Moreover, thermicity is increasing with the increase of xerogel loadings and decreasing with the increase thickness of coatings. Meanwhile, the reflective index is reducing with the increase of xerogel loading.

Chapter 6. Conclusions and recommendations

1. Conclusions

In this thesis, we utilized the in-situ polymerization and film casting method to introduce different nano-TiO_2 structures into polyurethane foams and coatings. It successfully reduced the agglomeration effect of nano-TiO_2 inside the polyurethane structure and enhanced the photoactivity along with other physic-chemical properties of polyurethane.

DMPA (2,2-dimethylolpropionic acid) functionalized anatse TiO_2 and P25was integrated into polyurethane foam with a "grafting-from" method and the agglomeration effect was successfully reduced. By applying Langmuir-Hinshelwood kinetics, the photodegradation of polyurethane foam appears to be a zero order reaction. Coordination of DMPA to TiO_2 gave DMPA-TiO_2(A) nanoparticles that at 3wt%, were able to increase the degradation rate of polyurethane foam by 120%. DMPA-P25 nanoparticles increased the degradation rate about 66% over unmodified polyurethane foam at a loading of 1wt%. After functionalized with DMPA, anatase TiO_2 becomes a better photocatalyst than P25 which is attributed from a reduction of electron transfer due to anatase/rutile surface interaction separation.

SiO_2 encapsulated anatase and rutile TiO_2 nanoparticles were successfully synthesized via a modified Stöber process, and integrated into polyurethane coatings. With a loading weight of $SiO_2 < 3.25$ wt%, the photocatalytic activity of anatase TiO_2 was enhanced with a reduction of agglomeration, while the rutile form TiO_2 was tuned to be photocatalytic due to light diffraction from the full coverage of SiO_2 on the surface. For loadings beyond 3.25wt%, the photocatalytic

activity of anatase TiO_2 decreases and rutile TiO_2 stays the same. When applied in polyurethane

coatings, with an increasing amount of SiO_2 on the surface, the contact angle was increased from

75° to 87° for anatase form and 70° to 78° for rutile form. The Young's Modulus was also

increased from 1.06GPa to 2.77GPa for anatase form and 1060MPa to 2170MPa for rutile form.

The thermal insulation property of polyurethane coatings is successfully enhanced by

encapsulating SiO_2 on the surface of TiO_2 with the thermal conductivity from 0.15 to 0.042

$W \cdot m^{-1} K^{-1}$ for anatase form and 0.069 to 0.037 $W \cdot m^{-1} K^{-1}$ for rutile form.

SiO_2 encapsulated TiO_2 nanofiber which was synthesized via an environmental friendly

supercritical CO_2 method and nanotube which was synthesized by conventional hydrothermal

reaction were also successfully synthesized via a modified Stöber process, and integrated into

polyurethane coatings. As of the TiO_2 nanofibers exhibit highest photoactivity, with more SiO_2

on the nanofiber surface blocking the UV absorbance and electron transfer, less photoactive the

nanofiber will be. As for higher specific area TiO_2 nanotube, the SiO_2 on the structure surface

will increase the photoactivity at first, and when the ratio of SiO_2 to TiO_2 past 10.8:100, the

photoactivity begin to decrease. When these nanostructures were addedd into polyurethane

coatings, the photoactivity of coatings exhibit the same catalytic activity trend. They both

strengthen the young's modulus of coatings and while the hydrophobicity did not change.

Nanofiber shaped TiO_2 xerogel synthesized via environmental friendly approach

supercritical CO_2 ($ScCO_2$) was mixed within polyurethane coatings through film casting method

and the coatings remain transparent. The synthesized TiO_2 xerogel nanofibers exhibited high UV

absorbance and UV protection property. When integrated into polyurethane coatings, more the

amount of xerogel inside the system, higher the UV shielding property without the decreasing of transparency in visible range. Moreover, thermicity is increasing with the increase of xerogel loadings and decreasing with the increase thickness of coatings. Meanwhile, the reflective index is reducing with the increase of xerogel loading.

2. Recommendations

Although the agglomeration effect is observed to be reduced inside the polyurethane coatings by apply SiO_2 on the surface of TiO_2, it is still not totally eliminated since the coatings are not as transparent as the ones with TiO_2 xerogel. It is because of during the Stöber process, TiO_2 nanoparticles still have agglomeration effect in solution. On the other hand, during the condensation step in the Stöber process, SiO_2 might link with each other and form a large cluster which contains a lot of TiO_2 nanoparticles. In order to conquer these problems, we would suggest investigating an in-situ Stöber process containing synthesis of TiO_2 or controlled Stöber process reducing SiO_2 self-linkage. Other encapsulating metal oxide replacing SiO_2 could also be investigated.

The coating transparency issue caused by agglomeration would not be a problem for the nanofiber-shaped TiO_2 xerogel since it dissolves in the methanol solution. However, it suffers from the solubility in methanol which limited the amount of TiO_2 xerogel mixed inside the polyurethane coatings. With less amount of methanol solution, the xerogel amount in coatings would be less and would not have a significant UV shielding property comparing with unmodified polyurethane coatings. With more amount of methanol solution, the xerogel would

be enough to provide a significant UV shielding property, but the coatings would suffer from lower mechanical strength. We suggest that either to figure out a solution possess a high solubility of TiO_2 xerogel or a solution which has no effect or even enhance the mechanical strength of coatings.

References

1.   Tummalapalli, N.K., et al., *Deposition and Characterization of CNT-Polyurethane Nanocomposite Films.* MRS Advances, 2017: p. 1-6.

2.   Tung, T., et al., *Enhancing the sensitivity of graphene/polyurethane nanocomposite flexible piezo-resistive pressure sensors with magnetite nano-spacers.* Carbon, 2016. **108**: p. 450-460.

3.   Strankowski, M., et al., *Polyurethane nanocomposites containing reduced graphene oxide, FTIR, raman, and XRD studies.* Journal of Spectroscopy, 2016. **2016**.

4.   Gupta, Y., et al., *Low temperature shape memory characteristics of segmented polyurethane-nanoclay composites.* Journal of Thermal Analysis and Calorimetry, 2016. **124**(3): p. 1449-1461.

5.   Shahrousvand, M., et al., *Flexible magnetic polyurethane/Fe 2 O 3 nanoparticles as organic-inorganic nanocomposites for biomedical applications: Properties and cell behavior.* Materials Science and Engineering: C, 2017. **74**: p. 556-567.

6.   Pielichowska, K., J. Bieda, and P. Szatkowski, *Polyurethane/graphite nano-platelet composites for thermal energy storage.* Renewable Energy, 2016. **91**: p. 456-465.

7.   *MarketsandMarkets: Global Polyurethanes Market will reach 17,946.20 Kilo Tons by 2016.* 2011.

8.   *Global MDI, TDI and Polyurethane Market by Type, Applications, Prices, Regulations Trends & Forecasts 2011-2016.* Journal of Transportation, 2011: p. 39.

9.   Winey, K.I. and R.A. Vaia, *Polymer Nanocomposites.* MRS Bulletin, 2007. **32**(4): p.

314-322.

10.   Mohammadi, A., M. Barikani, and M.M. Lakouraj, *Biocompatible polyurethane/thiacalix [4] arenes functionalized Fe 3 O 4 magnetic nanocomposites: Synthesis and properties.* Materials Science and Engineering: C, 2016. **66**: p. 106-118.

11.   Li, X., et al., *UV-Curable Polyurethane-Acrylate-Ag/TiO2 Nanocomposites with Superior UV Light Antibacterial Activity.* International Journal of Polymeric Materials and Polymeric Biomaterials, 2017(just-accepted).

12.   Akkoyun, M. and E. Suvaci, *Effects of TiO2, ZnO, and Fe3O4 nanofillers on rheological behavior, microstructure, and reaction kinetics of rigid polyurethane foams.* Journal of Applied Polymer Science, 2016. **133**(28).

13.   Qiu, S., et al., *Degradation of pollutant and antibacterial activity of waterborne polyurethane/doped TiO2.* Journal of Wuhan University of Technology-Mater. Sci. Ed., 2015. **30**(3): p. 447-451.

14.   Qiao, Q., et al., *Characteristics of water-soluble polythiophene: TiO2 composite and its application in photovoltaics.* Journal of Applied Physics, 2005. **98**(9): p. 094906.

15.   Jiang, J., G. Oberdörster, and P. Biswas, *Characterization of size, surface charge, and agglomeration state of nanoparticle dispersions for toxicological studies.* Journal of Nanoparticle Research, 2009. **11**(1): p. 77-89.

16.   Ratri, C.R. and Q. Sabrina. *Study on the Surface Morphology of PVdF-LiBOB Solid Polymer Electrolyte with TiO2 Filler for Lithium-Ion Battery Application.* in *Materials Science Forum.* 2016. Trans Tech Publ.

17.   Piegat, A., et al., *Inhibition of calcification of polymer–ceramic composites incorporating nanocrystalline TiO2.* Advances in Applied Ceramics, 2013.

18.   Liang, F., et al., *Dielectric performance of polymer-based composites containing core-shell Ag@ TiO2 nanoparticle fillers.* Applied Physics Letters, 2016. **108**(7): p. 072902.

19.   Dufresne, A., *Processing of polymer nanocomposites reinforced with polysaccharide nanocrystals.* Molecules, 2010. **15**(6): p. 4111-4128.

20.   Isayev, A., R. Kumar, and T.M. Lewis, *Ultrasound assisted twin screw extrusion of polymer–nanocomposites containing carbon nanotubes.* Polymer, 2009. **50**(1): p. 250-260.

21.   Pötschke, P., T. Fornes, and D. Paul, *Rheological behavior of multiwalled carbon nanotube/polycarbonate composites.* Polymer, 2002. **43**(11): p. 3247-3255.

22.   Chae, D.W. and B.C. Kim, *Characterization on polystyrene/zinc oxide nanocomposites prepared from solution mixing.* Polymers for advanced technologies, 2005. **16**(11‐12): p. 846-850.

23.   Park, C., et al., *Dispersion of single wall carbon nanotubes by in situ polymerization under sonication.* Chemical physics letters, 2002. **364**(3): p. 303-308.

24.   Xu, Z. and C. Gao, *In situ polymerization approach to graphene-reinforced nylon-6 composites.* Macromolecules, 2010. **43**(16): p. 6716-6723.

25.   Palkovits, R., et al., *Polymerization of w/o microemulsions for the preparation of transparent SiO2/PMMA nanocomposites.* Langmuir, 2005. **21**(13): p. 6048-6053.

26.   Yan, F. and J. Texter, *Capturing nanoscopic length scales and structures by polymerization in microemulsions.* Soft Matter, 2006. **2**(2): p. 109-118.

27.   Chen, X. and S.S. Mao, *Titanium dioxide nanomaterials: synthesis, properties, modifications, and applications.* Chemical reviews, 2007. **107**(7): p. 2891-2959.

28.   Tallósy, S.P., et al., *Investigation of the antibacterial effects of silver-modified TiO2 and ZnO plasmonic photocatalysts embedded in polymer thin films.* Environmental Science and Pollution Research, 2014. **21**(19): p. 11155-11167.

29.   Trenque, I., et al., *Encapsulation of ZnO particles by metal fluorides: Towards an application as transparent insulating coatings for windows.* Optical Materials, 2013. **35**(3): p. 661-667.

30.   Oertel, G. and L. Abele, *Polyurethane handbook: chemistry, raw materials, processing, application, properties*. 1985: Hanser Publishers. Distributed in USA by Scientific and Technical Books, Macmillan.

31.   Varron, C., P.c. Thomas, and S.T. Limited, *Polyurethanes*. Vol. v. III.;3.;. 1998, Chichester;London, UK;New York;: John Wiley & Sons.

32.   Hepburn, C., *Polyurethane elastomers*. 2012: Springer Science & Business Media.

33.   Reid, S.A. and D. Ontario Hydro. Research, *Rigid polyurethane foam: compressive strength variation with density and temperature*. Vol. 89-148-K. 1989, Toronto U6 - ctx_ver=Z39.88-2004&ctx_enc=info%3Aofi%2Fenc%3AUTF-8&rfr_id=info:sid/summon.serialssolutions.com&rft_val_fmt=info:ofi/fmt:kev:mtx:book&rft.genre=book&rft.title=Rigid+polyurethane+foam&rft.au=Reid%2C+S.A&rft.series=Report&rft.date=1989-01

-01&rft.pub=Ontario+Hydro%2C+Research+Division&rft.volume=89-148-K&rft.extern

alDocID=b39721012&paramdict=en-US U7 - Book: Ontario Hydro, Research Division.

34.   Zlatanić, A., et al., *Effect of structure on properties of polyols and polyurethanes based on different vegetable oils.* Journal of Polymer Science Part B: Polymer Physics, 2004. **42**(5): p. 809-819.

35.   Javni, I., et al., *Thermal stability of polyurethanes based on vegetable oils.* Journal of Applied Polymer Science, 2000. **77**(8): p. 1723-1734.

36.   Petrović, Z.S., *Polyurethanes from vegetable oils.* Polymer Reviews, 2008. **48**(1): p. 109-155.

37.   Bai, C.Y., et al., *A new UV curable waterborne polyurethane: Effect of C C content on the film properties.* Progress in Organic Coatings, 2006. **55**(3): p. 291-295.

38.   Asif, A., et al., *Physical and thermal properties of UV curable waterborne polyurethane dispersions incorporating hyperbranched aliphatic polyester of varying generation number.* Polymer, 2005. **46**(24): p. 11066-11078.

39.   Van Maris, R., et al., *Polyurethane catalysis by tertiary amines.* Journal of cellular plastics, 2005. **41**(4): p. 305-322.

40.   Silva, A.L. and J.C. Bordado, *Recent developments in polyurethane catalysis: catalytic mechanisms review.* Catalysis reviews, 2004. **46**(1): p. 31-51.

41.   Ashida, K., *Polyurethane and related foams: chemistry and technology.* 2006: CRC press.

42.   Yasunaga, K., et al., *Study of cell opening in flexible polyurethane foam.* Journal of

cellular plastics, 1996. **32**(5): p. 427-448.

43.   Jones, R. and G. Fesman, *Air flow measurement and its relations to cell structure,*

        physical properties, and processibility for flexible urethane foam. Journal of Cellular

        Plastics, 1965. **1**(1): p. 200-216.

44.   Zhang, X., et al., *Role of silicone surfactant in flexible polyurethane foam.* Journal of

        Colloid and Interface Science, 1999. **215**(2): p. 270-279.

45.   Kim, H., Y. Miura, and C.W. MacOsko, *Graphene/polyurethane nanocomposites for*

        improved gas barrier and electrical conductivity. Chemistry of Materials, 2010. **22**(11): p.

        3441-3450.

46.   Jain, P. and T. Pradeep, *Potential of silver nanoparticle‐coated polyurethane foam as an*

        antibacterial water filter. Biotechnology and bioengineering, 2005. **90**(1): p. 59-63.

47.   Guo, Z., et al., *Strengthening and thermal stabilization of polyurethane nanocomposites*

        with silicon carbide nanoparticles by a surface-initiated-polymerization approach.

        Composites Science and Technology, 2008. **68**(1): p. 164-170.

48.   Beneš, H., et al., *Utilization of Natural Oils for Decomposition of Polyurethanes.* Journal

        of Polymers and the Environment, 2012. **20**(1): p. 175-185.

49.   Bilbao, R., et al., *Kinetics of the thermal decomposition of polyurethane foams in*

        nitrogen and air atmospheres. Journal of Analytical and Applied Pyrolysis, 1996. **37**(1): p.

        69-82.

50.   Chambers, J., J. Jiricny, and C.B. Reese, *The thermal decomposition of polyurethanes*

        and polyisocyanurates. Fire and Materials, 1981. **5**(4): p. 133-141.

51. Kanaya, K. and S. Takahashi, *Decomposition of polyurethane foams by alkanolamines.* Journal of Applied Polymer Science, 1994. **51**(4): p. 675-682.

52. Watando, H., et al., *Improving chemical recycling rate by reclaiming polyurethane elastomer from polyurethane foam.* Polymer Degradation and Stability, 2006. **91**(12): p. 3354-3359.

53. Dai, Z., et al., *Effect of diaminotoluene on the decomposition of polyurethane foam waste in superheated water.* Polymer Degradation and Stability, 2002. **76**(2): p. 179-184.

54. Prager, F.H., et al., *Toxicity of the combustion and decomposition products of polyurethanes.* Fire and Materials, 1994. **18**(2): p. 107-119.

55. Zitting, A., et al., *Toxicity of polyurethane-derived oxidative thermal decomposition products.* Fire and Materials, 1982. **6**(2): p. 96-97.

56. Rek, V. and M. Bravar, *Ultraviolet Degradation of Polyester-Based Polyurethane.* Journal of Elastomers and Plastics, 1983. **15**(1): p. 33-42.

57. Açıkalın, E. and O. Atıcı, *Preparation of Waterborne Polyurethane‐OMt Nanocomposites and Effect of Clay on UV Degradation.* Macromolecular Symposia, 2014. **338**(1): p. 17-27.

58. Masumoto, Y. and T. Takagahara, *Semiconductor quantum dots: physics, spectroscopy and applications*. 2013: Springer Science & Business Media.

59. Fournier, J., et al., *Evidence of a green luminescence band related to surface flaws in high purity silica glass.* Optics express, 2010. **18**(21): p. 21557-21566.

60. Pan, L. and C.Q. Sun, *Coordination imperfection enhanced electron-phonon interaction.*

Journal of applied physics, 2004. **95**(7): p. 3819-3821.

61.   Franke, M.E., T.J. Koplin, and U. Simon, *Metal and metal oxide nanoparticles in chemiresistors: does the nanoscale matter?* Small, 2006. **2**(1): p. 36-50.

62.   Mather, G.C. and A. Martínez‐Arias, *Transport Properties and Oxygen Handling.* Synthesis, Properties, and Applications of Oxide Nanomaterials, 2007: p. 353-377.

63.   Tjong, S. and H. Chen, *Nanocrystalline materials and coatings.* Materials Science and Engineering: R: Reports, 2004. **45**(1): p. 1-88.

64.   Wang, Z., et al., *Anomalous quasihydrostaticity and enhanced structural stability of 3 nm nanoceria.* The Journal of Physical Chemistry C, 2007. **111**(32): p. 11756-11759.

65.   Jackson, S.D. and J.S. Hargreaves, *Metal oxide catalysis*. Vol. 1. 2009: Wiley Online Library.

66.   Goddard, W.A. *Detailed reaction mechanisms for selective transformation of alkanes to oxygenates by heterogeneous transition metal oxide catalysts*. in *Abstracts of Papers of the American Chemical Society*. 2015. American Chemical Society.

67.   Wan, Y., et al., *Ni-Mn bi-metal oxide catalysts for the low temperature SCR removal of NO with NH 3*. Applied Catalysis B: Environmental, 2014. **148**: p. 114-122.

68.   Lee, Y.S., et al., *Ultrathin amorphous zinc-tin-oxide buffer layer for enhancing heterojunction interface quality in metal-oxide solar cells.* Energy & Environmental Science, 2013. **6**(7): p. 2112-2118.

69.   You, J., et al., *Improved air stability of perovskite solar cells via solution-processed metal oxide transport layers.* Nature nanotechnology, 2016. **11**(1): p. 75-81.

70.   Shi, X., et al., *Enzymatic biosensors based on the use of metal oxide nanoparticles.* Microchimica Acta, 2014. **181**(1-2): p. 1-22.

71.   Prakash, S., et al., *Polymer thin films embedded with metal nanoparticles for electrochemical biosensors applications.* Biosensors and Bioelectronics, 2013. **41**: p. 43-53.

72.   Salarian, M., et al., *Angiogenic Rg1/Sr‐Doped TiO2 Nanowire/Poly (Propylene Fumarate) Bone Cement Composites.* Macromolecular Bioscience, 2016.

73.   Salarian, M., et al., *Synthesis and characterization of novel TiO 2-poly (propylene fumarate) nanocomposites for bone cementation.* Journal of Materials Chemistry B, 2014. **2**(32): p. 5145-5156.

74.   Topkaya, E., et al., *Pure ZnO and composite ZnO/TiO 2 catalyst plates: a comparative study for the degradation of azo dye, pesticide and antibiotic in aqueous solutions.* Journal of colloid and interface science, 2014. **430**: p. 6-11.

75.   Mortensen, P.M., et al., *Activity and stability of Mo 2 C/ZrO 2 as catalyst for hydrodeoxygenation of mixtures of phenol and 1-octanol.* Journal of Catalysis, 2015. **328**: p. 208-215.

76.   Guan, H., et al., *Enhanced performance of Rh1/TiO2 catalyst without methanation in water‐gas shift reaction.* AIChE Journal, 2016.

77.   Mootabadi, H. and A. Abdullah, *Response Surface Methodology for Simulation of Ultrasonic-assisted Biodiesel Production Catalyzed by SrO/Al2O3 Catalyst.* Energy Sources, Part A: Recovery, Utilization, and Environmental Effects, 2015. **37**(16): p.

1747-1755.

78.   Dieuzeide, M.L., M. Jobbagy, and N. Amadeo, *Vapor-Phase Hydrogenolysis of Glycerol to 1, 2-Propanediol over Cu/Al2O3 Catalyst at Ambient Hydrogen Pressure.* Industrial & Engineering Chemistry Research, 2016. **55**(9): p. 2527-2533.

79.   Lim, Z.-Y., et al., *A novel and anti-agglomerating Ni@ yolk–ZrO 2 structure with sub-10 nm Ni core for high performance steam reforming of methane.* RSC Advances, 2015. **5**(76): p. 61925-61932.

80.   Prashanthan, K., et al. *Effect of interface modifiers on hole mobility in Hybrid Nanoporous Titanium dioxide (TiO2)/Poly (3-hexylthiophene)(P3HT) solar cells*. in *Nanotechnology (IEEE-NANO), 2015 IEEE 15th International Conference on*. 2015. IEEE.

81.   Ren, Z., et al., *Amorphous TiO2 buffer layer boosts efficiency of quantum dot sensitized solar cells to over 9%.* Chemistry of Materials, 2015. **27**(24): p. 8398-8405.

82.   Baruah, S. and J. Dutta, *Hydrothermal growth of ZnO nanostructures.* Science and Technology of Advanced Materials, 2016.

83.   Borgohain, R. and S. Baruah, *Design and analysis of UV detector using ZnO nanorods on interdigitated electrodes.* ADBU Journal of Engineering Technology, 2016. **4**.

84.   Tan, X., et al., *Facile Synthesis of Bimodal Mesoporous Fe3O4@ SiO2 Composite for Efficient Removal of Methylene Blue.* European Journal of Inorganic Chemistry, 2015. **2015**(18): p. 2928-2933.

85.   Serna, J.J.T., et al., *Synthesis of geopolymer from spent FCC: Effect of SiO2/Al2O.*

Materiales de construcción, 2015(317): p. 6.

86.   Wang, X.-q., et al., *Preparation and properties of nano-TiO 2 modified interior wall paint.* Journal of Shanghai University (English Edition), 2007. **11**: p. 432-436.

87.   Jaroenworaluck, A., et al., *Characteristics of silica‐coated TiO2 and its UV absorption for sunscreen cosmetic applications.* Surface and Interface Analysis, 2006. **38**(4): p. 473-477.

88.   Tyner, K., et al., *The state of nano‐sized titanium dioxide (TiO2) may affect sunscreen performance.* International journal of cosmetic science, 2011. **33**(3): p. 234-244.

89.   Hanaor, D.A. and C.C. Sorrell, *Review of the anatase to rutile phase transformation.* Journal of Materials science, 2011. **46**(4): p. 855-874.

90.   Chen, X.D., et al., *Roles of anatase and rutile TiO 2 nanoparticles in photooxidation of polyurethane.* Polymer Testing, 2007. **26**(2): p. 202-208.

91.   Watanabe, T., et al., *Photocatalytic purification and treatment of water and air.* Elsevier, Amsterdam, 1993: p. 747.

92.   Linsebigler, A., G. Lu, and J.T. Yates Jr, *CO chemisorption on TiO2 (110): Oxygen vacancy site influence on CO adsorption.* The Journal of chemical physics, 1995. **103**(21): p. 9438-9443.

93.   Zhou, D., et al., *Influence of material properties on TiO 2 nanoparticle agglomeration.* PloS one, 2013. **8**(11): p. e81239.

94.   Li, G., et al., *Effect of the agglomeration of TiO 2 nanoparticles on their photocatalytic performance in the aqueous phase.* Journal of colloid and interface science, 2010. **348**(2):

p. 342-347.

95.   Nur, Y., J. Lead, and M. Baalousha, *Evaluation of charge and agglomeration behavior of TiO 2 nanoparticles in ecotoxicological media.* Science of The Total Environment, 2015. **535**: p. 45-53.

96.   Roy, P., S. Berger, and P. Schmuki, *TiO2 nanotubes: synthesis and applications.* Angewandte Chemie International Edition, 2011. **50**(13): p. 2904-2939.

97.   Sui, R., A.S. Rizkalla, and P.A. Charpentier, *Formation of titania nanofibers: a direct sol-gel route in supercritical CO2.* Langmuir, 2005. **21**(14): p. 6150-6153.

98.   Vajda, K., et al., *Shape-controlled agglomeration of TiO 2 nanoparticles. New insights on polycrystallinity vs. single crystals in photocatalysis.* Ceramics International, 2016. **42**(2): p. 3077-3087.

99.   Janković, I.A., et al., *New Hybrid Properties of TiO2 Nanoparticles Surface Modified With Catecholate Type Ligands.* Nanoscale Research Letters, 2010. **5**(1): p. 81-88.

100.   Liu, Y.Z., et al., *Enhanced Dispersion of TiO2 Nanoparticles in a TiO2/PEDOT:PSS Hybrid Nanocomposite via Plasma-Liquid Interactions.* SCIENTIFIC REPORTS, 2015. **5**: p. 15765.

101.   Rao, C.N.R., A. Müller, and A.K. Cheetham, *The chemistry of nanomaterials: synthesis, properties and applications*. 2006: John Wiley & Sons.

102.   Tachikawa, T., M. Fujitsuka, and T. Majima, *Mechanistic insight into the TiO2 photocatalytic reactions: design of new photocatalysts.* The Journal of Physical Chemistry C, 2007. **111**(14): p. 5259-5275.

103.   Thiruvenkatachari, R., S. Vigneswaran, and I.S. Moon, *A review on UV/TiO2 photocatalytic oxidation process (Journal Review).* Korean Journal of Chemical Engineering, 2008. **25**(1): p. 64-72.

104.   Almquist, C.B. and P. Biswas, *Role of synthesis method and particle size of nanostructured TiO 2 on its photoactivity.* Journal of Catalysis, 2002. **212**(2): p. 145-156.

105.   He, H., et al., *A feasible hydrogen evolution process of water electrolysis assisted by TiO2 nanotube photocatalysis.* Journal of Industrial and Engineering Chemistry, 2013. **19**(4): p. 1112-1116.

106.   Wang, M., et al., *Inorganic-modified semiconductor TiO2 nanotube arrays for photocatalysis.* ENERGY & ENVIRONMENTAL SCIENCE, 2014. **7**(7): p. 2182-222.

107.   Chacko, D.K., et al., *Ultrafine TiO2 nanofibers for photocatalysis.* RSC ADVANCES, 2013. **3**(47): p. 24858-24862.

108.   Mukherjee, K., et al., *Electron transport in electrospun TiO2 nanofiber dye-sensitized solar cells.* Applied Physics Letters, 2009. **95**(1).

109.   Ohsaki, Y., et al., *Dye-sensitized TiO2 nanotube solar cells: Fabrication and electronic characterization.* Physical Chemistry Chemical Physics, 2005. **7**(24): p. 4157-4163.

110.   Berger, S., et al., *Transparent TiO2 nanotube electrodes via thin layer anodization: Fabrication and use in electrochromic devices.* Langmuir, 2009. **25**(9): p. 4841-4844.

111.   Zalnezhad, E., et al., *TiO2 nanotube coating on stainless steel 304 for biomedical applications.* CERAMICS INTERNATIONAL, 2015. **41**(2): p. 2785-2793.

112.   Chen, X., et al., *Dual action antibacterial TiO2 nanotubes incorporated with silver*

nanoparticles and coated with a quaternary ammonium salt (QAS). Surface and Coatings Technology, 2013. **216**: p. 158-165.

113. Mohl, M., et al., *Titania nanofibers in gypsum composites: an antibacterial and cytotoxicology study.* JOURNAL OF MATERIALS CHEMISTRY B, 2014. **2**(10): p. 1307-1316.

114. Galkina, O.L., et al., *Cellulose nanofiber-titania nanocomposites as potential drug delivery systems for dermal applications.* JOURNAL OF MATERIALS CHEMISTRY B, 2015. **3**(8): p. 1688-1698.

115. Tan, A.W., et al., *Advances in fabrication of TiO2 nanofiber/nanowire arrays toward the cellular response in biomedical implantations: a review.* Journal of Materials Science, 2013. **48**(24): p. 8337-8353.

116. Song, Y.-Y., et al., *Amphiphilic TiO2 nanotube arrays: An actively controllable drug delivery system.* Journal of the American Chemical Society, 2009. **131**(12): p. 4230-4232.

117. Hoyer, P., *Formation of a titanium dioxide nanotube array.* Langmuir, 1996. **12**(6): p. 1411-1413.

118. Jung, J.H., et al., *Creation of novel helical ribbon and double-layered nanotube TiO2 structures using an organogel template.* Chemistry of materials, 2002. **14**(4): p. 1445-1447.

119. Gong, D., et al., *Titanium oxide nanotube arrays prepared by anodic oxidation.* Journal of Materials Research, 2001. **16**(12): p. 3331-3334.

120. Kasuga, T., et al., *Titania nanotubes prepared by chemical processing.* Advanced

Materials, 1999. **11**(15): p. 1307-1311.

121. Bavykin, D.V., et al., *The effect of hydrothermal conditions on the mesoporous structure of TiO 2 nanotubes.* Journal of Materials Chemistry, 2004. **14**(22): p. 3370-3377.

122. Yu, J., et al., *Preparation and photocatalytic activity of mesoporous anatase TiO 2 nanofibers by a hydrothermal method.* Journal of Photochemistry and Photobiology A: Chemistry, 2006. **182**(2): p. 121-127.

123. Kim, I.-D., et al., *Ultrasensitive chemiresistors based on electrospun TiO2 nanofibers.* Nano Letters, 2006. **6**(9): p. 2009-2013.

124. Chuangchote, S., T. Sagawa, and S. Yoshikawa, *Efficient dye-sensitized solar cells using electrospun TiO2 nanofibers as a light harvesting layer.* Applied Physics Letters, 2008. **93**(3): p. 33310-33310.

125. Zhan, S., et al., *Long TiO2 hollow fibers with mesoporous walls: sol-gel combined electrospun fabrication and photocatalytic properties.* The Journal of Physical Chemistry B, 2006. **110**(23): p. 11199-11204.

126. Sahena, F., et al., *Application of supercritical CO 2 in lipid extraction–a review.* Journal of Food Engineering, 2009. **95**(2): p. 240-253.

127. Watkins, J.J. and T.J. McCarthy, *Polymer/metal nanocomposite synthesis in supercritical CO2.* Chemistry of Materials, 1995. **7**(11): p. 1991-1994.

128. Park, J.H., S. Kim, and A.J. Bard, *Novel carbon-doped TiO2 nanotube arrays with high aspect ratios for efficient solar water splitting.* Nano letters, 2006. **6**(1): p. 24-28.

129. Tokudome, H. and M. Miyauchi, *N-doped TiO2 nanotube with visible light activity.*

Chemistry Letters, 2004. **33**(9): p. 1108-1109.

130. LI, J., et al., *Preparation and Photoelectrochemical Properties of Fe-doped TiO_2 Nanotube Arrays [J].* Electrochemistry, 2008. **2**: p. 020.

131. Yu, J., G. Dai, and B. Huang, *Fabrication and characterization of visible-light-driven plasmonic photocatalyst Ag/AgCl/TiO2 nanotube arrays.* The Journal of Physical Chemistry C, 2009. **113**(37): p. 16394-16401.

132. Mumin, M.A., G. Moula, and P.A. Charpentier, *Supercritical CO 2 synthesized TiO 2 nanowires covalently linked with core–shell CdS–ZnS quantum dots: enhanced photocatalysis and stability.* RSC Advances, 2015. **5**(83): p. 67767-67779.

133. Law, M., et al., *ZnO-Al2O3 and ZnO-TiO2 core-shell nanowire dye-sensitized solar cells.* The Journal of Physical Chemistry B, 2006. **110**(45): p. 22652-22663.

134. Cipagauta, S., A. Hernández-Gordillo, and R. Gómez, *TiO2 xerogels prepared by modified sol–gel method with ethylenediamine are photoactive for the 4-nitrophenol photoreduction.* Journal of Sol-Gel Science and Technology, 2014. **72**(2): p. 428-434.

135. Kalasina, S., T. Amornsakchai, and U. Asawapirom, *Nanocomposite TiO2 xerogel film for DSSC photoelectrode via simple modified sol–gel process.* Journal of Sol-Gel Science and Technology. **75**(1): p. 63-73.

136. Lee, J.-S., et al., *The effect of porosity on the CO sensing properties of TiO 2 xerogel thin films.* Thin Solid Films, 2013. **529**: p. 98-102.

137. Chou, T.P., X. Zhou, and G. Cao, *SiO2–TiO2 xerogels for tailoring the release of brilliant blue FCF.* Journal of sol-gel science and technology, 2009. **50**(3): p. 301-307.

138.   Ahn, W., K. Kang, and K. Kim, *Synthesis of TS-1 by microwave heating of template-impregnated SiO2–TiO2 xerogels.* Catalysis letters, 2001. **72**(3-4): p. 229-232.

139.   Lahcene, D., et al., *Synthesis, characterization and activity in cyclohexene epoxidation of V2O5–TiO2 anatase xerogel.* Journal of sol-gel science and technology, 2012. **64**(3): p. 637-642.

140.   Rodella, C.B., et al., *V2O5/TiO2 catalyst xerogels: method of preparation and characterization.* Journal of sol-gel science and technology, 2002. **25**(1): p. 75-82.

141.   El Mir, L., et al., *Preparation and optical characterization of transparent, microporous TiO 2 xerogel monoliths.* Materials Science and Engineering: B, 2008. **146**(1): p. 69-73.

142.   Schubert, U., *Chemical modification of titanium alkoxides for sol-gel processing.* Journal of Materials Chemistry, 2005. **15**(35-36): p. 3701-3715.

143.   Parra, R., et al., *Reaction pathway to the synthesis of anatase via the chemical modification of titanium isopropoxide with acetic acid.* Chemistry of Materials, 2008. **20**(1): p. 143-150.

144.   Gupta, K., et al., *Photocatalytic antibacterial performance of TiO2 and Ag-doped TiO2 against S. aureus. P. aeruginosa and E. coli.* Beilstein journal of nanotechnology, 2013. **4**(1): p. 345-351.

145.   Chen, Y., et al., *Microstructure and properties of polyester-based polyurethane/titania hybrid films prepared by sol–gel process.* Polymer, 2006. **47**(5): p. 1640-1648.

146.   Ogawa, M., N. Shimura, and A. Ayral, *Deposition of thin nanoporous silica layers on solid surfaces.* Chemistry of materials, 2006. **18**(7): p. 1715-1718.

147.   Ibrahim, I.A., A. Zikry, and M.A. Sharaf, *Preparation of spherical silica nanoparticles: Stober silica.* J. Am. Sci, 2010. **6**(11): p. 985-989.

148.   Stöber, W., A. Fink, and E. Bohn, *Controlled growth of monodisperse silica spheres in the micron size range.* Journal of colloid and interface science, 1968. **26**(1): p. 62-69.

149.   Masalov, V., et al., *Mechanism of formation and nanostructure of Stöber silica particles.* Nanotechnology, 2011. **22**(27): p. 275718.

150.   Mumin, M.A., W.Z. Xu, and P.A. Charpentier, *Quantum dots/silica/polymer nanocomposite films with high visible light transmission and UV shielding properties.* Nanotechnology, 2015. **26**(31): p. 315702.

151.   He, Y.-L. and T. Xie, *Advances of thermal conductivity models of nanoscale silica aerogel insulation material.* Applied Thermal Engineering, 2015. **81**: p. 28-50.

152.   Gunay, A.A., *Modeling, fabrication and optimization of optically transparent-thermally insulating silica aerogels for solar thermal applications*. 2016.

153.   Zhao, L., et al., *Modeling silica aerogel optical performance by determining its radiative properties.* AIP Advances, 2016. **6**(2): p. 025123.

154.   Dorcheh, A.S. and M. Abbasi, *Silica aerogel; synthesis, properties and characterization.* Journal of materials processing technology, 2008. **199**(1): p. 10-26.

155.   Kamiuto, K., S. Saitoh, and Y. Tokita, *Scattering phase function of a silica aerogel at 450 nm wavelength.* Journal of Quantitative Spectroscopy and Radiative Transfer, 1993. **50**(3): p. 293-299.

156.   Park, O.K. and Y.S. Kang, *Preparation and characterization of silica-coated TiO 2*

nanoparticle. Colloids and Surfaces A: Physicochemical and Engineering Aspects, 2005. **257**: p. 261-265.

157. Ide, Y., Y. Koike, and M. Ogawa, *Molecular selective photocatalysis by TiO 2/nanoporous silica core/shell particulates.* Journal of colloid and interface science, 2011. **358**(1): p. 245-251.

158. Son, S., et al., *Designed synthesis of SiO2/TiO2 core/shell structure as light scattering material for highly efficient dye-sensitized solar cells.* ACS applied materials & interfaces, 2013. **5**(11): p. 4815-4820.

159. Ren, Y., et al., *Fabrication of rattle-type TiO2/SiO2 core/shell particles with both high photoactivity and UV-shielding property.* Langmuir, 2010. **26**(13): p. 11391-11396.

160. Mahyar, A., M. Ali Behnajady, and N. Modirshahla, *Characterization and photocatalytic activity of SiO2-TiO2 mixed oxide nanoparticles prepared by sol-gel method.* Indian journal of chemistry. Section A, Inorganic, bio-inorganic, physical, theoretical & analytical chemistry, 2010. **49**(12): p. 1593.

161. Lee, J., et al., *Fabrication of SiO2/TiO2 Double-Shelled Hollow Nanospheres with Controllable Size via Sol–Gel Reaction and Sonication-Mediated Etching.* ACS applied materials & interfaces, 2014. **6**(17): p. 15420-15426.

162. Cao, F. and S.C. Jana, *Nanoclay-tethered shape memory polyurethane nanocomposites.* Polymer, 2007. **48**(13): p. 3790-3800.

163. Xu, B., et al., *Mechanical properties of attapulgite clay reinforced polyurethane shape-memory nanocomposites.* European Polymer Journal, 2009. **45**(7): p. 1904-1911.

164. Zou, H., C. Weder, and Y.C. Simon, *Shape-Memory Polyurethane Nanocomposites with Single Layer or Bilayer Oleic Acid-Coated Fe3O4Nanoparticles: Shape-Memory Polyurethane Nanocomposites: Influence of Layers.* Macromolecular Materials and Engineering, 2015. **300**(9): p. 885-892.

165. Jang, M.K., A. Hartwig, and B.K. Kim, *Shape memory polyurethanes cross-linked by surface modified silica particles.* Journal of Materials Chemistry, 2009. **19**(8): p. 1166.

166. 杜明亮, 徐.傅., *Investigation on Structures and Properties of Shape Memory Polyurethane/Silica Nanocomposites.* 中国化学：英文版, 2011. **29**(4): p. 703-710.

167. Gu, S., et al., *Carbon nanotube-polyurethane shape memory nanocomposites with low trigger temperature.* European Polymer Journal, 2013. **49**(12): p. 3867.

168. Jiu, H., et al., *Graphene-crosslinked two-way reversible shape memory polyurethane nanocomposites with enhanced mechanical and electrical properties.* Journal of Materials Science: Materials in Electronics, 2016. **27**(10): p. 10720-10728.

169. Athanasopoulos, N., et al., *Electrical conductivity of polyurethane/MWCNT nanocomposite foams.* Polymer Composites, 2012. **33**(8): p. 1302-1312.

170. Yun, S., H. Im, and J. Kim, *The effect of different hard segments in polyurethane on the electrical conductivity of polyurethane grafted multi-walled carbon nanotube/polyurethane nanocomposites.* Synthetic Metals, 2011. **161**(13): p. 1361-1367.

171. Saadat-Monfared, A., M. Mohseni, and M.H. Tabatabaei, *Polyurethane nanocomposite films containing nano-cerium oxide as UV absorber. Part 1. Static and dynamic light scattering, small angle neutron scattering and optical studies.* Colloids and Surfaces A:

Physicochemical and Engineering Aspects, 2012. **408**: p. 64-70.

172. Kanjwal, M.A., N.A.M. Barakat, and I.S. Chronakis, *Photocatalytic degradation of dairy effluent using AgTiO2 nanostructures/polyurethane nanofiber membrane.* Ceramics International, 2015.

173. Modesti, M., et al., *Synergism between flame retardant and modified layered silicate on thermal stability and fire behaviour of polyurethane nanocomposite foams.* Polymer Degradation and Stability, 2008. **93**(12): p. 2166-2171.

174. Jana, R.N. and J.W. Cho, *Thermal stability and molecular interaction of polyurethane nanocomposites prepared byin situ polymerization with functionalized multiwalled carbon nanotubes.* Journal of Applied Polymer Science, 2008. **108**(5): p. 2857-2864.

175. Pircheraghi, G., et al., *Effect of carbon nanotube dispersion and network formation on thermal conductivity of thermoplastic polyurethane/carbon nanotube nanocomposites.* Polymer Engineering & Science, 2016. **56**(4): p. 394-407.

176. Dai, Z., et al., *Synthesis and thermal properties of antimony doped tin oxide/waterborne polyurethane nanocomposite films as heat insulating materials.* Polymers for Advanced Technologies, 2011. **22**(12): p. 1905-1911.

177. Lv, C., et al., *Waterborne UV-curable polyurethane acrylate/silica nanocomposites for thermochromic coatings.* RSC Adv, 2015. **5**(33): p. 2573-25737.

178. Chen, J., et al., *Synthesis, characterization and infrared emissivity study of polyurethane/TiO2 nanocomposites.* Applied Surface Science, 2007. **253**(23): p. 9154-9158.

179. Sadu, R.B., et al., *Silver-Doped TiO2/Polyurethane Nanocomposites for Antibacterial Textile Coating.* BioNanoScience, 2014. **4**(2): p. 136-148.

180. Qiu, S., et al., *Degradation of pollutant and antibacterial activity of waterborne polyurethane/doped TiO2 nanoparticle hybrid films.* Journal of Wuhan University of Technology-Mater. Sci. Ed, 2015. **30**(3): p. 447-451.

181. Schreader, K.J., et al., *A polyurethane‐based nanocomposite biocompatible bone adhesive.* Journal of Applied Polymer Science, 2013. **127**(6): p. 4974-4982.

182. Meng, J., et al., *Improving the blood compatibility of polyurethane using carbon nanotubes as fillers and its implications to cardiovascular surgery.* Journal of Biomedical Materials Research Part A, 2005. **74A**(2): p. 208-214.

183. Barick, A.K. and D.K. Tripathy, *Effect of Organoclay on the Morphology, Mechanical, Thermal, and Rheological Properties of Organophilic Montmorillonite Nanoclay Based Thermoplastic Polyurethane Nanocomposites Prepared by Melt Blending.* Polymer Engineering and Science, 2010. **50**(3): p. 484-498.

184. Wang, X., et al., *Fabrication and characterization of graphene-reinforced waterborne polyurethane nanocomposite coatings by the sol–gel method.* Surface and Coatings Technology, 2012. **206**(23): p. 4778-4784.

185. Rashti, A., et al., *Development of novel biocompatible hybrid nanocomposites based on polyurethane-silica prepared by sol gel process.* Materials science & engineering. C, Materials for biological applications, 2016. **69**: p. 1248-1255.

186. Aslzadeh, M.M., G. Mir Mohamad Sadeghi, and M. Abdouss, *Synthesis and*

characterization of chlorine‐containing flame‐retardant polyurethane nanocomposites via in situ polymerization. Journal of Applied Polymer Science, 2012. **123**(1): p. 437-447.

187. Reid, D., et al., *In-Situ Synthesis of Polyurethane-TiO2 Nanocomposite and Performance in Solid Propellants.* Journal of Materials Chemistry A, 2013.

188. Lee, S.K., et al., *Waterborne polyurethane nanocomposites having shape memory effects.* Journal of Polymer Science, Part A: Polymer Chemistry, 2011. **49**(3): p. 634-641.

189. Mohammadi, A., M. Barikani, and M.M. Lakouraj, *Biocompatible polyurethane/thiacalix[4]arenes functionalized Fe3O4 magnetic nanocomposites: Synthesis and properties.* Materials Science & Engineering C, 2016. **66**: p. 106-118.

190. Charpentier, P.A., et al., *Nano-TiO2/polyurethane composites for antibacterial and self-cleaning coatings.* NANOTECHNOLOGY, 2012. **23**(42): p. 425606.

191. Zia, K.M., H.N. Bhatti, and I.A. Bhatti, *Methods for polyurethane and polyurethane composites, recycling and recovery: A review.* Reactive and functional polymers, 2007. **67**(8): p. 675-692.

192. Shah, A.A., et al., *Biological degradation of plastics: a comprehensive review.* Biotechnology advances, 2008. **26**(3): p. 246-265.

193. Howard, G.T., *Biodegradation of polyurethane: a review.* International Biodeterioration & Biodegradation, 2002. **49**(4): p. 245-252.

194. Loredo-Treviño, A., et al., *Microbial enzymes involved in polyurethane biodegradation: a review.* Journal of Polymers and the Environment, 2012. **20**(1): p. 258-265.

195. Rek, V., H.J. Mencer, and M. Bravar, *GPC and structural analysis of polyurethane*

degradation. Polymer photochemistry, 1986. **7**(4): p. 273-283.

196.   Açıkalın, E. and O. Atıcı. *Preparation of Waterborne Polyurethane‐OMt*

Nanocomposites and Effect of Clay on UV Degradation. in *Macromolecular Symposia.*

2014. Wiley Online Library.

197.   Chen, L., et al., *Fabrication and characterization of TiO2–SiO2 composite nanoparticles*

and polyurethane/(TiO2–SiO2) nanocomposite films. Colloid and Polymer Science, 2007.

285(13): p. 1515-1520.

198.   Charpentier, P.A., et al., *Nano-TiO2/polyurethane composites for antibacterial and*

self-cleaning coatings. Nanotechnology, 2012. **23**(42): p. 425606.

199.   Wold, A., *Photocatalytic properties of titanium dioxide (TiO2).* Chemistry of Materials,

1993. **5**(3): p. 280-283.

200.   Fujishima, A., T.N. Rao, and D.A. Tryk, *Titanium dioxide photocatalysis.* Journal of

Photochemistry and Photobiology C: Photochemistry Reviews, 2000. **1**(1): p. 1-21.

201.   Cho, S. and W. Choi, *Solid-phase photocatalytic degradation of PVC–TiO 2 polymer*

composites. Journal of Photochemistry and Photobiology A: Chemistry, 2001. **143**(2): p.

221-228.

202.   Khaled, S., et al., *Synthesis of TiO2-PMMA nanocomposite: using methacrylic acid as a*

coupling agent. Langmuir, 2007. **23**(7): p. 3988-3995.

203.   Hojjati, B., R. Sui, and P.A. Charpentier, *Synthesis of TiO 2/PAA nanocomposite by RAFT*

polymerization. Polymer, 2007. **48**(20): p. 5850-5858.

204.   Kumar, K.V., K. Porkodi, and F. Rocha, *Langmuir–Hinshelwood kinetics–a theoretical*

study. Catalysis Communications, 2008. **9**(1): p. 82-84.

205.   Mehrotra, K., G.S. Yablonsky, and A.K. Ray, *Kinetic studies of photocatalytic degradation in a TiO2 slurry system: Distinguishing working regimes and determining rate dependences.* Industrial & engineering chemistry research, 2003. **42**(11): p. 2273-2281.

206.   Cauich-Rodríguez, J.V., et al., *Degradation of polyurethanes for cardiovascular applications.* 2013: INTECH Open Access Publisher.

207.   Radovic, L.R., *Chemistry & Physics of Carbon.* 2012: Taylor & Francis.

208.   Hurum, D.C., et al., *Explaining the enhanced photocatalytic activity of Degussa P25 mixed-phase TiO2 using EPR.* The Journal of Physical Chemistry B, 2003. **107**(19): p. 4545-4549.

209.   Mandzy, N., E. Grulke, and T. Druffel, *Breakage of TiO 2 agglomerates in electrostatically stabilized aqueous dispersions.* Powder Technology, 2005. **160**(2): p. 121-126.

210.   Bajsić, E.G. and V. Rek, *Thermal stability of polyurethane elastomers before and after UV irradiation.* Journal of applied polymer science, 2001. **79**(5): p. 864-873.

211.   Xia, X., et al., *Synthesis and photocatalytic properties of TiO 2 nanostructures.* Materials Research Bulletin, 2008. **43**(8): p. 2187-2195.

212.   González, E., et al., *Photoactive self-cleaning polymer coatings by TiO2 nanoparticle Pickering miniemulsion polymerization.* Chemical Engineering Journal, 2015. **281**: p. 209-217.

213.   Seentrakoon, B., B. Junhasavasdikul, and W. Chavasiri, *Enhanced UV-protection and antibacterial properties of natural rubber/rutile-TiO2 nanocomposites.* Polymer Degradation and Stability, 2013. **98**(2): p. 566-578.

214.   Qi, L., et al., *Photostabilization of polypropylene by surface modified rutile‐type TiO2 nanorods.* Journal of Applied Polymer Science, 2014. **131**(16): p. n/a-n/a.

215.   Hamming, L.M., et al., *Effects of dispersion and interfacial modification on the macroscale properties of TiO 2 polymer–matrix nanocomposites.* Composites science and technology, 2009. **69**(11): p. 1880-1886.

216.   Shen, Y., et al. *Preparation and characterization of titania/silicone nanocomposite material.* in *IOP Conference Series: Materials Science and Engineering.* 2015. IOP Publishing.

217.   Kickelbick, G., *The search of a homogeneously dispersed material—the art of handling the organic polymer/metal oxide interface.* Journal of Sol-Gel Science and Technology, 2008. **46**(3): p. 281-290.

218.   Chen, C., Y. Tang, and P.A. Charpentier, *Grafting from approach to the synthesis of photo-degrading polyurethane foams utilizing 2, 2-dimethylolpropionic acid functionalized nano-TiO 2.* Polymer, 2015. **77**: p. 345-353.

219.   Bellardita, M., et al., *Photocatalytic activity of TiO 2/SiO 2 systems.* Journal of Hazardous Materials, 2010. **174**(1): p. 707-713.

220.   Moongraksathum, B. and Y.-W. Chen, *Preparation and characterization of SiO2–TiO2 neutral sol by peroxo sol–gel method and its application on photocatalytic degradation.*

Journal of Sol-Gel Science and Technology, 2016. **77**(2): p. 288-297.

221. Ishibashi, K.-i., et al., *Quantum yields of active oxidative species formed on TiO 2 photocatalyst.* Journal of Photochemistry and Photobiology A: Chemistry, 2000. **134**(1): p. 139-142.

222. Ishibashi, K.-I., et al., *Detection of active oxidative species in TiO 2 photocatalysis using the fluorescence technique.* Electrochemistry Communications, 2000. **2**(3): p. 207-210.

223. Allan, J.M., et al., *Silica aerogel‐poly(ethylene‐co‐vinyl acetate) composite for transparent heat retention films.* Journal of Polymer Science Part B: Polymer Physics, 2014. **52**(14): p. 927-935.

224. Nilchi, A., S. Janitabar-Darzi, and S. Rasouli-Garmarodi, *Sol-gel preparation of nanoscale TiO2/SiO2 composite for eliminating of Con Red azo dye.* Materials Sciences and Applications, 2011. **2**(05): p. 476.

225. Sirimahachai, U., et al., *Nanosized TiO2 particles decorated on SiO2 spheres (TiO2/SiO2): synthesis and photocatalytic activities.* Journal of sol-gel science and technology, 2010. **56**(1): p. 53-60.

226. MUSTAFE, A.M.B.M., *FTIR studies on 2K polyurethane paint*. 2005.

227. Plummer, J.D., M.D. Deal, and P.B. Griffin, *Silicon VLSI technology: fundamentals, practice and modeling*. 2000, Upper Saddle River, NJ: Prentice Hall.

228. Zhang, Y., et al., *TiO2/SiO2 hybrid nanomaterials: synthesis and variable UV-blocking properties.* Journal of sol-gel science and technology, 2011. **58**(1): p. 326-329.

229. Li, K., et al., *Comparative study of the effects of anatase and rutile titanium dioxide*

nanoparticles on the structure and properties of waterborne polyurethane. Colloids and Surfaces A: Physicochemical and Engineering Aspects, 2015. **470**: p. 92-99.

230.   Shafaei, A., M. Nikazar, and M. Arami, *Photocatalytic degradation of terephthalic acid using titania and zinc oxide photocatalysts: Comparative study.* Desalination, 2010. **252**(1): p. 8-16.

231.   Bolis, V., et al., *Hydrophilic/hydrophobic features of TiO 2 nanoparticles as a function of crystal phase, surface area and coating, in relation to their potential toxicity in peripheral nervous system.* Journal of colloid and interface science, 2012. **369**(1): p. 28-39.

232.   Diebold, U., *The surface science of titanium dioxide.* Surface science reports, 2003. **48**(5): p. 53-229.

233.   Che, X.-C., Y.-Z. Jin, and Y.-S. Lee, *Preparation of nano-TiO 2/polyurethane emulsions via in situ RAFT polymerization.* progress in Organic Coatings, 2010. **69**(4): p. 534-538.

234.   Hinkley, J., *A blister test for adhesion of polymer films to SiO2.* The Journal of Adhesion, 1983. **16**(2): p. 115-125.

235.   Mumin, M.A., et al., *Multifunctional mesoporous silica nanoparticles in poly (ethylene‐co‐vinyl acetate) for transparent heat retention films.* Journal of Polymer Science Part B: Polymer Physics, 2015. **53**(12): p. 851-859.

236.   Lee, H., *Rapid measurement of thermal conductivity of polymer films.* Review of Scientific Instruments, 1982. **53**(6): p. 884-887.

237.   Tessema, A. and A. Kidane, *The Effect of Particles Size on the Thermal Conductivity of*

Polymer Nanocomposite, in *Composite, Hybrid, and Multifunctional Materials, Volume 4*. 2015, Springer. p. 151-156.

238.   Wang, J., J. Kuhn, and X. Lu, *Monolithic silica aerogel insulation doped with TiO 2 powder and ceramic fibers.* Journal of non-crystalline solids, 1995. **186**: p. 296-300.

239.   Du, M., B. Guo, and D. Jia, *Thermal stability and flame retardant effects of halloysite nanotubes on poly (propylene).* European Polymer Journal, 2006. **42**(6): p. 1362-1369.

240.   Ghassemi, H., J.E. McGrath, and T.A. Zawodzinski, *Multiblock sulfonated–fluorinated poly (arylene ether) s for a proton exchange membrane fuel cell.* Polymer, 2006. **47**(11): p. 4132-4139.

241.   O'connell, M.J., *Carbon nanotubes: properties and applications*. 2006: CRC press.

242.   Inagaki, M., Y. Yang, and F. Kang, *Carbon nanofibers prepared via electrospinning.* Advanced Materials, 2012. **24**(19): p. 2547-2566.

243.   Rao, C.N.R. and M. Nath, *Inorganic nanotubes.* Dalton Transactions, 2003(1): p. 1-24.

244.   Xia, Y., et al., *One‐dimensional nanostructures: synthesis, characterization, and applications.* Advanced materials, 2003. **15**(5): p. 353-389.

245.   Charpentier, P.A. and K.D. Burgess, *Self-cleaning coatings*. 2015, Google Patents.

246.   Xu, Q.F., et al., *Superhydrophobic TiO2–polymer nanocomposite surface with UV-induced reversible wettability and self-cleaning properties.* ACS applied materials & interfaces, 2013. **5**(18): p. 8915-8924.

247.   Vuong, D., et al., *Hydrothermal synthesis and photocatalytic properties of TiO2 nanotubes*, in *Physics and Engineering of New Materials*. 2009, Springer. p. 95-101.

248. Chen, Q., et al., *The structure of trititanate nanotubes.* Acta Crystallographica Section B: Structural Science, 2002. **58**(4): p. 587-593.

249. Inagaki, M., et al., *Structure and photoactivity of titania derived from nanotubes and nanofibers.* Journal of Hazardous Materials, 2009. **161**(2): p. 1514-1521.

250. Radtke, A., et al., *The structure and the photocatalytic activity of titania based nanotube and nanofiber coatings.* Applied Surface Science, 2016. **368**: p. 165-172.

251. González, E., et al., *Photoactive self-cleaning polymer coatings by TiO 2 nanoparticle Pickering miniemulsion polymerization.* Chemical Engineering Journal, 2015. **281**: p. 209-217.

252. Smirnova, I., S. Suttiruengwong, and W. Arlt, *Feasibility study of hydrophilic and hydrophobic silica aerogels as drug delivery systems.* Journal of Non-Crystalline Solids, 2004. **350**: p. 54-60.

253. Moniruzzaman, M. and K.I. Winey, *Polymer nanocomposites containing carbon nanotubes.* Macromolecules, 2006. **39**(16): p. 5194-5205.

254. Koo, J.H., *Polymer nanocomposites*. 2006: McGraw-Hill Professional Pub.

255. Kim, H., A.A. Abdala, and C.W. Macosko, *Graphene/polymer nanocomposites.* Macromolecules, 2010. **43**(16): p. 6515-6530.

256. Chau, J.L.H., et al., *Transparent high refractive index nanocomposite thin films.* Materials Letters, 2007. **61**(14): p. 2908-2910.

257. Meng, X., et al., *Transparent poly (methyl methacrylate)/TiO2 nanocomposites for UV-shielding applications.* Polymer Science Series A, 2011. **53**(10): p. 977-983.

258.	KHOROSHKO, L., et al. *PHOTOCATALYTIC ACTIVITY OF TiO2 AND SrTiO3*

XEROGELS EMBEDDED IN POROUS ANODIC ALUMINA. in *Physics, Chemistry and*

Applications of Nanostructures: Proceedings of International Conference

Nanomeeting–2015. 2015.

259.	Paez, C.A., et al., *Unpredictable photocatalytic ability of H-2-reduced rutile-TiO2*

xerogel in the degradation of dye-pollutants under UV and visible light irradiation.

APPLIED CATALYSIS B-ENVIRONMENTAL, 2010. **94**(3-4): p. 263-271.

260.	Sukanek, P.C., *Dependence of film thickness on speed in spin coating.* Journal of The

Electrochemical Society, 1991. **138**(6): p. 1712-1719.

261.	Zhang, F., et al., *Ultrathin Film Organic Transistors: Precise Control of Semiconductor*

Thickness via Spin‐Coating. Advanced Materials, 2013. **25**(10): p. 1401-1407.

262.	Allan, J.M., et al., *Silica aerogel‐poly (ethylene‐co‐vinyl acetate) composite for*

transparent heat retention films. Journal of Polymer Science Part B: Polymer Physics,

2014. **52**(14): p. 927-935.

263.	Koenig, J.L., *Application of Fourier transform infrared spectroscopy to chemical systems.*

Applied Spectroscopy, 1975. **29**(4): p. 293-308.

264.	Mumin, M.A., et al., *Multifunctional mesoporous silica nanoparticles in poly(ethylene‐*

co‐vinyl acetate) for transparent heat retention films. Journal of Polymer Science Part B:

Polymer Physics, 2015. **53**(12): p. 851-859.

265.	Fang, V., et al., *A review of near infrared reflectance properties of metal oxide*

nanostructures. 2013.

266.   Chang, C.-C., et al., *TiO2 nanoparticles synthesized in an aprotic solvent and applied to prepare high-refractive-index TiO2-polyimide hybrid thin films.* Journal of sol-gel science and technology, 2014. **71**(1): p. 129-135.

267.   Maeda, S., et al., *Preparation of Transparent Bulk TiO2/PMMA Hybrids with Improved Refractive Indices via an in Situ Polymerization Process Using TiO2 Nanoparticles Bearing PMMA Chains Grown by Surface-Initiated Atom Transfer Radical Polymerization.* ACS Applied Materials & Interfaces, 2016. **8**(50): p. 34762-34769.

268.   Noack, J., et al., *Metal fluoride-based transparent nanocomposites with low refractive indices.* Dalton Transactions, 2013. **42**(16): p. 5706-5710.

Appendices

Appendix A: support information
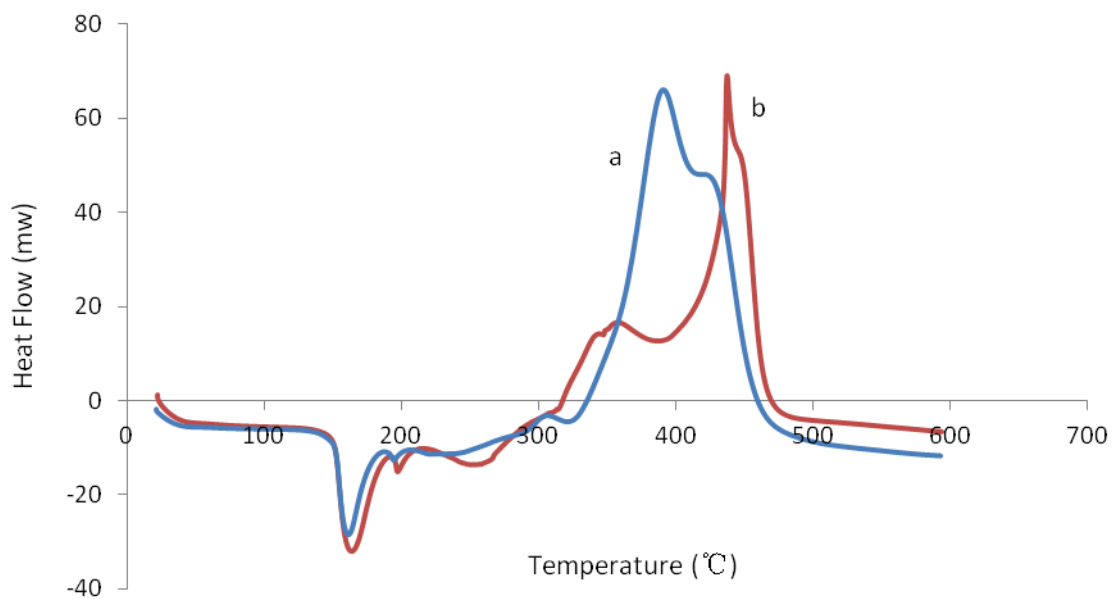
Supporting Information 2.1. DSC of DMPA and DMPA functionalized anatase TiO_2 in air.

(a):DMPA; (b):DMPA-TiO_2(A).
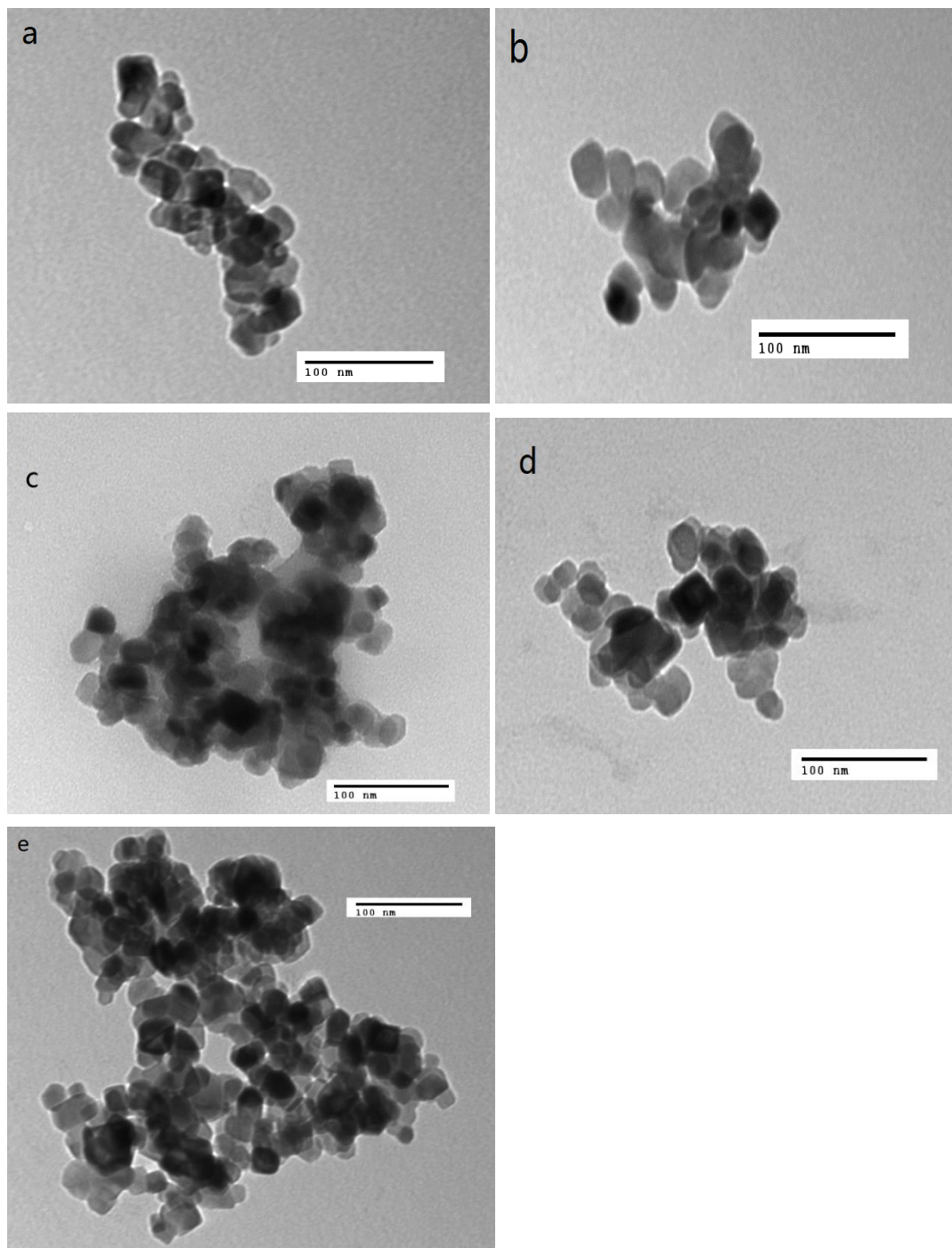
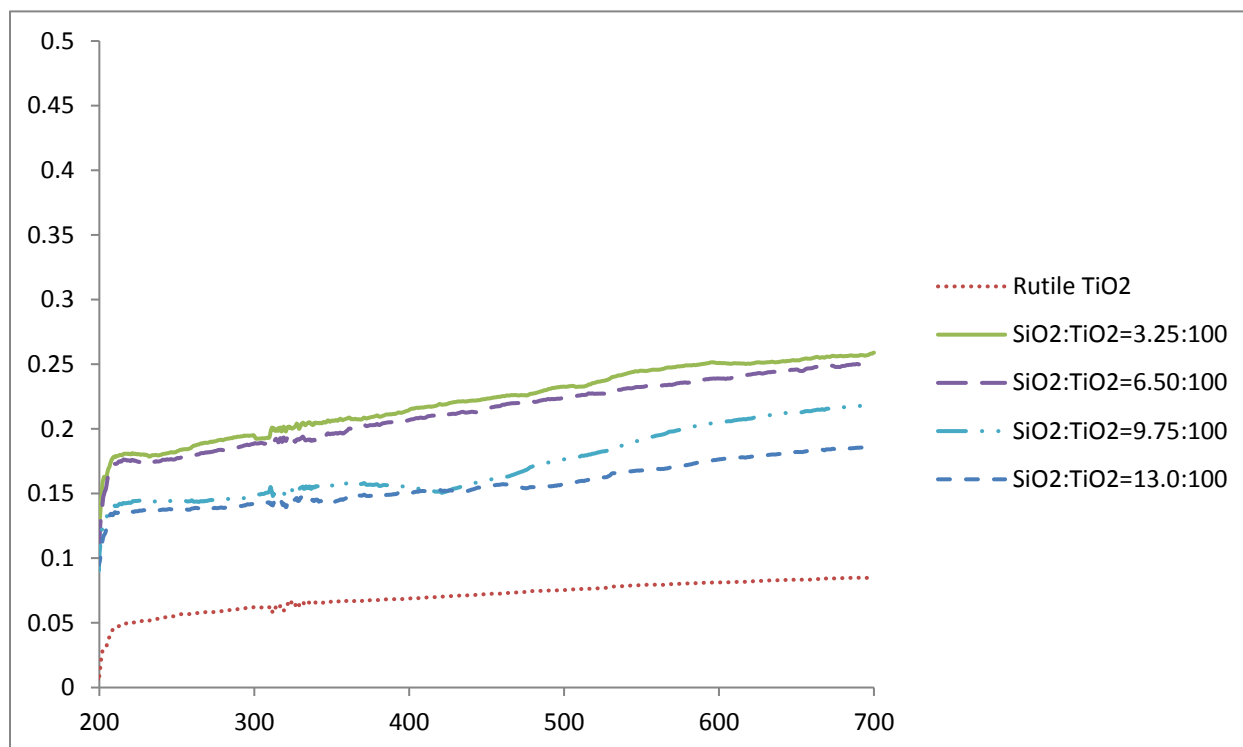**Supporting information 3.1**. TEM image of SiO_2-TiO_2(A) nanoparticles. a: A1. b: A2. c: A3. d: A4. e: A0.
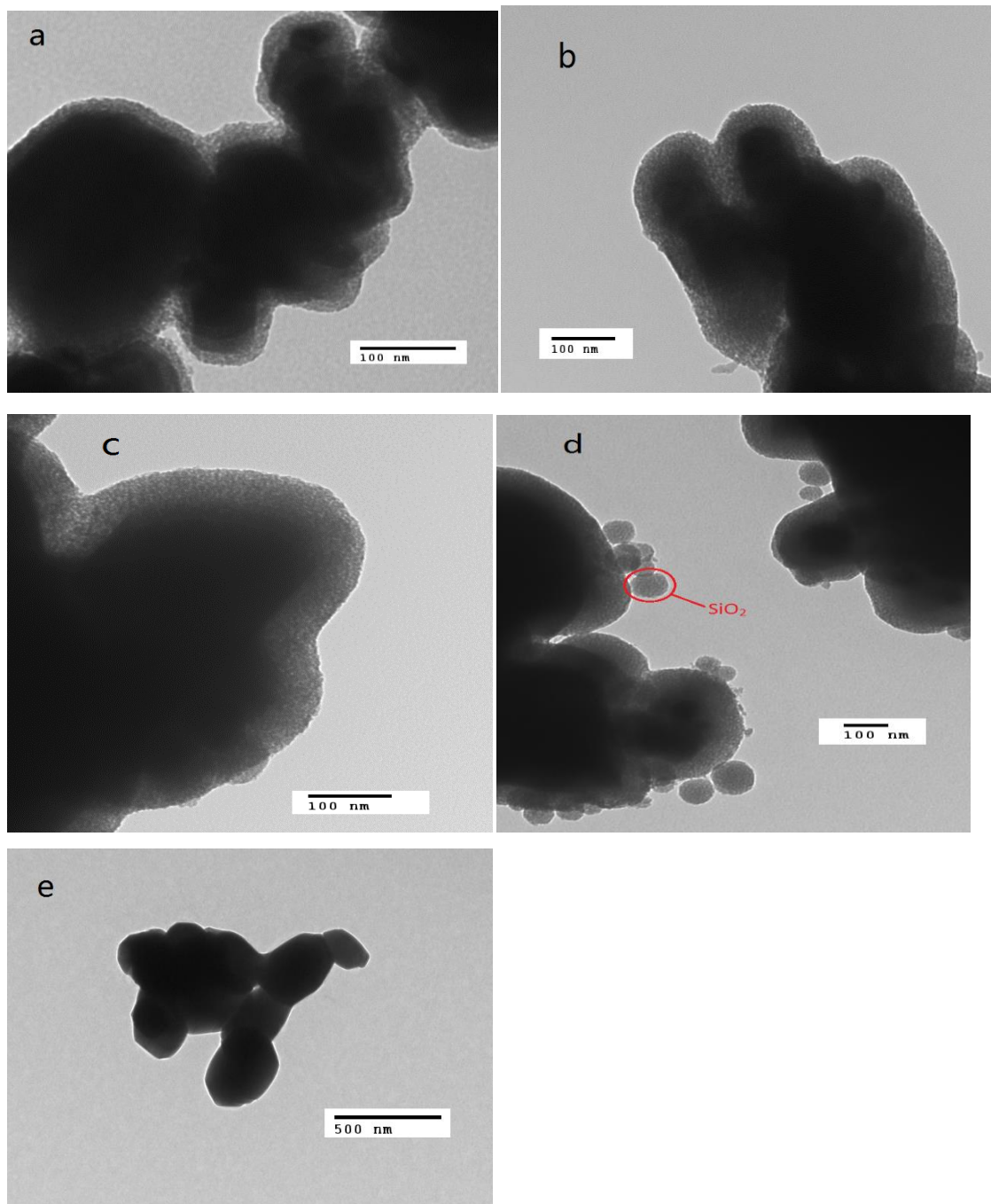
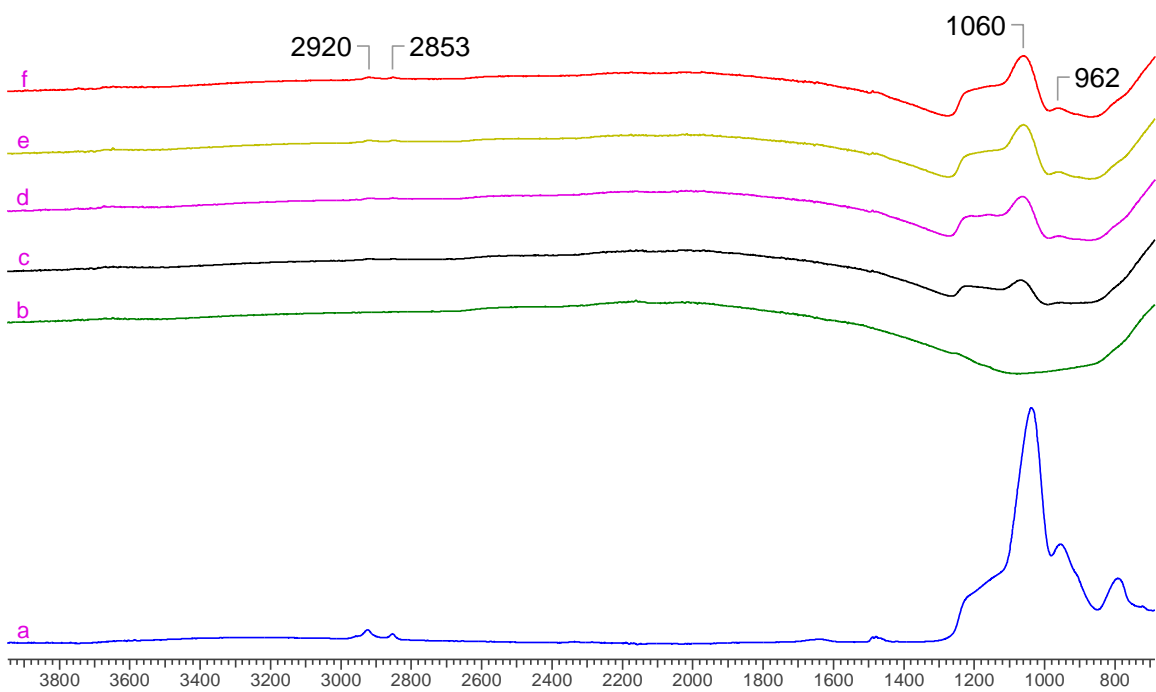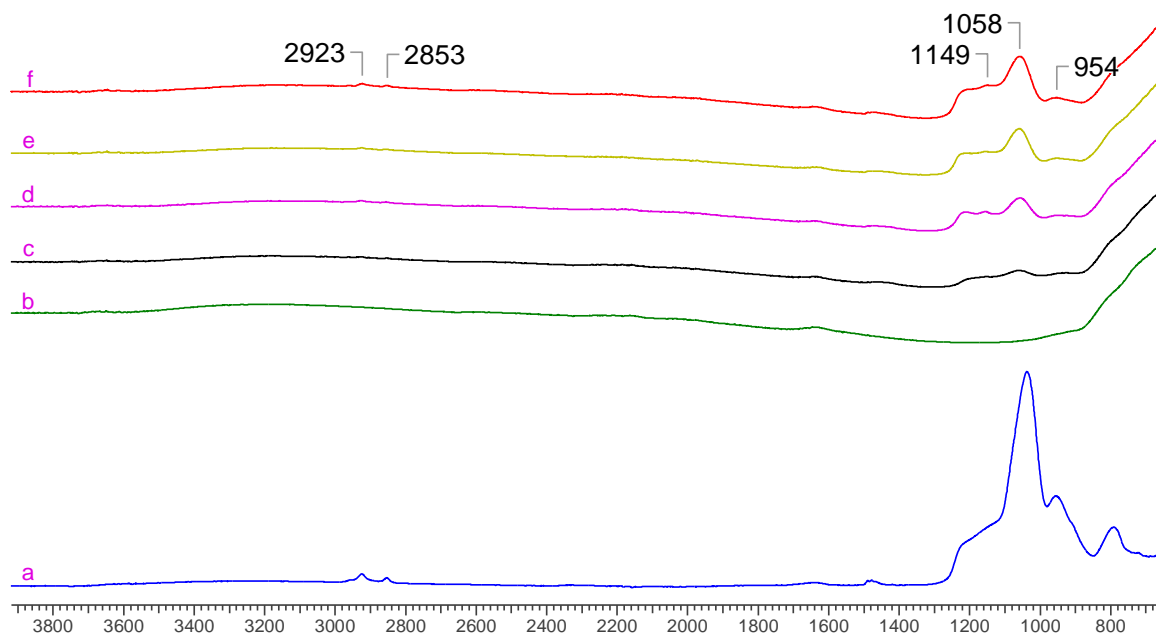**Supporting information 3.2**. TEM image of SiO_2-TiO_2(R) nanoparticles. a: A1. b: A2. c: A3. d: A4. e: A0.
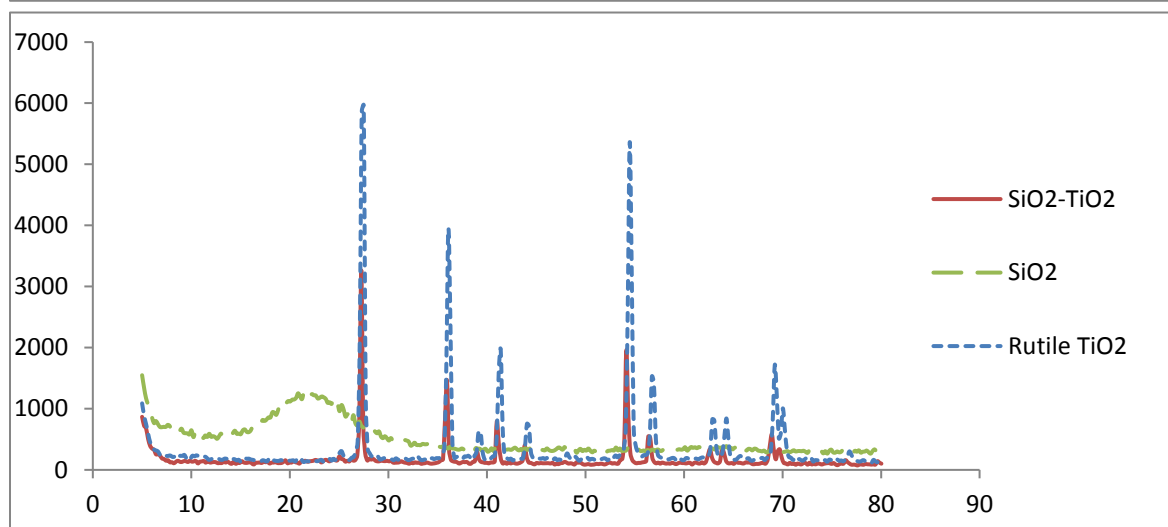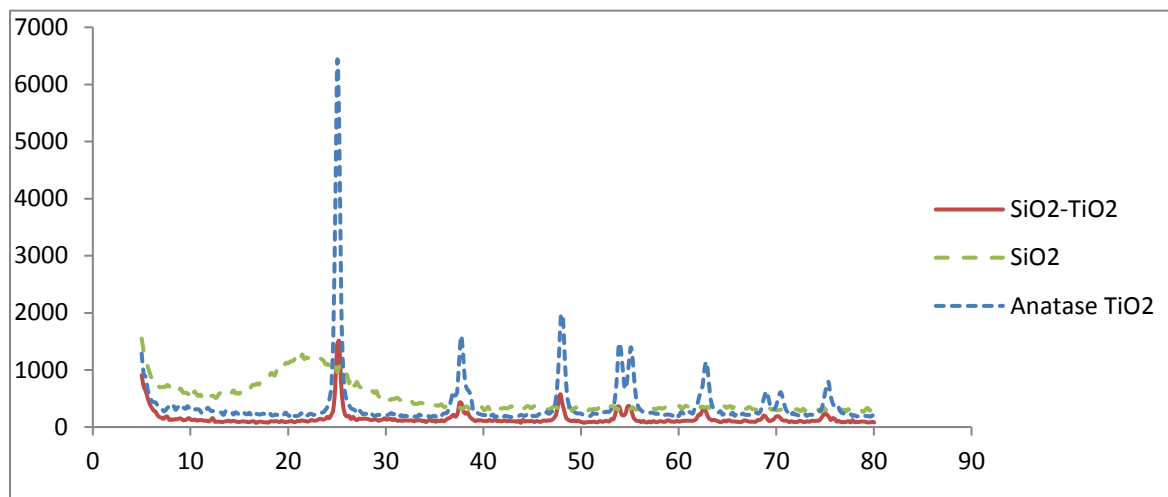
Supporting information 3.3. XRD of different SiO_2-TiO_2 nanoparticles.

**Supporting information 3.4.** UV-vis spectra of SiO2 coated the rutile form of TiO_2.

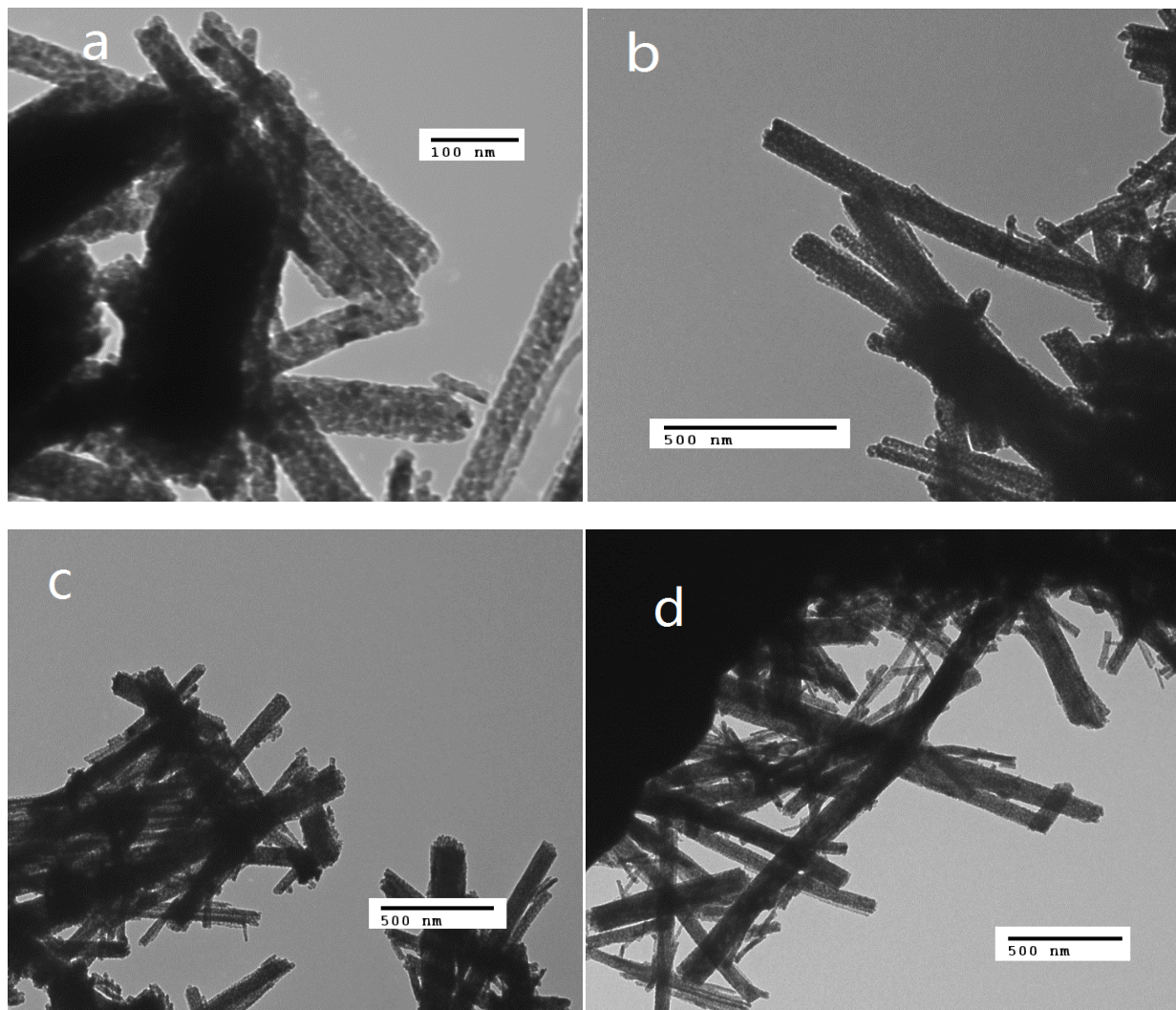**Supporting information 3.5.** FTIR spectra of SiO_2-TiO_2 nanoparticles. Anatse TiO_2 (a: SiO_2. b: A0. c: A1. d: A2. e: A3. f: A4.) Rutile TiO_2 (g: SiO_2. h: R0. i: R1. j: R2. k: R3. l: R4.)
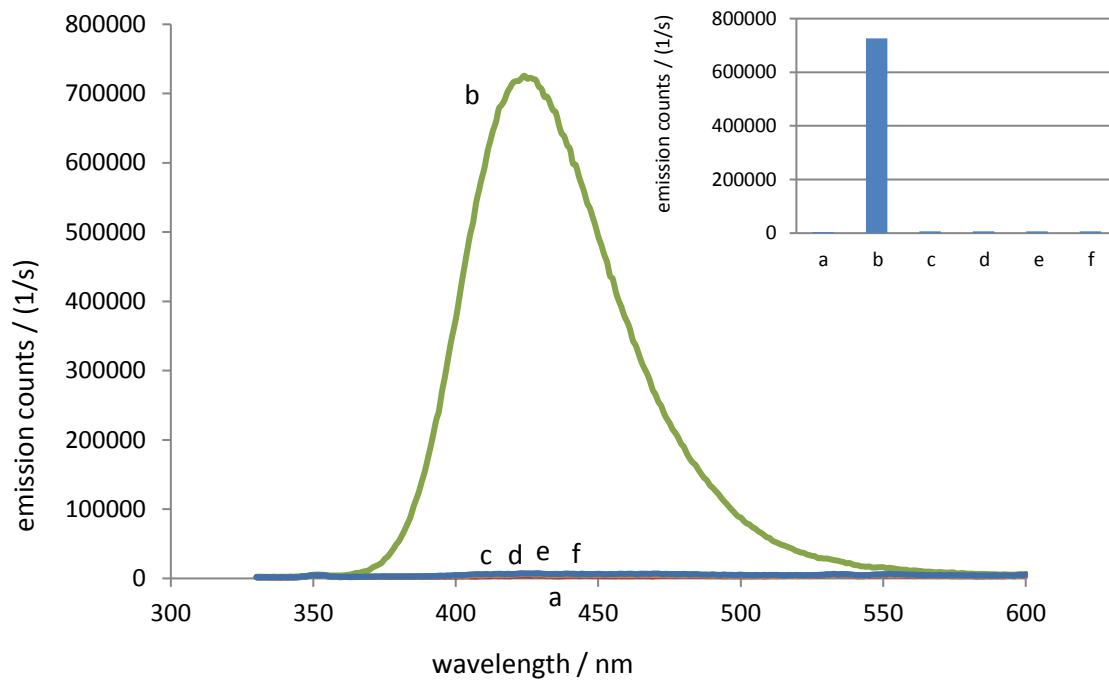
Supporting information 3.6. Photoluminescence spectra of SiO_2-TiO_2(R) nanoparticles in basic

solution under full light illumination of 1 sun for 10 min. a: blank. b: R0. c: R1. d: R2. e: R3. f:
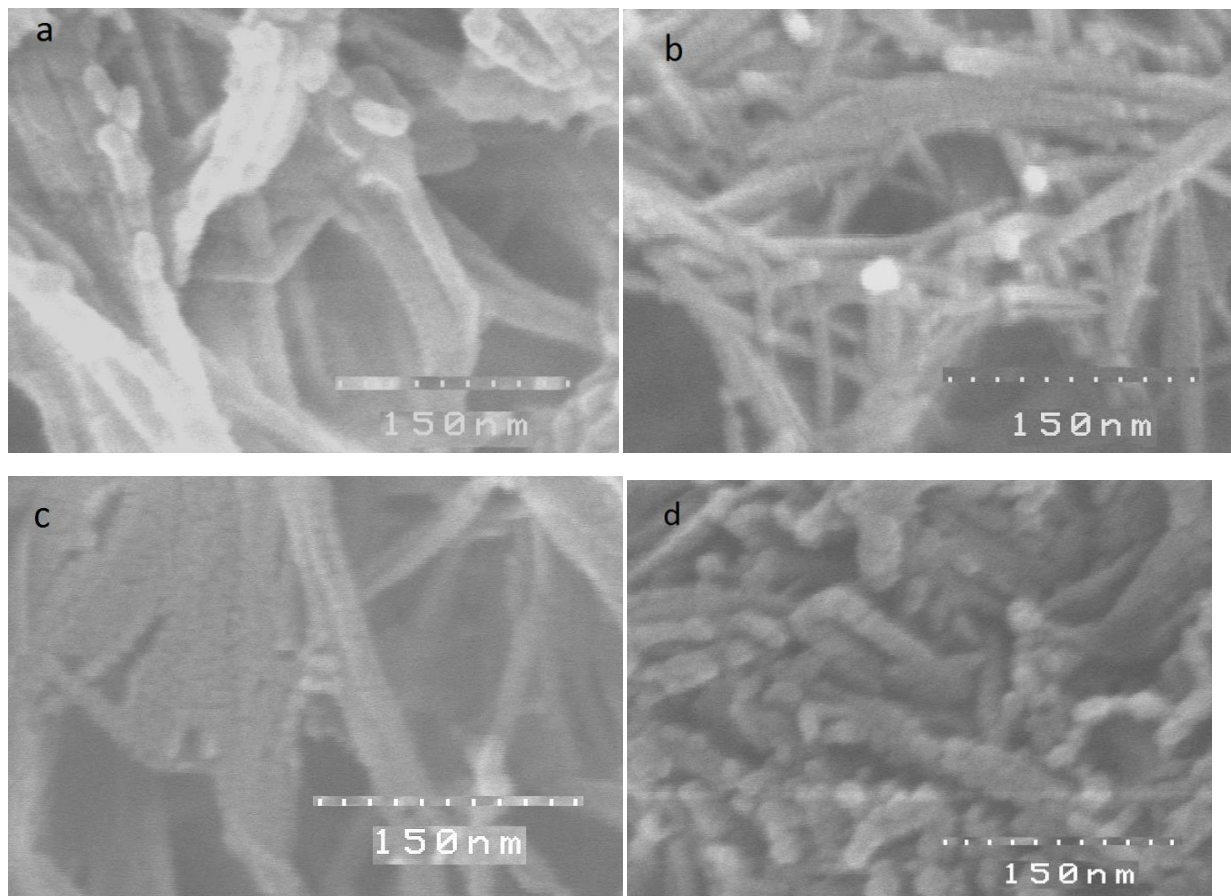
R4.
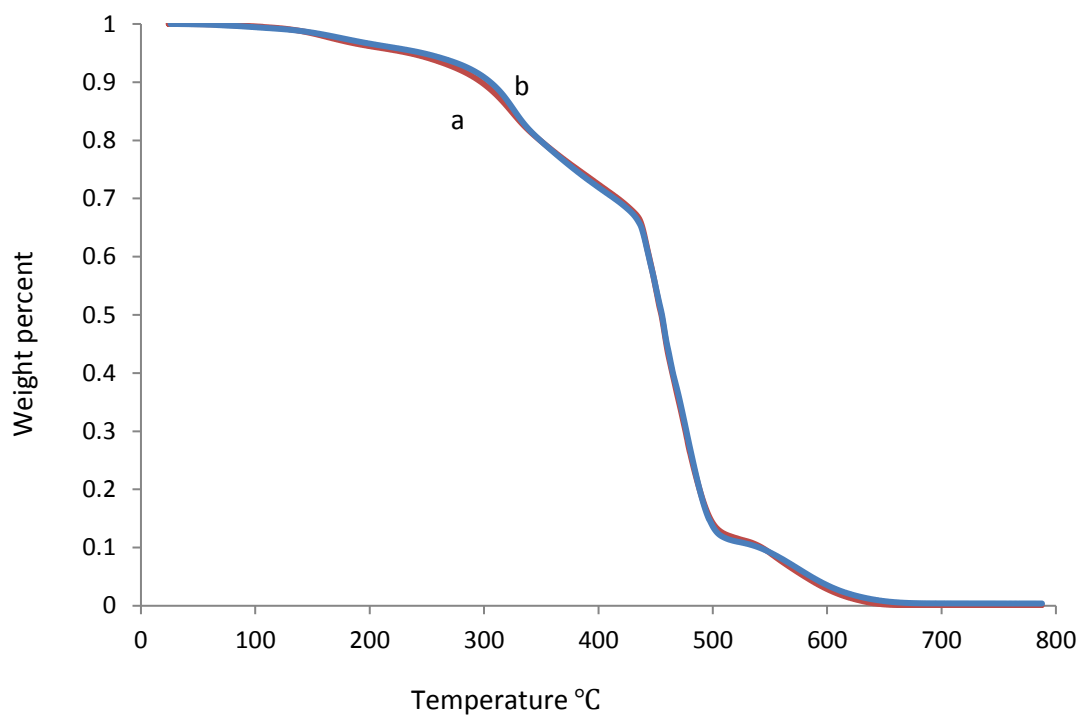
Supporting information 3.7. TGA curves of polyurethane coatings with and without

nanoparticles. a: pure polyurethane; b: polyurethane with A1.

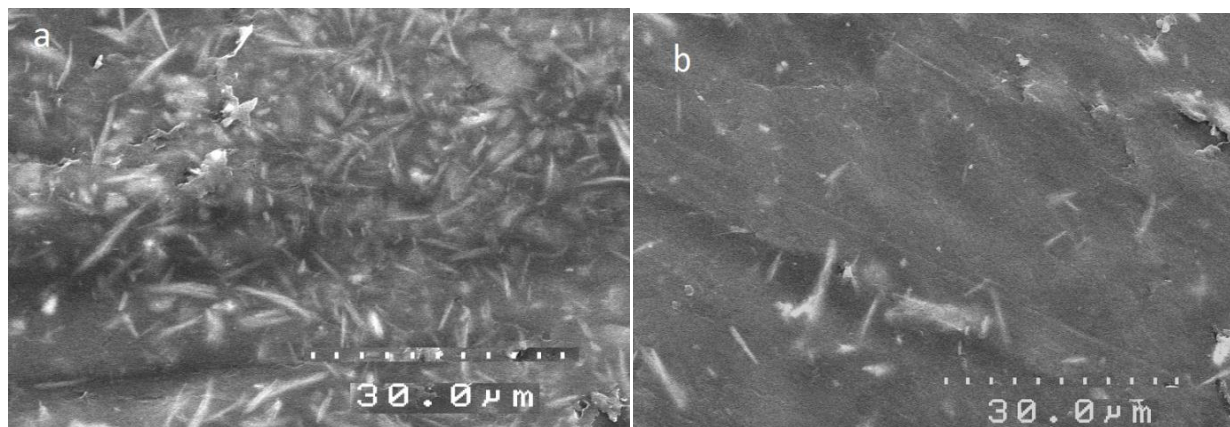**Supporting information 4.1**. TEM image of SiO_2-TiO_2 nanofiber. a: F0. b: F5. c: F10. d: F16.
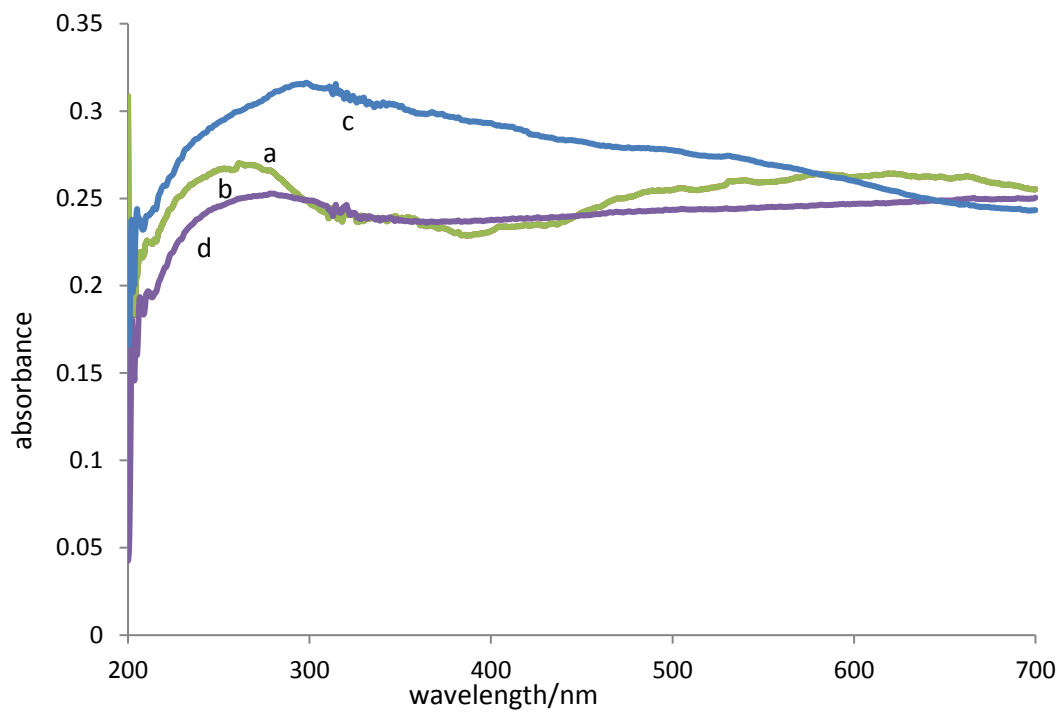
Supporting information 4.2. UV-vis spectra of SiO_2-TiO_2 nanotube. a: T0. b: T5. c: T10. d: T16.
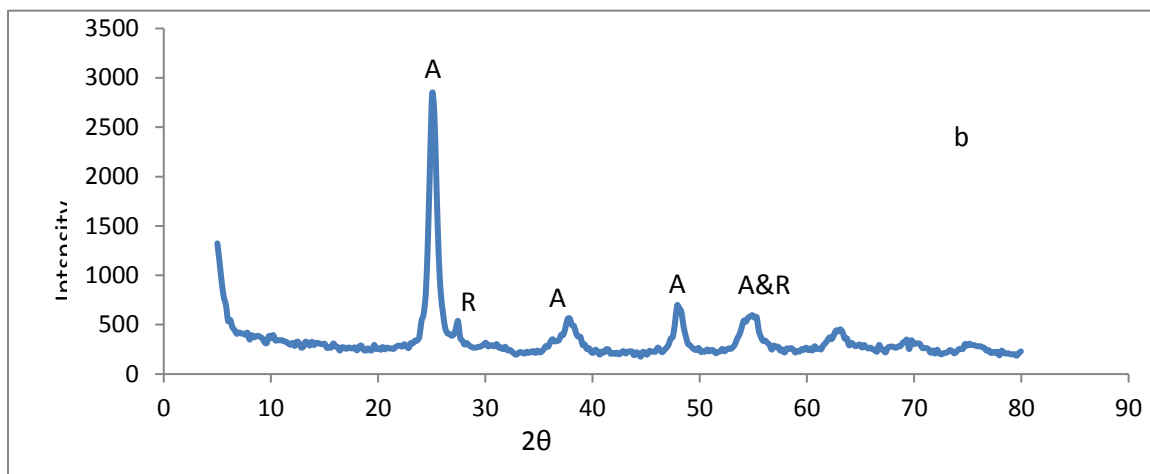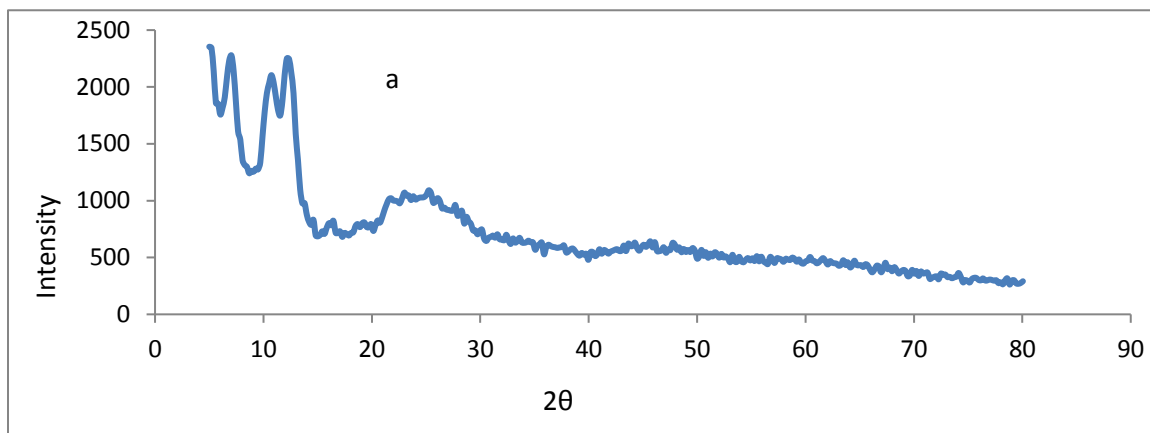
Supporting information 4.3. SEM images of TiO2 nanotubes calcined at different temperatures.

(a) before calcination; (b) 200 °C; (c) 300°C; (d) 400 °C.

Supporting information 4.4. SEM images of PU nanocomposites with different nanoparticles after methylene blue tests. (a) F0; (b) F2.

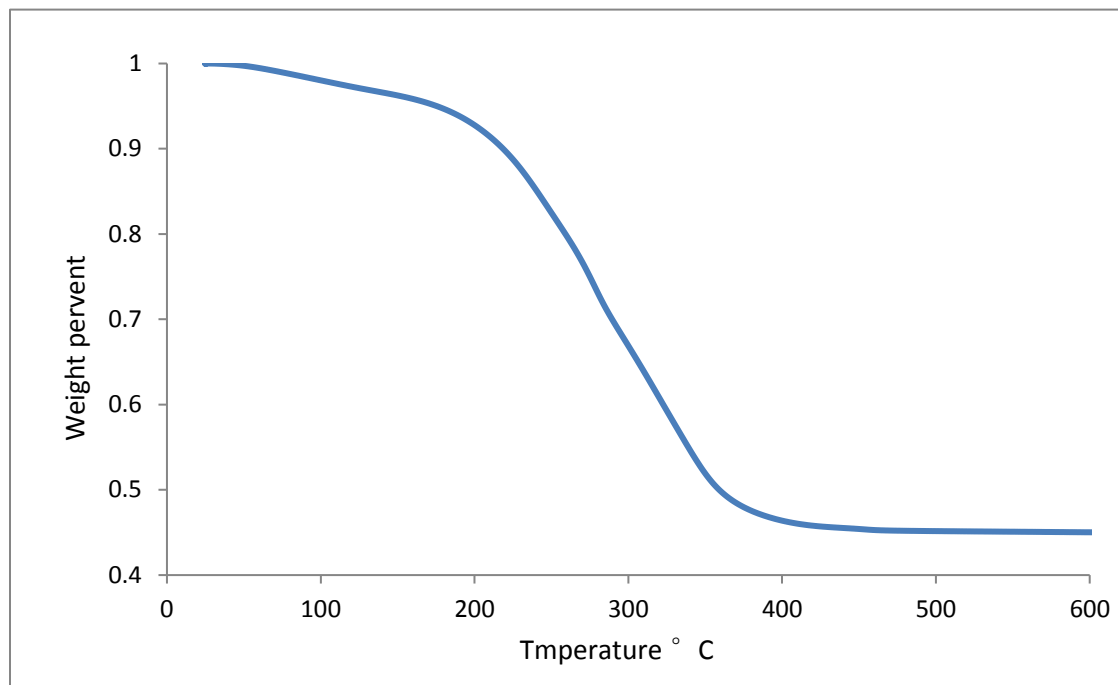**Support information 5.1:** XRD spectra of TiO_2 xerogel nanofiber. a: TiO_2 xerogel nanofiber, b: TiO_2 xerogel nanofiber calcinated at 400℃ for 1 hour.
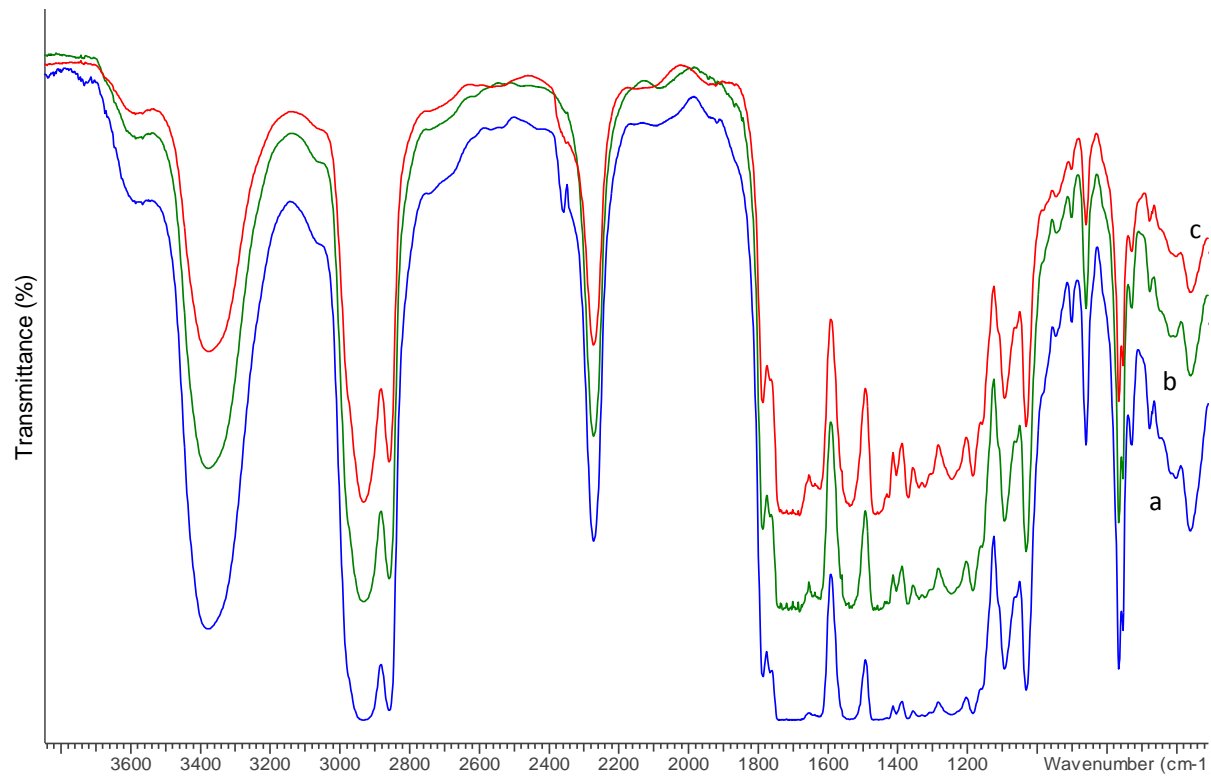
Support information 5.2. FTIR spectra of polyurethane coatings with 15 mg TiO_2 xerogel at different spinning speed. a: 1000rpm. b: 2000rpm. c: 3000rpm.

Support information 5.3: TGA spectrum of TiO_2 xerogel nanofibers treated in air.

Appendix B: personal CV

Chao Chen

EDUCATION

Chemical and biochemical engineering, Specialization in biomaterial and biochemical engineering

University of Western Ontario (PhD)   **2012-2017**

- Supervised by Professor Paul A. Charpentier.

- Focused on modify the physical and chemical properties (such as Young's Modulus, UV proofing, thermal conductivity, and degradation ability under sunlight) of polyurethane foams and coatings by mixing with various modified Titanium Dioxide based nanostructures.

Chemical and biochemical engineering, Specialization in biomaterial and biochemical engineering

University of Western Ontario (Master of Engineering)   **2010-2011**

- Performed a project in Professor Paul A. Charpentier's group.

- Investigated the degradation of polyurethane foams under sunlight by mixing with different Titanium Dioxide nanoparticles.

Material science, Specialization in material chemistry

Fudan University (Bachelor of Science)   **2005-2009**

- Performed the study of the enzymatic degradation of Copolymer.

WORK EXPERIENCES

Teaching Assistant   **2012 - 2015**

University of Western Ontario, London, Ontario

- Designed and supervised undergraduate labs

- Provided guidelines and procedures to safely and successfully complete lab requirements

- Evaluated lab reports, and provided feedbacks for improvements

Graduate Research Assistant   **2012 - 2016**

University of Western Ontario, London, Ontario

- Synthesized DMPA functionalized TiO_2 nanostructures and integrated with polyurethane foams and characterize both of the nanostructures and polymers with TGA, FTIR, SEM etc. for a successful scholarly publication about photo-degradation polyurethane foam.

- Synthesized SiO_2 encapsulated TiO_2 nanostructures (Anatase, Rutile, Nanofiber, Nanotube) and integrated with polyurethane coatings for reducing the agglomeration effect of TiO_2 nanostructures and prevent the coatings aging under UV light.

- Synthesized nanofiber shaped TiO_2 xerogel via supercritical CO_2 method. Developing UV proofing transparent polyurethane coatings by integrating prepared Xerogel.

- Managed the basic maintenance and user training of XRD, and perform sample characterizations with TGA and XRD for colleagues' research project and scholarly publication.

EXPERTISE

Software:

- Familiar with Microsoft Office Excel, Word, and PowerPoint to prepare experiment reports, papers for publication, and presentation.

- Familiar with ChemDraw and CAD for preparation of chemical structures and reaction schemes for publication and presentation.

Instrumentation:

- Familiar with various characterization method as X-ray Diffraction, Thermal gravimetric analysis, Fourier transform infrared spectroscopy, Transmission electron microscopy, UV-Vis, Instron mechanical tests, GPC analysis.

- Familiar with the basic maintenance of XRD equipment and repair performance.

PUBLICATIONS

Chen, C., & Charpentier, P. A. (2014). The effect of TiO_2 nanostructures on self-degrading polyurethane foams. In *AIP Conference Proceedings*, Singh, M. R. (ed.).*1590* (1), 251-258.

Chen, C., Tang, Y., & Charpentier, P. A. (2015). Grafting from approach to the synthesis of photo-degrading polyurethane foams utilizing 2,2-dimethylolpropionic acid functionalized nano-TiO_2. *Polymer, 77*, 345-353.

Chen, C., Wu, W., Xu, W. Z., & Charpentier, P. A. (2017). The effect of silica thickness on nano

 TiO$_2$ particles for functional polyurethane nanocomposites. *Nanotechnology*, *28* (11),

 115709.

Hu, K., Chen, C., Meng, Q., Williams, Z., & Xu, W. (2016). Scientific profile of brain–computer

 interfaces: Bibliometric analysis in a 10-year period. *Neuroscience Letters*, *635*, 61-66.